Engineering

STUDIA UNIVERSITATIS BABEŞ-BOLYAI

Engineering

The Journal of the Faculty of Engineering at Reşiţa

Babeş-Bolyai University from Cluj-Napoca

EDITOR-IN-CHIEF:

Nicoleta GILLICH

BBU University Center in Reşiţa – Romania
Faculty of Engineering
nicoleta.gillich@ubbcluj.ro

Table of content

The contribution of statistical processes in the control of technological processes

Olga-Ioana Amariei, Codruța-Oana Hamat[*], Alexandru-Victor Amariei

Abstract. *In this paper, a manufacturing process is analyzed, having as quality characteristic the "height of the screw head", using analyzes and representative diagrams. Based on this case study, the way to solve these types of problems using the Quality Control Chart module of the WinQSB program, as well as the XLSTAT program is presented.*

Keywords: *WinQSB, XLSTAT, statistical control, control sheets, centering, accuracy*

1. Introduction

The manufacture of high quality products is of particular economic importance, "a first-class requirement of industrial enterprises" [7]. Products that have a higher quality are much more sought after by customers and purchased in a much larger volume, and the lack of this quality affects the entire organization.

Industrial enterprises use "two product quality control groups, namely:

a) deterministic control methods;

b) probabilistic or statistical control methods" [7].

"The main statistical procedures used in the study of processes are the so-called Process Control Chats, which although they have a long "historical career" – the first statistical control sheet being practically invented and applied in 1924 – did not "age" with the entry in the age of digitalization. On the contrary, the current possibilities of calculation allow, together with the use of modern means of measurement, to obtain larger data collections, and their statistical processing to take place almost instantly" [15].

2. Input data of the problem

The studied reference is represented by an M8 screw with a fully threaded hexagonal head, and the quality characteristic of interest is the height of the screw head (Characteristic 1) of size 5.2 ± 0.05 mm. In this sense, 4 samples of 5 measurements per day were taken from the production process, at an interval of 2 hours per shift, for a week.

Number	Date	Time	Subgroup	Characteristic 1
1	08.06.2020	10	1	5.17
2	08.06.2020	10	1	5.15
3	08.06.2020	10	1	5.16
4	08.06.2020	10	1	5.17
5	08.06.2020	10	1	5.15
6	08.06.2020	12	1	5.15
7	08.06.2020	12	1	5.17
8	08.06.2020	12	1	5.15
9	08.06.2020	12	1	5.16
10	08.06.2020	12	1	5.17
11	08.06.2020	14	1	5.17
12	08.06.2020	14	1	5.15
13	08.06.2020	14	1	5.17
14	08.06.2020	14	1	5.20
15	08.06.2020	14	1	5.22
16	08.06.2020	16	1	5.26
17	08.06.2020	16	1	5.25
18	08.06.2020	16	1	5.17
19	08.06.2020	16	1	5.26
20	09.06.2020	16	1	5.25
21	09.06.2020	10	2	5.15
22	09.06.2020	10	2	5.16
23	09.06.2020	10	2	5.18
24	09.06.2020	10	2	5.17
25	09.06.2020	10	2	5.19
26	09.06.2020	12	2	5.19
27	09.06.2020	12	2	5.17
28	09.06.2020	12	2	5.15
29	09.06.2020	12	2	5.16
30	09.06.2020	12	2	5.14
31	09.06.2020	14	2	5.13
32	09.06.2020	14	2	5.19
33	09.06.2020	14	2	5.19
34	09.06.2020	14	2	5.26
35	09.06.2020	14	2	5.17
36	09.06.2020	16	2	5.17
37	09.06.2020	16	2	5.26
38	09.06.2020	16	2	5.25
39	09.06.2020	16	2	5.26
40	09.06.2020	16	2	5.25
41	10.06.2020	10	3	5.17
42	10.06.2020	10	3	5.15
43	10.06.2020	10	3	5.16
44	10.06.2020	10	3	5.15
45	10.06.2020	10	3	5.17
46	10.06.2020	12	3	5.19
47	10.06.2020	12	3	5.19
48	10.06.2020	12	3	5.17
49	10.06.2020	12	3	5.15
50	10.06.2020	12	3	5.16
51	10.06.2020	14	3	5.15
52	10.06.2020	14	3	5.16
53	10.06.2020	14	3	5.26
54	10.06.2020	14	3	5.19
55	10.06.2020	14	3	5.19
56	10.06.2020	16	3	5.16
57	10.06.2020	16	3	5.26
58	10.06.2020	16	3	5.25
59	10.06.2020	16	3	5.20
60	10.06.2020	16	3	5.17
61	11.06.2020	10	4	5.15
62	11.06.2020	10	4	5.16
63	11.06.2020	10	4	5.17
64	11.06.2020	10	4	5.17
65	11.06.2020	10	4	5.24
66	11.06.2020	12	4	5.24
67	11.06.2020	12	4	5.26
68	11.06.2020	12	4	5.25
69	11.06.2020	12	4	5.15
70	11.06.2020	12	4	5.16
71	11.06.2020	14	4	5.14
72	11.06.2020	14	4	5.13
73	11.06.2020	14	4	5.17
74	11.06.2020	14	4	5.19
75	11.06.2020	14	4	5.19
76	11.06.2020	16	4	5.23
77	11.06.2020	16	4	5.26
78	11.06.2020	16	4	5.25
79	11.06.2020	16	4	5.14
80	11.06.2020	16	4	5.13
81	12.06.2020	10	5	5.17
82	12.06.2020	10	5	5.22
83	12.06.2020	10	5	5.15
84	12.06.2020	10	5	5.16
85	12.06.2020	10	5	5.15
86	12.06.2020	12	5	5.22
87	12.06.2020	12	5	5.17
88	12.06.2020	12	5	5.17
89	12.06.2020	12	5	5.15
90	12.06.2020	12	5	5.19
91	12.06.2020	14	5	5.19
92	12.06.2020	14	5	5.15
93	12.06.2020	14	5	5.16
94	12.06.2020	14	5	5.22
95	12.06.2020	14	5	5.14
96	12.06.2020	16	5	5.13
97	12.06.2020	16	5	5.26
98	12.06.2020	16	5	5.25
99	12.06.2020	16	5	5.14
100	12.06.2020	16	5	5.13

Figure 1. The input data of the problem using the WinQSB program

The data collected (measured values for each product unit in the sample) are entered in the Quality Control Chart module of the WinQSB program, in fig. 1.

3. Analysis

We first perform a statistical analysis of the recorded data, by subgroups (days) and total [9]. So the statistical control is applied using the method of the arithmetic average and the amplitude of the scattering for each sample of size n = 5 pcs, and the obtained results are presented in fig. 2.

	23:03:22		Monday	July	19	2021			
Sample	Sample Size	Mean	Median	Midrange	Variance	S.D.	Range	Maximum	Minimum
1	20	5.1850	5.1700	5.2050	0.0016	0.0398	0.1100	5.2600	5.1500
2	20	5.1895	5.1750	5.1950	0.0018	0.0427	0.1300	5.2600	5.1300
3	20	5.1825	5.1700	5.2050	0.0013	0.0355	0.1100	5.2600	5.1500
4	20	5.1890	5.1700	5.1950	0.0022	0.0470	0.1300	5.2600	5.1300
5	20	5.1760	5.1650	5.1950	0.0015	0.0390	0.1300	5.2600	5.1300
Overall	20	5.1844	5.1700	5.1990	0.0017	0.0408	0.1220	5.2600	5.1300

Figure 2. Summary analysis

The arithmetic mean "represents the best estimator of the central position of the distribution of measured values" [18] and "measures the stability over time of the process adjustment, and the amplitude measures the stability of the accuracy over time of the manufacturing process" [14].

For each quality control problem the module predefines a set of 14 rules (fig. 3), which can be modified using the *Edit* menu options:

Number	Rule Description
1	Single Point Above UCL
2	Single Point Below LCL
3	2 of 3 Points Above 2 Sigma
4	2 of 3 Points Below 2 Sigma
5	4 of 5 Points Above 1 Sigma
6	4 of 5 Points Below 1 Sigma
7	8 Points in a Row Above CL
8	8 Points in a Row Below CL
9	8 Points in a Row Above Median
10	8 Points in a Row Below Median
11	8 Points in a Row Up
12	8 Points in a Row Down
13	Single Point Jumps Up 2 Sigma
14	Single Point Jumps Down 2 Sigma
15	Rule 15

Figure 3. The 14 rules offered by the WinQSB program

The analysis is continued with the "elaboration of representative diagrams, available in the Gallery menu, first of all the control sheets for data obtained" by measurement "which can be of several types:
- control sheets for averages/mean (X-bar (Mean) Chart – fig. 4);
- amplitude control sheets (R chart – fig. 12);
- control sheets for standard deviation of the sample "[6].

The average of these subgroups is under control, due to the fact that it does not violate any of the 14 rules presented in figure 3.

Figure 4. X-bar (Mean) Chart

In fig. 5 are presented the results provided by XLSTAT in tabular form, in fig. 6, in graphical form, as well as the descriptive statistical parameters (fig. 7).

Time\Subgroup	1	2	3	4	5
10.00	5,160	5,170	5,160	5,178	5,170
12.00	5,160	5,160	5,172	5,212	5,180
14.00	5,178	5,188	5,190	5,164	5,172
16.00	5,238	5,238	5,208	5,202	5,182

Subgroup\Time	10.00	12.00	14.00	16.00
1	5,160	5,160	5,178	5,238
2	5,170	5,160	5,188	5,238
3	5,160	5,172	5,190	5,208
4	5,178	5,212	5,164	5,202
5	5,170	5,180	5,172	5,182

Figure 5. Mean by time factor and subgroup factor,
respectively by the subgroup factor
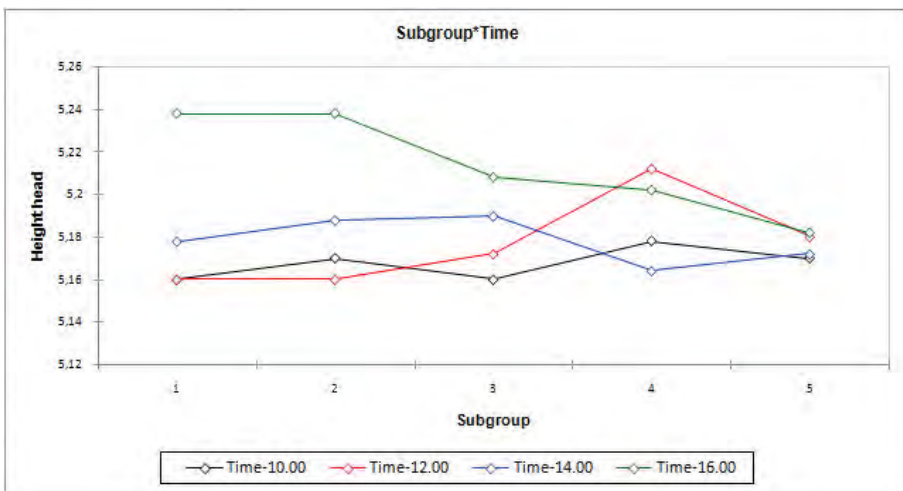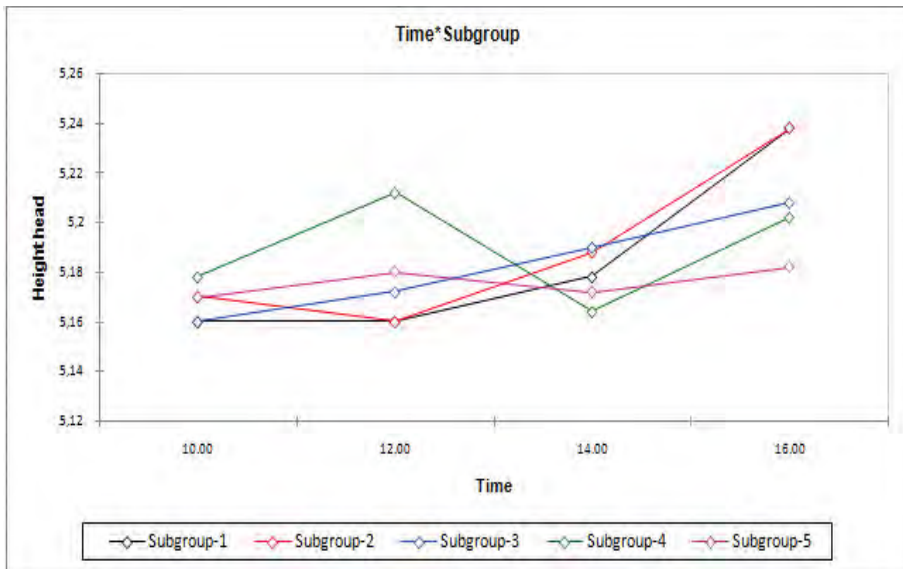
Figure 6. Graphic representation of the average/mean the time factor, rspectively by the subgroup factor

Statistiques descriptives (Données quantitatives) :

Statistique	Height head
Nb. d'observations	100
Minimum	5,130
Maximum	5,260
1er Quartile	5,150
Médiane	5,170
3ème Quartile	5,205
Moyenne	5,184
Variance (n-1)	0,002
Ecart-type (n-1)	0,041
Asymétrie (Pearson)	0,774
Asymétrie (Fisher)	0,786
Aplatissement (Pearson)	-0,734
Aplatissement (Fisher)	-0,709

Figure 7. Descriptive Statistics

The average estimated by the time factor is presented in matrix and graph form in fig. 8, and by the subgroup factor in fig. 9.

Modalité	Moyenne estimées	Erreur standard	Borne inférieure (95%)	Borne supérieure (95%)
10.00	5,168	0,007	5,153	5,182
12.00	5,177	0,007	5,162	5,192
14.00	5,176	0,008	5,161	5,191
16.00	5,214	0,007	5,199	5,228
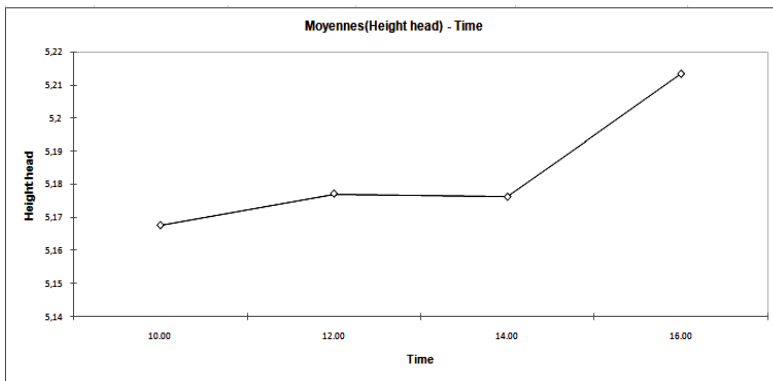
Figure 8. Estimated average by time factor

Modalité	Moyenne estimées	Erreur standard	Borne inférieure (95%)	Borne supérieure (95%)
1	5,184	0,008	5,167	5,201
2	5,190	0,008	5,173	5,206
3	5,183	0,008	5,166	5,199
4	5,189	0,008	5,172	5,206
5	5,173	0,009	5,156	5,190
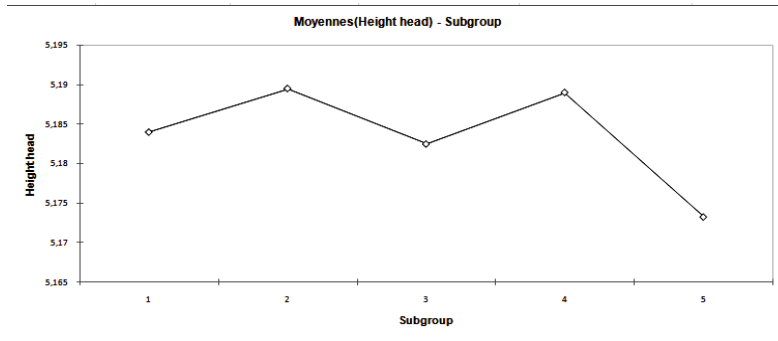
Figure 9. Estimated average by the subgroup factor

The CUSUM Chart for average diagram represents the dispersion of the average values from the central average value and has the role of highlighting the smallest deviations of the manufacturing processes. It is followed if from this point of view the values fall within normal limits, and in this case, due to the fact that all points are represented in green (fig.10), it results that there are no uncontrolled values, as in the case of the sheet control for environments (fig. 4).

It can be stated that "the CUSUM diagram is a" zoom "given to our process in order to better understand and observe its unnatural behaviors and to react in time to avoid waste from production" [5].
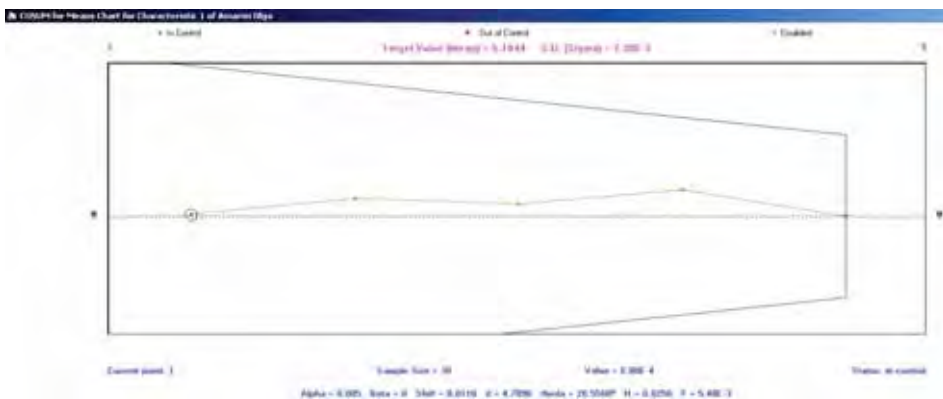
Figure 10. CUSUM for Mean Chart

In order to be able to follow "the evolution of a quality characteristic on which a single measurement is performed at a given time interval" [10], the X chart is used for individual values (fig.11).
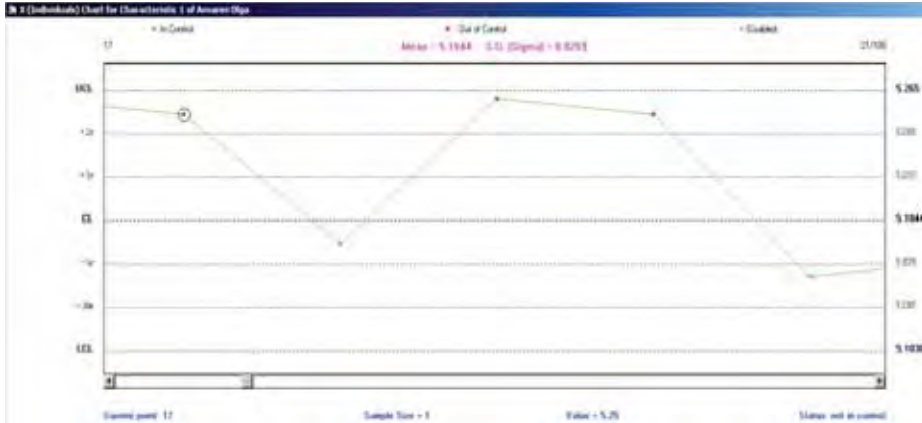
Figure 11. X (Individuals) Chart for points 17÷21

In Figure 11 it can be seen that points 17, 19 and 20 are out of control. But there are other parts out of control, and this can be seen in fig. 12.

The parts 8÷13, from 08.06.2020, ie the last three parts measured at 12 o'clock, as well as the first three, from 14 o'clock, violated rule 8 from the list of the 14 offered by the program. This is 8 Points in a Row Below CL, and this may be due to the following causes:
- incorrect adjustment of the machine;
- replacement of operators on machines;
- fatigue or inattention of operators when performing measurements.

Rule 3, namely: 2 of 3 Points Above 2 Sigma is violated by parts 17, 19, 20, (measurements also performed on 08.06.2020, but at 16 o'clock), 38÷40 (09.06.2020, 16 o'clock), 58 (10.06.2020, 4 pm), 66÷68 (11.06.2020, 12 noon), 78 (11.06.2020, 4 pm) and 98 (12.06.2020, 4 pm), and parts 19, 20, 40 and 68 also violates rule 5, ie 4 of 5 Points Above 1 Sigma.

Single Point Jumps Down 2 Sigma - rule 14 violated by marks 79 (11.06.2020, 4 pm) and 99 (12.06.2020, 4 pm), and this may be due to the following causes:
- power failure
- tool breakage
- interruption of the supply of raw material
- calculation error etc.

12

	00.97.00		07-20-2021		00.07.00		07-20-2021
Sample	Value	Status	Rule Violation	Sample	Value	Status	Rule Violation
1	5.1700	In control	No rule violated	26	5.1900	In control	No rule violated
2	5.1500	In control	No rule violated	27	5.1700	In control	No rule violated
3	5.1600	In control	No rule violated	28	5.1500	In control	No rule violated
4	5.1700	In control	No rule violated	29	5.1600	In control	No rule violated
5	5.1500	In control	No rule violated	30	5.1400	In control	No rule violated
6	5.1500	In control	No rule violated	31	5.1300	In control	No rule violated
7	5.1700	In control	No rule violated	32	5.1900	In control	No rule violated
8	5.1500	Not in control	8	33	5.1900	In control	No rule violated
9	5.1600	Not in control	8	34	5.2600	In control	No rule violated
10	5.1700	Not in control	8	35	5.1700	In control	No rule violated
11	5.1700	Not in control	8	36	5.1700	In control	No rule violated
12	5.1500	Not in control	8	37	5.2600	In control	No rule violated
13	5.1700	Not in control	8	38	5.2500	Not in control	3
14	5.2000	In control	No rule violated	39	5.2600	Not in control	3
15	5.2200	In control	No rule violated	40	5.2500	Not in control	3 5
16	5.2600	In control	No rule violated	41	5.1700	In control	No rule violated
17	5.2500	Not in control	3	42	5.1500	In control	No rule violated
18	5.1700	In control	No rule violated	43	5.1600	In control	No rule violated
19	5.2600	Not in control	3 5	44	5.1500	In control	No rule violated
20	5.2500	Not in control	3 5	45	5.1700	In control	No rule violated
21	5.1500	In control	No rule violated	46	5.1900	In control	No rule violated
22	5.1600	In control	No rule violated	47	5.1900	In control	No rule violated
23	5.1800	In control	No rule violated	48	5.1700	In control	No rule violated
24	5.1700	In control	No rule violated	49	5.1500	In control	No rule violated
25	5.1500	In control	No rule violated	50	5.1600	In control	No rule violated

	00.97.00		07-20-2021		00.07.00		07-20-2021
Sample	Value	Status	Rule Violation	Sample	Value	Status	Rule Violation
51	5.1500	In control	No rule violated	75	5.1900	In control	No rule violated
52	5.1600	In control	No rule violated	76	5.2300	In control	No rule violated
53	5.2600	In control	No rule violated	77	5.2600	In control	No rule violated
54	5.1900	In control	No rule violated	78	5.2500	Not in control	3
55	5.1900	In control	No rule violated	79	5.1400	Not in control	14
56	5.1600	In control	No rule violated	80	5.1300	In control	No rule violated
57	5.2600	In control	No rule violated	81	5.1700	In control	No rule violated
58	5.2500	Not in control	3	82	5.2200	In control	No rule violated
59	5.2000	In control	No rule violated	83	5.1500	In control	No rule violated
60	5.1700	In control	No rule violated	84	5.1600	In control	No rule violated
61	5.1500	In control	No rule violated	85	5.1500	In control	No rule violated
62	5.1600	In control	No rule violated	86	5.2200	In control	No rule violated
63	5.1700	In control	No rule violated	87	5.1700	In control	No rule violated
64	5.1700	In control	No rule violated	88	5.1700	In control	No rule violated
65	5.2400	In control	No rule violated	89	5.1500	In control	No rule violated
66	5.2400	Not in control	3	90	5.1900	In control	No rule violated
67	5.2600	Not in control	3	91	5.1900	In control	No rule violated
68	5.2500	Not in control	3 5	92	5.1500	In control	No rule violated
69	5.1500	In control	No rule violated	93	5.1600	In control	No rule violated
70	5.1600	In control	No rule violated	94	5.2200	In control	No rule violated
71	5.1800	In control	No rule violated	95	5.1400	In control	No rule violated
72	5.1300	In control	No rule violated	96	5.1300	In control	No rule violated
73	5.1700	In control	No rule violated	97	5.2600	In control	No rule violated
74	5.1900	In control	No rule violated	98	5.2500	Not in control	3
75	5.1900	In control	No rule violated	99	5.1400	Not in control	14
				100	5.1300	In control	No rule violated

Figure 12. Matrix results

We move on to the verification of the inclusion in the accepted minimum and maximum limits of the average values on subgroups, ie R (Range) chart – figure 13.

Figure 13. R (Range) chart

Figure 14 shows the CUSUM for range chart. According to R chart and CUSUM for range chart, all subgroups fall within the required limits.
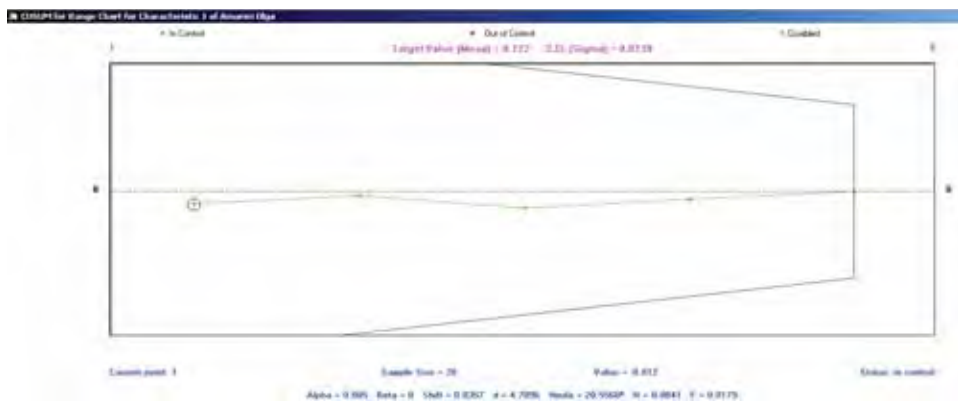
Figure 14. CUSUM for Range Chart

4. Conclusion

The average of the subgroups is under control, due to the fact that it does not violate any of the 14 rules predefined by the WinQSB program module. Also, the CUSUM Chart for Mean diagram, which represents the dispersion of the average values from the central average value and has the role of highlighting the smallest deviations of the manufacturing processes, shows that there are no uncontrolled values, as in the case of the control for environments. The verification of the inclusion in the

accepted minimum and maximum limits of the average values by subgroups led to the same conclusion, namely that all subgroups fall within the required limits.

Regarding the X diagram for individual values, it is observed that out of the 100 parts that are the subject of this study, 20 violate one or even two rules (tests) offered by the program. Most of the measured parts that violate these rules are from the samples at 12 o'clock, namely parts, after the lunch break or at 4 o'clock (11 parts), before the end of the activity on that day.

References

[1] Alexandru A., Ion R., Stanciu A., *Reprezentarea grafică a seriilor de date statistice ca formă de manifestare a „calității" în sistemele de producție, Revista Română de Informatică și Automatică*, 8(1), 1998, pp. 27-33.

[2] Amariei O.-I., *Contribuții privind modelarea, simularea și optimizarea fluxurilor de producție utilizând programe dedicate,* Editura Politehnica Timișoara, Teze de doctorat ale UPT, 8 (62), 2014.

[3] Amariei O.-I., *Aplicații ale programului WinQSB în simularea proceselor de producție,* Editura Eftimie Murgu Reșița, 2009.

[4] Amariei O.-I., Frunzăverde D., Popovici Gh., Hamat C.-O., *WinQSB simulation software – a tool for professional development,* World Conference on Educational Sciences, Nicosia, North Cyprus, 4-7 February 2009, pp 2786-2790.

[5] Amariței (Bogdan) D., *Contribuții privind îmbunătățirea proceselor mecanice pe baza controlului statistic, Universitatea Tehnică "Gheorghe Asachi" din Iași, Facultatea de Construcții de Mașini și Management Industrial*, Teză de doctorat, 2014, http://www.tuiasi.ro/uploads/files/Rezumat_Amaritei_Daniela.pdf (downloaded at August 04rd, 2021).

[6] Axinte E., *Elements of quality insurance in industrial engineering*, Demiurg Editorial House, Iași, 2007.

[7] Bărbulescu C., *Managementul producției industriale. Vol. 2*, Editura Sylvi, București, 2000.

[8] Boboc C., *Analiză statistică multidimensională. Aplicații în cadrul studiului produselor și serviciilor*, Editura Meteor Press, București, 2007.

[9] Hamat C.-O., Amariei O.-I, Dumitrescu C.D., *Analysis of the Quality Control problems using the WinQSB Software Product,* The 19th International DAAAM Symposium, 22-25 Oct. 2008, Trnava, Slovakia, pp. 583-584.

[10] Isaic-Maniu A., Vodă V.Gh., *Abordarea Șase Sigma. Interpretări, controverse, proceduri*, Editura Economică, București, 2008.

[11] Isaic-Maniu A., Vodă V.Gh., *Proiectarea statistică a experimentelor. Fundamente și studii de caz*, Editura Economică, București, 2006.

[12] Mihalca, R; Fabian, C., *The use of the software products - Word, Excel, PMT, WinQSB, Systat*, ASE Publishing House, Bucharest, 2003.

[13] Olaru M., *Tehnici şi instrumente utilizate în managementul calităţii*, Editura Economică, Bucureşti, 2000.
[14] Olaru M., *Quality Management*, ASE Publishing House, Bucharest, 1999.
[15] Petrescu E., Vodă V.Gh., *Fişe de control de proces. Teorie şi studii de caz*, Ed. Economică, Bucureşti, 2002.
[16] Rusu C., *Bazele managementului calităţii*, Editura Dacia, Cluj–Napoca, 2002
[17] Toma C.*,* Capitolul IV. Metode statistice pentru controlul calităţii și fiabilităţii produselor, la https://www.academia.edu/34522960/Capitolul_-IV_METODE_STATISTICE_PENTRU_CONTROLUL_CALIT%C4%82%C5%A2II_%C5%9EI_FIABILIT%C4%82%C5%A2II_PRODUSELOR (downloaded at August 08rd, 2021).
[18] Tovissi L., Vodă V.Gh., *Metode statistice. Aplicaţii în producţie*, Ed. Ştiinţifică și Enciclopedică, Bucureşti, 1982.
[19] http://mpt.upt.ro › cursuri ›IMC›Curs_IMC_Pugna, Pugna A., *Ingineria şi managementul calităţii*, curs, 2017 (downloaded at July 18rd, 2021).
[20] Wheeler, D.J., Shewhart, Deming and Six Sigma, in „W. Edwards Deming 2007 Fall Conference", http://www.spcpress.com/pdf/DJW187.pdf (downloaded at August 08rd, 2021).

Addresses:

- Lect. Dr. Eng. Olga-Ioana Amariei, Babeș-Bolyai University, Faculty of Engineering, Piaţa Traian Vuia, nr. 1-4, 320085, Reşiţa, Romania
  olga.amariei@ubbcluj.ro
- Prof. Dr. Eng. Codruţa-Oana Hamat, Babeș-Bolyai University, Faculty of Engineering, Piaţa Traian Vuia, nr. 1-4, 320085, Reşiţa, Romania
  codruta.hamat@ubbcluj.ro
  (*corresponding author)
- Eng. Alexandru-Victor Amariei, Desengpro SRL, str. Fântînilor, nr. 1, Reşiţa, Romania
  desengpro@yahoo.com

Dimensionless wave numbers evolution of a three spans simply supported beam when the intermediate supports are moving along the whole beam

Zeno-Iosif Praisach[*], Dorel Ardeljan, Constantin-Viorel Pașcu

Abstract. *Continuous beams simply supported with several intermediate supports are very common in engineering achievements everywhere. The paper shows the evolution of the dimensionless wave number in 3D format, respectively of the eigenfrequencies for a continuous beam with three openings when the intermediate supports take any position inside the beam. The frequency equation for calculating the dimensionless wave number is presented and the modal function is given with an example for the case where the eigenfrequency has the maximum value at fist vibration mode.*

Keywords*: natural frequency, dimensionless wave number, mode shape*

1. Introduction

Beams that have more than one span and there are continuous throughout their lengths are known as continuous beams. A continuous beam is a statically indeterminate multispan beam on hinged supports.

There are several methods to analyze the dynamic behavior of continuous beams, such as: transfer-matrix technique [1], wave-propagation approach, Rayleigh-Ritz procedure, iterative procedure, conventional method of solving the equation of motion directly, the finite element method.

Continuous structures such as beams, can be modeled by discrete mass and stiffness parameters and analyzed as multi-degree of freedom systems [3, 4]. For these types of structures, it is necessary to assume homogeneous and isotropic material that follows Hooke's law [2, 6].

For a continuous beam of constant section, the natural frequency (1) for each vibration mode can be determined if the dimensionless wave number is known.

$$f_n = \frac{a_n^2}{2\pi} \sqrt{\frac{E \cdot I}{m \cdot L^4}} \tag{1}$$

where,

f_n [Hz] is the natural frequency;

a_n - dimensionless wave number;
E [N/m^2] – Young's modulus;
I [m^4] - moment of inertia;
m [kg] – beam mass;
$L = l_1 + l_2 + l_3$ [m] – beam length;
$n = 1, 2, …, \infty$ – number of vibration mode.

The dimensionless wave number is important both for calculating the natural frequencies and for the relationship of the mode shapes for each vibration mode. The precision of evaluating the natural frequencies is crucial, because small structural changes lead to reduced modal parameter changes [10].

2. Boundary conditions and frequency equation

In this paper it is considered a continuous beam supported at 4 (four) hinges, that means three spans (fig. 1). It is known that the deflection and the bending moment is zero for the end hinges. Since the beam is continuous, the slope and bending moment to the left and to the right of the intermediate supports are the same. Also, the deflection is zero for the intermediate supports [7, 8, 9].
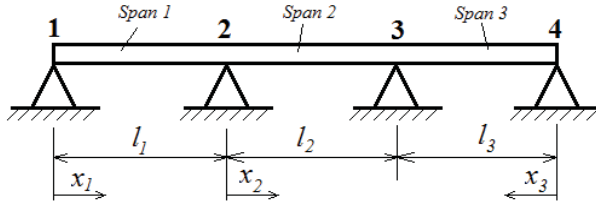
Figure 1. Continuous beam with three spans

Based on the above statements, for each support (1, 2, 3, 4), it can be written:

$$
\text{1.}\begin{cases} W_1(0)=0 \\ \dfrac{d^2 W_1(0)}{dx^2}=0 \end{cases}
\qquad
\text{3.}\begin{cases} W_2(l_2)=0 \\ W_3(l_3)=0 \\ \dfrac{dW_2(l_2)}{dx}=-\dfrac{dW_3(l_3)}{dx} \\ \dfrac{d^2 W_2(l_2)}{dx^2}=\dfrac{d^2 W_3(l_3)}{dx^2} \end{cases}
$$

$$
\text{2.}\begin{cases} W_1(l_1)=0 \\ W_2(0)=0 \\ \dfrac{dW_1(l_1)}{dx}=\dfrac{dW_2(0)}{dx} \\ \dfrac{d^2 W_1(l_1)}{dx^2}=\dfrac{d^2 W_2(0)}{dx^2} \end{cases}
\qquad
\text{4.}\begin{cases} W_3(0)=0 \\ \dfrac{d^2 W_3(0)}{dx^2}=0 \end{cases}
$$

(2)

where, the characteristic function or normal mode of span can be expressed:

$$W_i(x_i) = A_i \sin(a_n x_i) + B_i \cos(a_n x_i) + C_i \sinh(a_n x_i) + D_i \cosh(a_n x_i) \tag{3}$$

with $i = 1, 2, 3$ represents the number of spans.

After solving the system of equations (2) for calculating the integration coefficients: A_i, B_i, C_i, D_i by using the following notation (4) for the terms with constant value for a certain configuration of the continuous beam between two consecutive supports:

$$(1-2) \begin{cases} Z_{11} = \cos(a_n l_1) - \dfrac{\sin(a_n l_1)}{\sinh(a_n l_1)} \cosh(a_n l_1) \\ Z_{12} = 2\sin(a_n l_1) \end{cases}$$

$$(2-3) \begin{cases} Z_{21} = 1 - \cos(a_n l_2)\cosh(a_n l_2) \\ Z_{22} = \cos(a_n l_2)\sinh(a_n l_2) - \sin(a_n l_2)\cosh(a_n l_2) \\ Z_{23} = 2\sin(a_n l_2)\sinh(a_n l_2) \end{cases} \tag{4}$$

$$(3-4) \begin{cases} Z_{31} = \cos(a_n l_3) - \dfrac{\sin(a_n l_3)}{\sinh(a_n l_3)} \cosh(a_n l_3) \\ Z_{32} = 2\sin(a_n l_3) \end{cases}$$

the frequency equation of the system (2), which allows us to obtain the dimensionless wave number a_n, for a continuous beam with three spans, becomes:

$$(Z_{12} \cdot Z_{21} + Z_{11} \cdot Z_{22}) \cdot Z_{32} + (Z_{12} \cdot Z_{22} + Z_{11} \cdot Z_{23}) \cdot Z_{31} = 0 \tag{5}$$

The solutions of equation (5) represent the dimensionless wave numbers for the n vibration modes with which we can calculate the natural frequencies (1) and also, we can plot the normalized mode shapes (3) for the continuous beam with three spans.

3. Mode shape equation and integration constants

The normalized mode shape equation for the continuous beam with three spans are obtained by solving the system (2) with the results replaced in (3).

Thus, for each span, the functions result:

$$h\begin{cases} W_1(x_1) = A_1\left[\sin(a_n x_1) - \dfrac{\sin(a_n l_1)}{\sinh(a_n l_1)}\sinh(a_n x_1)\right] \\ W_2(x_2) = A_2\sin(a_n x_2) + B_2\left[\cos(a_n x_2) - \cosh(a_n x_2)\right] + C_2\sinh(a_n x_2) \quad (6) \\ W_3(x_3) = A_3\left[\sin(a_n x_3) - \dfrac{\sin(a_n l_3)}{\sinh(a_n l_3)}\sinh(a_n x_3)\right] \end{cases}$$

with $x_1 \in \left[0,\ l_1\right]$, $x_2 \in \left[0,\ l_2\right]$, $x_3 \in \left[0,\ l_3\right]$.

The integration constants from (6) are:

$$\begin{cases} A_2 = -\dfrac{A_1}{\sin(a_n l_2) - \sinh(a_n l_2)}\left[Z_{12}\dfrac{\cos(a_n l_2) - \cosh(a_n l_2)}{2} + Z_{11}\sinh(a_n l_2)\right] \\ B_2 = A_1\dfrac{Z_{12}}{2} \\ C_2 = A_1 \cdot Z_{11} - A_2 \\ A_3 = -\dfrac{A_1}{\sin(a_n l_2) - \sinh(a_n l_2)} \cdot \dfrac{Z_{12}\cdot Z_{21} + Z_{11}\cdot Z_{22}}{Z_{32}} \end{cases} \qquad (7)$$

and the constant A_1 has the value so that the mode shape function (6) to be normalized by the entire length of the continuous beam for each vibration mode separately.

Dimensionless wave numbers evolution when the intermediate supports are moving along the whole beam

We will take into account the fact that the intermediate supports (fig. 1) can be in any position along the normalized continuous beam ($l_1 + l_2 + l_3 = 1$, or $l_3 = 1 - l_1 - l_2$). This means that, for each location of the intermediate supports, from relation (5), values of the dimensionless wave number are obtained for each vibration mode.

By plotting all the obtained values of the dimensionless wave number in a 3D diagram, for each vibration mode separately, we obtain a surface that gives us a general image on the evolution of the wave number depending on the position that the intermediate supports can have.

Figures 2 - 7 show the evolution of the dimensionless wave number for the first six vibration modes ($n = 6$) for the normalized continuous beam with three spans.
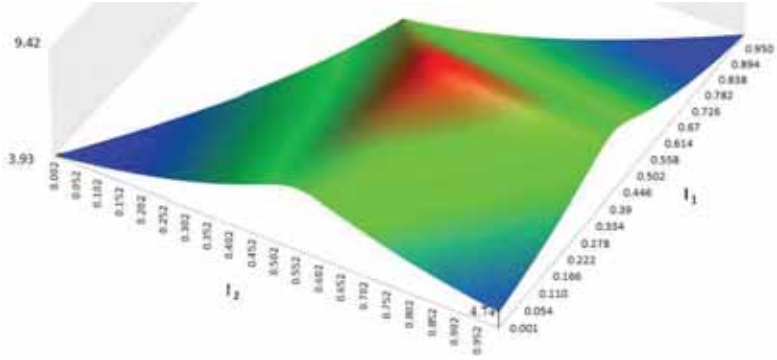
Figure 2. Dimensionless wave number evolution for the 1st vibration mode.
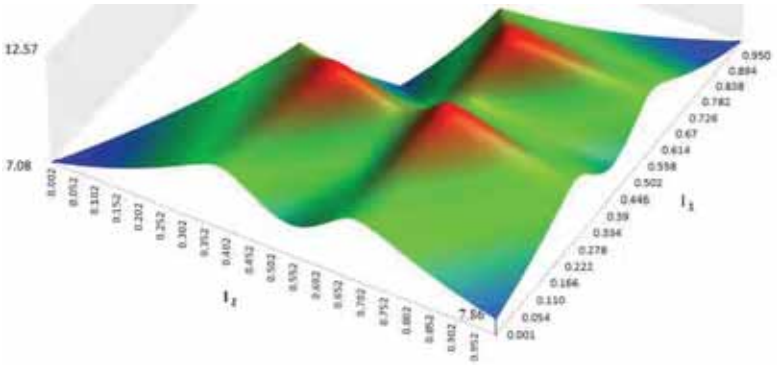
Figure 3. Dimensionless wave number evolution for the 2nd vibration mode.
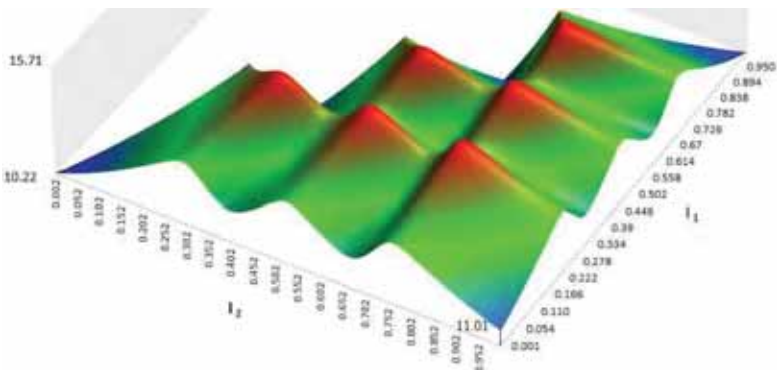
Figure 4. Dimensionless wave number evolution for the 3rd vibration mode.

21
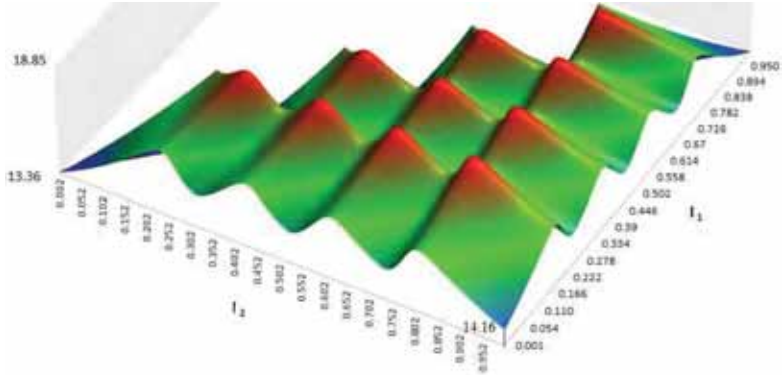
Figure 5. Dimensionless wave number evolution for the 4th vibration mode.
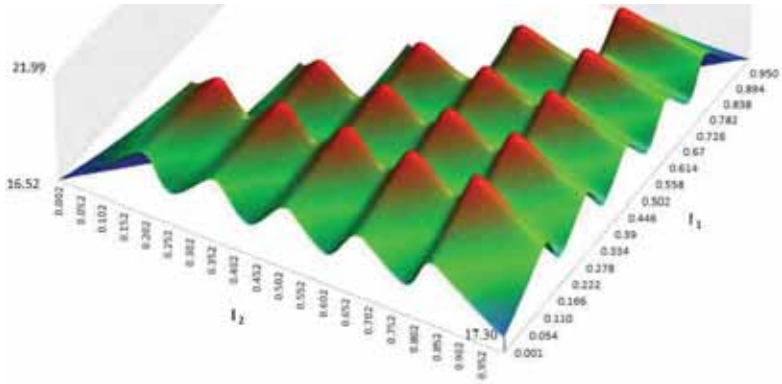
Figure 6. Dimensionless wave number evolution for the 5th vibration mode.
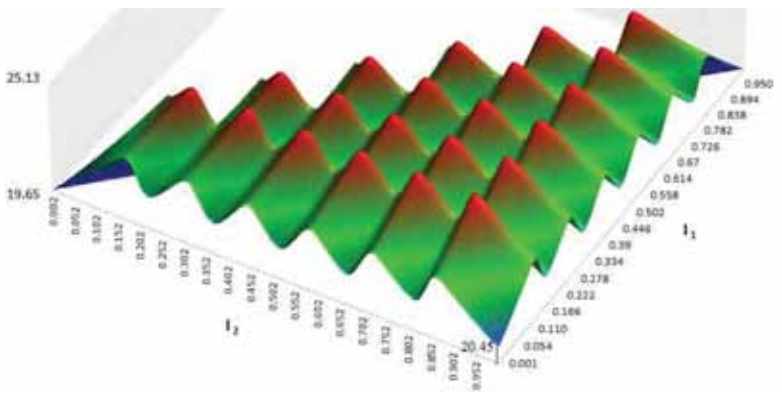
Figure 7. Dimensionless wave number evolution for the 6th vibration mode.

4. Conclusion

By analyzing figures 2 - 7, the following conclusions can be drawn:

1. for first vibration mode, the maximum dimensionless wave number is obtained when the intermediate supports are placed equidistantly (fig. 8), $l_1 = l_2 = l_3$. Taking into account the relation (1), for this configuration of the continuous beam we also have the maximum eigenfrequency;

2. when $l_1 \rightarrow 0$ and $l_2 \rightarrow 0$, the continuous beam behaves like a beam clamped at the left end and hinged at the right end;

3. when $l_1 \rightarrow 1$ and $l_2 \rightarrow 1$, the continuous beam behaves like a beam hinged at the left end and clamped at the right end;

4. when $l_1 \rightarrow 0$ and $l_2 \rightarrow 1$, the continuous beam behaves like a beam clamped at the both ends;

Knowing the analytical expression of the modal function, it is easy to obtained the mode shape curvature function, on which depends the establishment of the location of a damage on the beam [5], in case of its appearance.
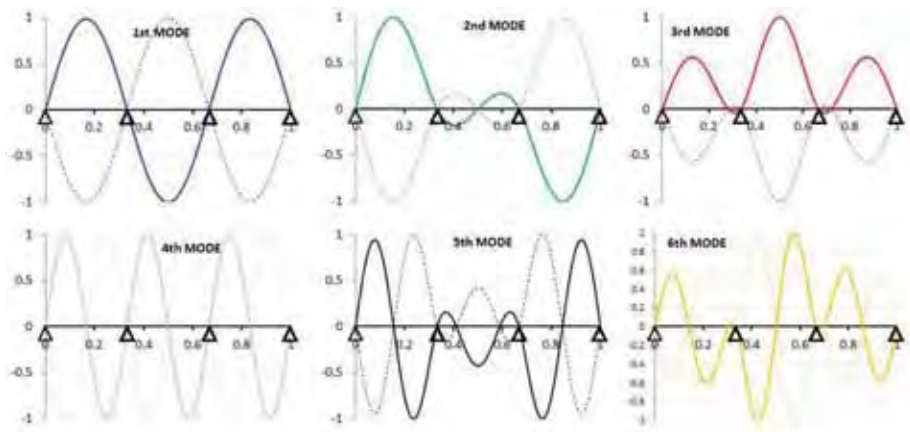
Figure 8. Continuous beam with intermediate supports placed equidistantly – the first six normalized mode shapes.

References

[1] Sule S., Nwofor T.C., Application of Matrix Iteration for Determining the Fundamental Frequency of Vibration of a Continuous Beam, *International Journal of Engineering Reearch and Development*, Vol. a(12), 2012, pp. 30-36.

[2] Ebrahimi F., *Advances in Vibration Analysis Research*, Published by InTech, Croatia, 2011.

[3] Khodabakhsh S., Rama B.B., Clustered Natural Frequencies in Multi-Span Beams with Constrained Characteristic Functions, *Shock and Vibration,* 18(5), 2011, pp. 697-707.

[4] Ichikawa M., Miyakawa Y., Matsuda A., Vibration analysis of the continuous beam subjected to a moving mass, *Journal of Sound and Vibration* 230(3), 2000, pp. 493-506.

[5] Gillich G.R., Praisach Z.I., Modal identification and damage detection in beam-like structures using the power spectrum and time-frequency analysis, *Signal Processing,* 96, Special Issue: SI, Part: A, 2014, pp. 29-44.

[6] Mead D.J., Yaman Y., The harmonic response of uniform beams on multiple linear supports: A flexural wave analysis, *Journal of Sound and Vibration*, 141(3), 1990, pp. 465–484.

[7] Ntakpe J.L., Praisach Z.I, Mituletu C.I., Gillich G.R., Muntean F., Natural frequency changes of two-span beams due to transverse cracks, *Journal of Vibration Engineering & Technologies,* 5(3), 2017, pp. 229-238.

[8] Gillich G.R., Ntakpe J.L., Wahab M.A., Praisach Z.I., Mimis M.C., Damage detection in multi-span beams based on the analysis of frequency changes *Journal of Physics: Conference* Series 842 (1), 2017, 012033.

[9] Gillich G.R., Praisach Z.I., Hamat C., Gillich N., Ntakpe J.L., Crack localization in L-shaped frames, *Acoustics and Vibration of Mechanical Structures - AVMS-2017*, 2018, pp. 315-322.

[10] Ntakpe J.L., Gillich G.R., Mituletu I.C., Praisach Z.I., Gillich N., An Accurate Frequency Estimation Algorithm with Application in Modal Analysis. *Romanian Journal of Acoustics & Vibration*, 13(2), 2016, pp. 98-103.

Addresses:

- Lect. Dr. Eng. Habil. Zeno-Iosif Praisach, Babeș-Bolyai University, Faculty of Engineering, Piața Traian Vuia, nr. 1-4, 320085, Reşiţa, Romania zeno.praisach@ubbcluj.ro
  ([*]corresponding author)

- PhD. Stud. Dorel Ardeljan, Babeș-Bolyai University, Faculty of Engineering, Piața Traian Vuia, nr. 1-4, 320085, Reşiţa, Romania dorel.ardeljan@ubbcluj.ro

- PhD. Stud. Constantin-Viorel Pașcu, Babeș-Bolyai University, Faculty of Engineering, Piața Traian Vuia, nr. 1-4, 320085, Reşiţa, Romania constantin.pascu@ubbcluj.ro

An assessment of physical properties and water holding capacity of soil under different fertilizer applications

Adeniyi Afolabi Rodiya[*], Dauda Aluyah Okodugha,
Emmanuel Aleonolu Adoga, Samuel Olaiya, Michael Okafor

Abstract. *This study was carried out at the Teaching and Research Farm of the Department of Agricultural and Bio-Environmental Engineering, School of Engineering, The Federal Polytechnic, Ado-Ekiti to evaluate the water holding capacities of soil under different fertilizers. The experiment was laid out in randomized complete block design (RCBD). The treatments: control, poultry waste, biochar and urea fertilizer replicated four times were incorporated into the soil and maize seed planted. Data collected were subjected to statistical analysis. Soil samples were analyzed for moisture contents, bulk densities, particle densities and water holding capacities. Maize yield was also analyzed. The result obtained showed a significant (p< 0.05) changes in maize yield for the different fertilizers. It also shows a non-significant (p<0.05) effect on water holding capacities of the soils incorporated with different fertilizers. The study concluded that fertilizers has no effect on the water holding capacity of the soil and that poultry waste amended soil will produce higher yield.*

Keywords*: water holding capacity, biochar, poultry waste, urea fertilizer*

1. Introduction

Water holding capacity designates the ability of a soil to hold water. It is useful information for irrigation scheduling, crop selection, groundwater contamination considerations, estimating runoff and determining when plants will become stressed [1, 2, 3]. Understanding some physical characteristics of the soil is useful to determine the strengths and weaknesses of different soil types. Soil moisture limits forage production potential the mostly in semiarid regions [4, 5, 6]. Estimated water use efficiency for irrigated and dry-land crop production systems is 50 percent, and available soil water has a large impact on management decisions producers make throughout the year (Hatfield and Dold, 2019) Fertilizers are mainly applied in form of farmyard manure and crop residues. Nevertheless, a study on soil fertility management on smallholder farms in western Kenya [7, 8, 9] showed that many of the farmers are using fertilizers but the application rates are low and differ between farm types.

Within that study, the farm types were classified by wealth; production orientation (self-consumption or market-oriented); constraints to land, labor and capital; family structure and main source of income. Mineral fertilizers are mainly applied as di ammonium phosphate and calcium ammonium nitrate and urea for top dressing. Small sized farms are less self-sufficient in food production and relay more on off-farm jobs, but dispose over a higher capital for mineral fertilizer purchase (Tisdale *et al.,* 1997).

However, decreasing soil fertility, the parasitic weed Striga spp is a major problem for agricultural productivity in SSA [10, 11]. Maize, which is one of the most important food crops in rural areas of Nigeria is greatly affected by this weed. Due to the land pressure and intensification of agricultural practices, the fallow periods tend to be shorter and the diversity of the crops lower (Mertz, 2002). This and the decline in soil fertility create an ideal environment for Striga and other weeds. Farmers have little knowledge about Striga control [12, 13]. Soil moisture available for plant growth makes up approximately 0.01 percent of the world's stored water [14]. Soil texture and structure greatly influence water infiltration, permeability, and water-holding capacity [15].

Soil texture refers to the composition of the soil in terms of the proportion of small, medium, and large particles (clay, silt, and sand, respectively) in a specific soil mass [16]. For example, a coarse soil is sand or loamy sand, a medium soil is a loam, silt loam, or silt, and a fine soil is a sandy clay, silt clay, or clay. Water holding capacity varies by soil texture. Permeability refers to the movement of air and water through the soil, which is important because it affects the supply of root-zone air, moisture, and nutrients available for plant uptake. A soil's permeability is determined by the relative rate of moisture and air movement through the most restrictive layer within the upper 40 inches of the effective root zone. Water-holding capacity is controlled primarily by soil texture and organic matter. Soils with smaller particles (silt and clay) have a larger surface area than those with larger sand particles, and a large surface area allows a soil to hold more water.

2. Materials and Methods

2.1. Site description

The experiment was carried out at the Teaching and Research Farm of the Department of Agricultural and Bio Environmental Engineering, School of Engineering, The Federal Polytechnic, Ado-Ekiti, Ekiti State. The area lies on longitude 5° 13' 17.0004'' E and latitude 7° 37' 15.9996'' N in the derived tropical rainfall of southwestern Nigeria [14]. The climate of the area is classified as tropical. The average annual temperature of the area is 25.1^oC and rainfall average is 1334 mm. The relative humidity of the area is between 60 – 80% [15]. The major materials used for the experiment are plastic buckets, (perforated) container of the same size, biochar, urea

fertilizer and poultry waste. The biochar was purchased at Ado-Ekiti market and the urea fertilizer was obtained from Ondo state Agricultural Development Programme (OSADP) Ikare Akoko. The poultry waste was obtained from the poultry farms of the Department of Agricultural and Bio Environmental Engineering and Department of Agricultural Technology, The Federal Polytechnic Ado-Ekiti, Ekiti state. Other materials are Axe, tractor, motor saw, digger, cutlass, and shovel, hoe, and rake for land preparation. Mortal and sieve were used for the preparation of the biochar. Weighing balance, core sampler and mason jar were used to take measurement and the soil bulk density. While soil textural triangle was used to determine the soil structural classes. The water holding capacity was determined using plastic buckets which have been perforated.

2.2. Land preparation

The experimental site measured 19 x19 m (0.0361ha) was on a flat terrain which had been fallow for more than three (3) years. The vegetation on the area (trees and grasses) was removed using Axe, cutlass, hoe, and motor saw. The area was tilled mechanically using plough and harrow. While the marking out (the division into treatment plots) was done using measuring tape and pegs.

2.3. Experimental design

The experiment was laid out in a randomized complete block design (RCBD) with four replications and four treatments. A total at sixteen (16) plots each measured 4 m x 4 m (16 m^2) were used for the experiment, the replicate was 1 m apart. The treatments were control, biochar, urea fertilizer and poultry waste. Treatments were uniformly incorporated to the plots after making the bed using plough and harrow [4, 9, 10]. Few weeks later, the soil samples from those treatment plots was collected at the same quantity and was put into the perforated buckets to determine their water holding capacity and other physical properties.

2.4. Soil sampling

2.4.1. Water holding capacity

A 10 kg soil sample was collected from each of the treatment's plots, 2500 ml of water was added into it and was left for 24 hours. The water that infiltrate into the containers was collected and was turn into measuring cylinder and measured. These were done for four times per treatment plot and the average was estimated.

2.4.2. Bulk density

The soil sample was collected using core sampler and it was measured to be 0.1433 kg/m^3 before taking to the laboratory to determine the volume and the cross-sectional area of the core sampler. It was done for four times per treatment plots.

2.4.3. Moisture content

This method is used to determine the percentage of water in a sample by drying the sample to a constant weight. The water content is expressed as the percentage by weight of the sample as shown in equation (1):

$$\%W = \frac{W_{wet} - W_{dry}}{W_{dry}} \times 100 \tag{1}$$

where: %W - Percentage of moisture in the sample
   Wwet - weight of wet samples in grams (g)
   Wdry - weight of dry sample grams (g)

2.4.4. Yield test

Five cobs were harvested at random from those treatment plots and weighed to determine the yield. This procedure was replicated four time per treatment.

2.4.5. ANOVA

Analysis of Variance (ANOVA) will be used to test for variation in water holding capacity of the soil under different fertilizer application as well as variation in physical properties of the soil (bulk density and particle density).

3. Results and discussion

3.1. Physical properties

Results of the treatment plots based on physical properties are as shown in Tables 1, 2, 3, and 4. Table 5 and 4.6 shows the effect of biochar, poultry waste and urea fertilizer on physical properties of the soil. The results show that the application of fertilizers causes significant difference in the soil's physical properties (moisture content, bulk density, and particle density). The significant value is less than the α value of 0.05. This shows that all the fertilizers incorporated into the soil will change the physical properties of the soil as seen in the multiple comparison test in Table 6. The findings agree with [15].

3.2 Water holding capacity

The effect of those soil on water holding capacity is shown in Tables 7 and 8. The application of biochar, poultry waste, and urea fertilizer has no significant difference in water holding capacity according to the analysis of variance (ANOVA) shown in Table 8.

3.3. Yield

The result of the effect of those treatments on crops planted into that treatment plot is shown in Tables 9 and 10. While Table 9 shows the raw data are collected on yield. Table 10 shows the analysis of variance of yield and 11 shows the multiple

comparisons for yield. The tables show that there is a significant difference between those treatments and maize yield. The plot at which poultry waste and urea fertilizer was added has a highly significant.

Table 1. Control experimentation

Trails	Moisture content (%)	Bulk density (kg/cm^3)	Particle density (kg/cm^3)
Trial1	22.22	0.0018	3.5
Trial 2	16.66	0.0018	5.0
Trial 3	17.88	0.0018	4.6
Trial 4	15.56	0.0018	5.4
Average	18.08	0.0018	4.6

Table 2. Treatment with poultry waste

Trials	Moisture content (%)	Bulk density (kg/cm^3)	Particle density (kg/cm^3)
Trial 1	13.33	0.0018	6.5
Trial 2	15.55	0.0018	5.4
Trial 3	14.44	0.0018	5.9
Trial 4	16.66	0.0018	5.0
Average	15.00	0.0018	5.7

Table 3. Treatment with biochar

Trials	Moisture (%)	Bulk density (kg/cm^3)	Particle density kg/cm^3
Trial 1	20.00	0.0018	4.0
Trial 2	17.77	0.0018	4.6
Trial 3	15.56	0.0018	5.4
Trial 4	17.78	0.0018	4.6
Average	17.78	0.0018	4.7

Table 4. Treatment with Urea

Trials	Moisture %	Bulk density kg/cm^3	Particle density kg/cm^3
Trial 1	14.44	0.0018	5.9
Trial 2	16.66	0.0018	5
Trial 3	18.88	0.0018	4.3
Trial 4	15.55	0.0018	5.4
Average	16.38	0.0018	5.2

Table 5. Variation in Physical Properties

Source	Type III Sum of Squares	Df	Mean Square	F
Corrected Model	595.499a	5	119.1	120.746
Intercept	636.96	1		
Fertilizer	0.816	3		
Physical Properties	594.683	2		
Error	5.918	6		
Total	1238.376	12		
Corrected Total	601.417	11		

a. R Squared = .990 (Adjusted R Squared = .982)

Table 7. Variation in Water Holding Capacity

Trials	Control (ml)	Poultry waste (ml)	Biochar (ml)	Urea(ml)
Trial 1	420	320	450	795
Trial 2	420	253	320	225
Trial 3	210	300	250	200
Trial 4	285	426	350	275
Mean average	334	325	343	374

Table 8. Water holding capacity. Dependent Variable: Observation

Source	Type III Sum of Squares	Df
Corrected Model	9411.687a	3
Intercept	1838058.063	1
Fertilizer	9411.687	3
Error	297739.25	12
Total	2145209	16
Corrected Total	307150.937	15

a. R Squared = .031 (Adjusted R Squared = -.21)

Table 9.

TRIALS	Poultry Waste (kg)	Biochar (kg)	Urea (kg)	Control (kg)
Trial 1	0.40	0.25	0.15	0.25
Trial 2	0.20	0.22	0.15	0.10
Trial 3	0.35	0.24	0.20	0.15
Trial 4	0.25	0.20	0.17	0.10
Mean average	0.30	0.23	0.17	0.15

Table 10. Multiple Comparisons for yield

(I) Fertilizer	(J) Fertilizer	Mean Difference(I-J)	Std. Error	Sig.
Control	Poultry Waste	-.1500*	0.0424	0.004
	Biochar	-0.0775	0.0424	0.093
	Urea	-0.0175	0.0424	0.687
Poultry Waste	Control	.1500*	0.0424	0.004
	Biochar	0.0725	0.0424	0.113
	Urea	.1325*	0.0424	0.009
Biochar	Control	0.0775	0.0424	0.093
	Poultry Waste	-0.0725	0.0424	0.113
	Urea	0.06	0.0424	0.182
Urea	Control	0.0175	0.0424	0.687
	Poultry Waste	-.1325*	0.0424	0.009
	Biochar	-0.06	0.0424	0.182

The error term is Mean Square (Error) = .004.
*. The mean difference is significant at the 0.05 level.

4. Conclusion

It is concluded that the different fertilizers incorporated into the soil has no effect on the water-holding capacity of the soil but have an effect on the physical properties of the soil and yield of maize. According to results obtained from the experiment, farmers are advised to use any fertilizer at any point in time because there is no effect at all on the water holding capacity of the soil. Fertilizers should also be applied to the soil to increase yield and the physical properties of the soil when the need arises.

References

[1] Adediran J.A., Banjoko V.A., Response of maize to N, P, and K fertilizers in the savanna zone of Nigeria, *Commun. Soil Sci. Plant Anal.*, 26, 2012, pp. 593-606.

[2] Adu S.V., *Soils of the Kumasi Region, Ashanti Region, Ghana. Soil Research Institute* (Council for Scientific and Industrial Research). Memoir No. 8, 2014.

[3] Aggarwal P.K., Singh A.K., Chaturvedi G.S., Sinha S.K., Performance of wheat and triticale cultivars in a variable soil-water environment. II. Evapotranspiration, WUE, harvest index and grain yield. *Field Crops Research*, 13, 2009, pp. 301-315.

[4] Akande M.O., Adediran J.A., Oluwatoyinbo F.I., Effects of rock phosphate amended with poultry manure on soil available P and yield of maize and cowpea. *Afr. J. Biotechnol*. 4, 2008, pp.444-448.

[5] Black C.A., *Soil-Plant Relationships*, Department of Agronomy, Iowa State College, Ames, Iowa. Published by John Wiley & Sons, Inc, 1965.

[6] Baanante C.A., Thompson T., Acheampong K., Rhodes E.R., Pouzet D., Opoku S., *Fertilizer use and agricultural development in the Ashanti Region of Ghana. An analysis of farm survey data*, IFDC, Muscle Shoals A1. USA, 2010.

[7] Bationo A., Mokwunye A.U., Role of manures and crop residue in alleviating soil fertility constraints to crop production: With special reference to the Sahelian and Soudanian zones of West Africa, *Fertilizer Research*, 29, 2004, pp. 217-225.

[8] Bergmann W., *Nutritional disorders of plants*. 2nd ed. Gustav Fischer Verlag, Jena, Germany, 2009.

[9] Bray R.H., Kurtz L.T., Determination of total organic and available forms of phosphorus in soil, *Soil Science*, 599, 2011, pp. 39-45.

[10] Boateng, J.K., Oppong J., *Proceedings of Seminar on organic and sedentary agriculture held at the Science and Technology Policy Research Institute (C.S.I.R)* Accra. 1-3 Nov, 1995, p. 85.

[11] Buol S.W., Stokes M.L., Soil profile alteration under long-term high-inputagri-culture. In: R. J. Buresh, P. A. Sanchez and F. Calhoun (eds.): Replenishing soil fertility in Africa. Special Publication No. 51. *Soil Sci. Soc. Am.,* Madison, WI, 1997.

[12] Cleaver K.M., Schreiber G.A., *Reserving the spiral; the population, agriculture and environment nexus in sub-Saharan Africa*, World Bank, Washington, DC, 2008.

[14] Chand S., Anwar M., Patra D.D., Influence of long-term application of organic and inorganic fertilizer to build up soil fertility and nutrient uptake in mint mustard cropping sequence, *Communications in Soil Science and Plant Analysis*, 37, 2006.

[15] Chang C., Sommerfeldt T.G., Entz T., Rates of soil chemical changes with eleven annual applications of cattle feedlot manure, *Can. J. Soil Sci.*, 70, 1990, pp. 673 - 681.

[16] CAST.1996. *Integrated animal waste management. Task Force Report. No. 128.* Council for Agricultural Science and Technology. Ames. Iowa.

Addresses:

- Engr. Adeniyi Afolabi Rodiya, Department of Agricultural & Bio-Environmental Engineering, The Federal Polytechnic, Ado-Ekiti, Nigeria
  afolabrodiya@yahoo.com
  ([*]corresponding author)
- Engr. (Dr.) Daudua Aluyah Okodugha, Department of Civil Engineering, Auchi Polytechnic, Auchi, Edo State, Nigeria
  aluyahd@gmail.com
- Engr. Emmanuel Aleonolu Adoga, Department of Civil Engineering, Auchi Polytechnic, Auchi, Edo State, Nigeria
- Engr. Samuel Olaiya, Department of Civil Engineering, Auchi Polytechnic, Auchi, Edo State, Nigeria
- Engr. Michael Okafor, Department of Civil Engineering, Auchi Polytechnic, Auchi, Edo State, Nigeria

Acoustic emission as a valuable technique used for monitoring polymer failures

Jakub Skoczylas[*], Sylwester Samborski, Mariusz Kłonica

Abstract. *In the paper, acoustic emission (AE) system was presented as a method that can be used to monitor polymer material failures. Samples fabricated of two aluminum profiles bonded together with a thick layer of cured epoxy resin were subjected to fracture tests. Epidian 53 epoxy resin cured with Z1 curing agent as well as Epidian 5 epoxy resin cured with PAC curing agent were selected as adhesives. Acoustic emission parameters were acquired during Double Cantilever Beam (DCB) tests. The frequencies of elastic waves released during failure were then analyzed using both Fast Fourier Transformation (FFT) and Wavelet Transformation (WT) for the two materials.*

Keywords*: acoustic emission, DCB test, epoxy resin, wavelets, Wavelet Transformation*

1. Introduction

Polymers consisting of epoxy resins are nowadays widely used especially as a fiber reinforced polymer (FRP) composites' matrices but also as adhesives and coatings in many branches of contemporary engineering e.g. automotive industry, aerospace industry, marine industry and electronics. Besides their excellent chemical and corrosion resistance, high tolerance to different environmental conditions [1] and adhesive properties [2], epoxy resins are classified as brittle materials with low crack propagation resistance and weak fracture toughness [3]. Thus, it is important to examine the mechanical behavior of these materials as well as to detect failures that may occur just at their origin to prevent further damages.

Acoustic emission (AE) is described as a useful technique applied for health monitoring [4, 5] and failure detection [6–8]. The term "acoustic" seems to be a little bit misleading because human ear is not able to hear the frequencies which are referred to this technique, with a range of 100 kHz – 1 MHz [6]. This method let to classify material defects with relation to appropriate ranges of signal frequencies. The main AE advantage is that it gives the opportunity to indicate damage onset just while the propagation initiates [9, 10] whereas other traditional methods allow to notice material failures until as they are much more advanced. Most commonly occurring material defects can be correlated with specific frequencies of the elastic

waves [5–8, 11–14]. However, the frequency ranges depend on the materials. In addition, various matrices can generate various AE signals while cracking [9] as well as ply geometry and orientation of fibers and matrices can also affect the emission [15]. Thus, it is crucial to deeply analyze the behavior of particular materials before AE can be successfully used for defect recognition and health monitoring.

Typical AE system consists of piezoelectric sensors, preamplifier, A/D card and a PC equipped with a dedicated software [6, 12]. Data registered by AE sensors are hits and counts in classical approach. Today, however the AE systems enable much more sophisticated analysis of the registered elastic waves: not only energy or amplitude of the signal can be derived, but also FFT and wavelet analyses [13, 15]. In order to make it possible to distinguish different types of damage processes based on signal analysis it is essential to categorize the collected signals into clusters. It can be obtained using K-means method [5, 16, 17] based on calculating Euclidean distances.

So far, many AE researches have been already conducted on matrix-fiber effect appearing in various material types. Different defects were classified such as matrix cracking, matrix-fiber debonding, delamination, fiber breakage or fiber pull out and assigned to AE frequencies [5–8, 11–14]. Moreover, some additional examinations were done on fibers separated from matrices to confirm the range of frequency for fiber breakage [13]. It was also proved by AE that higher number of hits was registered in case of samples without self-healing capability than in case of samples with self-healing capability which was caused by constantly matrix repairing [5]. Furthermore, the number of hits can be also correlated with the course of stress-strain curve [13] and in-plane shear modulus [15].

Based on the open literature the different ranges of frequencies of acoustic waves emitted during failure can be correlated with appropriate types of damages appeared inside testing materials. Following groups of AE frequencies were distinguished for CFRP composites: 0–50 kHz, 50–150 kHz, 200–300 kHz, 400–500 kHz and 500–600 kHz, which could be referred to matrix cracking, delamination, debonding and fiber failure or fiber pull out, respectively [14]; for GFRP composites: 140–250 kHz, 250–350 kHz and 350–450 kHz, which corresponded to matrix cracking, debonding and fiber breakages, respectively [11]; 0–150 kHz, 150–400 kHz and 400–550 kHz, which could be attributed to matrix cracking, interface failures and fiber breakage, respectively [5]; 60–150 kHz, 200–300 kHz and 400–500 kHz, which were associated with matrix cracking, delamination and fiber cracking, respectively [6]; 63.1 kHz, 129.5 kHz and 213.3 kHz, which were connected to matrix cracking (without fiber bridging or fiber pull out), delamination (with fiber pull out) and fiber breakage, respectively [12]; for hybrid CFRP/GFRP composites: 50–160 kHz, 150–300 kHz, 300–400 kHz and 400–600 kHz, which corresponded to matrix cracking, interface failure, fiber pull out and fiber breakage, respectively [13]. As it can be noticed, for each material the failure classification looks similar referring to raising frequency. The lowest frequencies corresponded to intra-ply cracking, whereas the

highest ones were reserved for fiber breakages and fiber bridging. Furthermore, medium frequencies were related to interlaminar cleavage. However, frequency ranges might vary in each case depending on different types of composites and specimens preparation, also among the same type e.g. GFRPs. Moreover, different types of damages occurring inside breaking specimens could be referred to different ranges of elastic waves amplitudes. As described in [7] following ranges were distinguished: 40–50 dB, 45–60 dB, 65–80 dB, which corresponded to matrix micro-cracking, fiber/matrix debonding and fiber pull out, respectively. Hence, it can be inferred that raising amplitudes corresponded to material failures in a similar way that they corresponded to raising frequencies.

Analysis of acoustic emission waveforms is based on applying signal analysis tools such as Fast Fourier Transformation (FFT) and Wavelet Transformation (WT). Acoustic emission systems are equipped with a specialized frequency analysis computer software which helps to interpret the results using both FFT and WT, providing particular information on acoustic wave propagation, as well as damage mechanisms and their origin. However, it is worth to notice that WT has some advantages over FFT. The most important of them is that this method of analysis let to obtain more accurate results as it is localized not only in frequency as FFT, but also in time. Hence, additional information is given on when in time a specific frequency occurs [18, 19], which makes WT a valuable mathematical tool helping to deeply examine signal structure [20]. Because of that, WT can help with analyzing complicated issues that are unable to resolve using FFT only [16].

Signals are represented in WT as a linear combination of wavelets [18] which have limited duration and are located where concerned [21]. While FFT bases on wave analysis, WT focuses on wavelet which is explained as a "small wave", having its energy focused in time [17]. Thus, it gives the ability to conduct simultaneous time and frequency analysis using appropriate mathematical solutions. One of the most significant wavelets property is that they are smooth which means that they are the best basis for representing signals consisting of freely many singularities. This means that function of *n* derivatives can be represented by a wavelet that is n times continuously differentiable. In case when not enough information is given about a signal, using wavelets is a good choice for classifying different varieties of functions because wavelets have the unconditional basis property, described additionally as a near-optimal property. Likewise, nonlinear thresholding and coefficient vector truncation are both optimal in case of signal recovery, statistical estimation and data compression. Moreover, WT is computationally less expensive than FFT and can be easily adopted to inhomogeneous functions [17].

Generally, WT is a transformation similar to FFT because both of them are based on the operation of multiplying the signal function *f(t)* by transformation kernel. The difference is that FFT uses periodic sine and cosine functions representing defined frequency whereas WT's transformation kernel bases on wavelets. The using

of WT requires that only one elementary wavelet is applied, defined as a mother wavelet. In order to decompose the signal, mother wavelet copies are used. They come into being due to mother wavelet scaling and relocating, according to formula (1) where t is time or space coordinate and b is mother wavelet relocation in time or space domain. Thus, Continuous Wavelet Transformation can be calculated as the integral of signal function multiplied by wavelet function, using the formula (2) which may be also expressed as (3). Function $\overline{\psi_{a,b}}$ is defined as a complex wavelet function coupled to $\psi_{a,b}$ [22].

$$\psi_{a,b} = \frac{1}{\sqrt{|a|}} \psi\left(\frac{t-b}{a}\right)$$

(1)

$$W_{f(a,b)} = \frac{1}{\sqrt{|a|}} \int\limits_{-\infty}^{+\infty} f(t) \cdot \overline{\psi\left(\frac{t-b}{a}\right)} dt = \langle f(t), \psi_{a,b}\rangle$$

(2)

$$\langle f, \psi_{a,b}\rangle = \int\limits_{t \in R} f(t) \cdot \overline{\psi_{a,b}} \, dt$$

(3)

After substitution $a = \frac{1}{2^j}$ and $b = \frac{k}{2^j}$, k, j $\in$ C to formula (1) a new wavelet family is created which is a basis of Discrete Wavelet Transformation expressed by formula (4).

$$W_{f(j,k)} = 2^{j/2} \int\limits_{-\infty}^{+\infty} f(t) \cdot \overline{\psi(2^j t - k)} \, dt = \langle f(t), \psi_{j,k}\rangle$$

(4)

Furthermore, it should be emphasized that the same signal can be interpreted in a different way depending on the basis wavelet that has been chosen. Hence, selecting the appropriate basis wavelet plays an important role in whole analysis process. Different wavelets can be used as a basis for computation, including Haar wavelet, Morlet wavelet, Meyer wavelet, Mexican Hat wavelet [21].

Application areas of WT include: harmonic analysis; numerical solutions; mathematical problems; signal processing e.g. medical, biomedical, seismic, geophysical; image processing e.g. medical, biomedical; fractals and chaotic systems; radaring; automatic target recognition [16, 17]. Moreover, since middle 90s it has been also applied for cutting the noise from audio files [23].

2. Methods and materials

In the paper AE was used to monitor polymer failures during Double Cantilever Beam (DCB) test, which was conducted in accordance with ASTM D5528-13 Standard. DCB is a mode I fracture test [24]. In this case, failure is caused due to a load attached in perpendicular direction to a specimen surface [25]. The schematic view of a specimen with dimensions indicated is shown in Fig. 1.
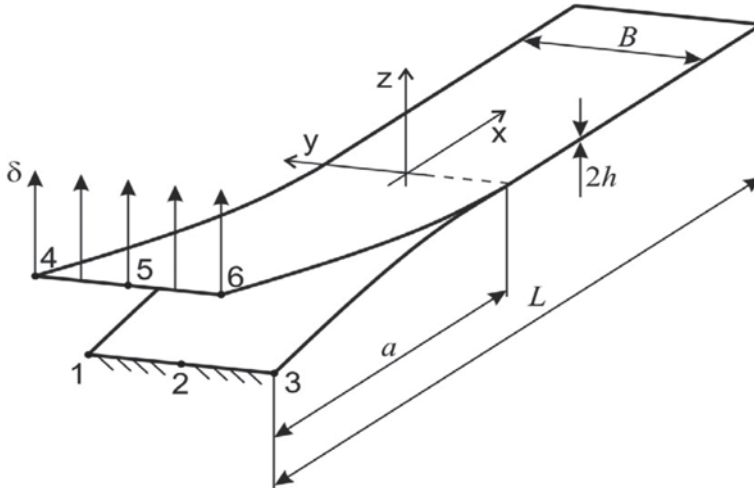
igure 1. Schematic view of DCB specimen [25].

Samples with following dimensions (according to Fig. 1) were used: length L = 210 mm, pre-crack length a = 65 mm, width B = 25 mm, thickness 2h = 8 mm. Specimens were fabricated of two aluminum profiles thick on 2 mm and a polymer layer thick on 4 mm. Polymer layer was made of cured epoxy resin, wherein two kinds of epoxy resins as well as two kinds of curing agents were used to produce the specimens at ambient conditions by bending the appropriate amounts of the ingredients. Materials' details are given in Table 1.

Table 1. Cured epoxy resins prepared for testing

Material symbol	Material designation	Epoxy resin	Curing agent	The amount of curing agent added expressed as a % of a total weight of resin
I	E53/Z1/100:10	Epidian 53	Z1	10
II	E5/PAC/100:60	Epidian 5	PAC	60

In order to prepare DCB samples a silicone form was used with recesses 210 mm x 25 mm x 8 mm. To obtain the appropriate length and thickness of cured epoxies, rectangular aluminum pieces thick on 4mm were used to set a distance between profiles, as shown in Fig 2. After curing and 3-day acclimatization the pieces were removed. Subsequently, notches deep on 20-30 mm were cut in the middle of polymer layer.
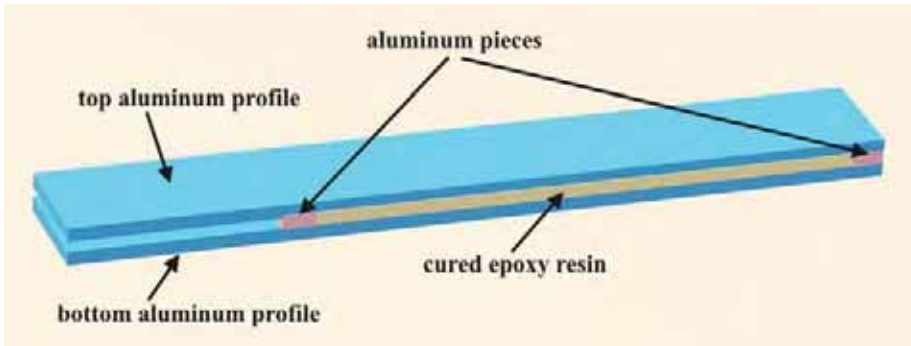
igure 2. The model of DCB sample taken out of the form.

The samples were then subjected to DCB tests using the Autograph AGS-X 5kN universal testing machine. The photo presenting a loaded specimen is shown in Fig. 3.
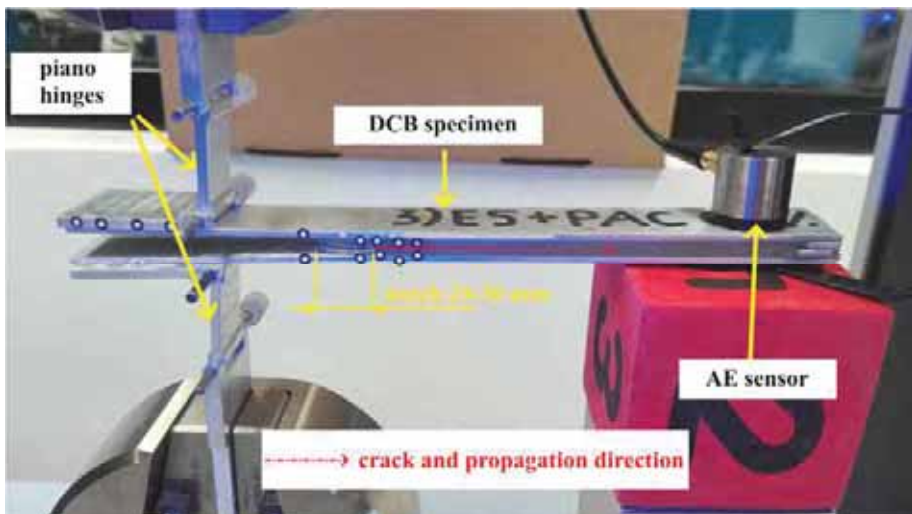
igure 3. View of a loaded specimen during DCB test.

Firstly, piano hinges were bonded to each specimen. Secondly, DCB samples were loaded quasi-statically at vertical speed equal to 1 mm/min. During DCB test, acoustic emission system AMSY-5 was used to register acoustic emission parameters. AE sensor was placed in 30 mm distance from specimen's end. The acquired data was collected on computer's hard drive. Finally, dedicated software was applied to conduct the analysis.

3. Results and discussion

During DCB tests AE parameters such as frequencies (f_{AE}), hits, counts, amplitudes, as well as forces and corresponding energies were registered by AE system. In Fig. 4 mean values of frequency were plotted for the two tested specimen types. As it can be seen mean value of frequency was equal to 117.5 kHz and 45 kHz for material I and material II, respectively. Thus, the frequency for material II was over 60% lower than for material I. This proves that AE frequency registered during fracture depends on material type.
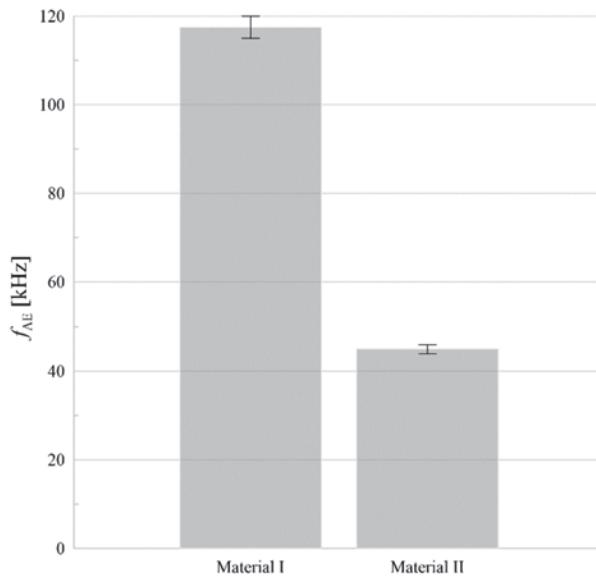
igure 4. Mean values of acoustic emission frequency for the two tested materials.

Moreover, wavelet analysis tool was applied to determine the time range when AE frequency occurred. One specimen for material I and II was selected to prepare visualization based on wavelets, as presented in Fig. 5. This way of results presentation uses a contour diagram in which WT coefficients are indicated by color map.

As it can be noticed the measurement points with the highest intensity of WT coefficients may be simply localized in both frequency and time and peak frequencies obtained from FFT analysis correspond well with the results of WT. In Fig. 5a and 5c color map of WT coefficients is shown for material I and II, respectively. Furthermore, in Fig. 5b and 5d the respective FFT plots are given. In the case of both materials the mean value of frequency 117.5 kHz and 45 kHz is related with the highest intensity of WT coefficients presented in Fig. 5a and 5c and is localized in the time range of 55-60 µs and 30-35 µs, respectively. To summarize, emission of elastic waves was more intense in case of material I, because the higher AE frequency was registered as well as the signal duration was longer, over 80 µs and over 50 µs in case of material I and II, respectively. However, a time duration was relatively low in both cases.
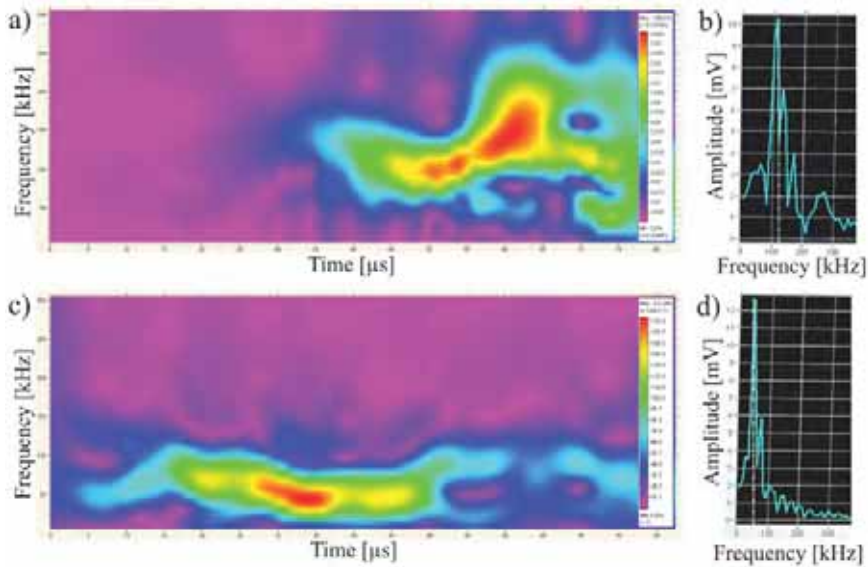
igure 5. Contour maps of WT coefficients: a) material I; c) material II and respective FFT plots: b) material I; d) material II

For the purpose of this research the AE frequency was only analyzed although other AE parameters were also registered during the tests. It would be interesting to conduct deeper analysis of the problem with additional relation to number of hits, counts, acoustic energy, as well as force. This will be the objective of further research.

4. Conclusion

Based on the experimental analysis it can be concluded that:

1) It was proved that acoustic emission may be successfully used for monitoring failures in case of both selected materials: Epidian 53 epoxy resin cured with Z1 curing agent (marked as material I) as well as Epidian 5 epoxy resin cured with PAC curing agent (marked as material II).

2) According to the results mean values of AE frequency registered during failure for the two tested materials varied depending on material type.

3) DCB test can be applied not only to laminates and adhesively bonded parts but also to analyze the behavior of cracking appeared inside the thick adhesive layer.

4) Wavelet analysis is a promising tool which helps to examine AE signal in detail regarding time, frequency and WT coefficients.

References

[1] Kubit A., Trzepiecinski T., Kłonica M., Hebda M., Pytel M., The Influence of Temperature Gradient Thermal Shock Cycles on the Interlaminar Shear Strength of Fibre Metal Laminate Composite Determined by the Short Beam Test, *Composites Part B: Engineering*, 176, 2019.

[2] Jin F.-L., Li X., Park S.-J., Synthesis and Application of Epoxy Resins: A Review, *Journal of Industrial and Engineering Chemistry*, 29, 2015, pp. 1–11.

[3] Zheng T., Xi H., Wang Z., Zhang X., Wang Y., Qiao Y., Wang P., Li, Q., Li Z., Ji C., Wang X., The Curing Kinetics and Mechanical Properties of Epoxy Resin Composites Reinforced by PEEK Microparticles, *Polymer Testing*, 91, 2020.

[4] Aggelis D. G., De Sutter S., Verbruggen S., Tsangouri E., Tysmans T,. Acoustic Emission Characterization of Damage Sources of Lightweight Hybrid Concrete Beams, *Engineering Fracture Mechanics*, 210, 2019, pp. 181–188.

[5] Seyyed Monfared Zanjani J., Saner Okan B., Yilmaz C., Menceloglu Y., Yildiz M., Monitoring the Interface and Bulk Self-Healing Capability of Tri-Axial Electrospun Fibers in Glass Fiber Reinforced Epoxy Composites, *Composites Part A: Applied Science and Manufacturing*, 99, 2017, pp. 221–232.

[6] Kubiak T., Samborski S., Teter A., Experimental Investigation of Failure Process in Compressed Channel-Section GFRP Laminate Columns Assisted with the Acoustic Emission Method, *Composite Structures*, 133, 2015, pp. 921–929.

[7]   Haggui M., El Mahi A., Jendli Z., Akrout A., Haddar M., Static and Fatigue Characterization of Flax Fiber Reinforced Thermoplastic Composites by Acoustic Emission, *Applied Acoustics*, 147, 2019, pp. 100–110.

[8]   Ben Ameur M., El Mahi A., Rebiere J.-L., Gimenez I., Beyaoui M., Abdennadher M., Haddar M., Investigation and Identification of Damage Mechanisms of Unidirectional Carbon/Flax Hybrid Composites Using Acoustic Emission, *Engineering Fracture Mechanics*, 216, 2019.

[9]   Barile C., Innovative Mechanical Characterization of CFRP by Using Acoustic Emission Technique, *Engineering Fracture Mechanics*, 210, 2019, pp. 414–421.

[10] Berro Ramirez J. P., Halm D., Grandidier J.-C., Assessment of a Damage Model for Wound Composite Structures by Acoustic Emission, *Composite Structures*, 214, 2019, pp. 414–421.

[11] Fotouhi M., Najafabadi M.A., Acoustic Emission-Based Study to Characterize the Initiation of Delamination in Composite Materials, *Journal of Thermoplastic Composite Materials*, 2014.

[12] Samborski S., Gliszczynski A., Rzeczkowski J., Wiacek N., Mode I Interlaminar Fracture of Glass/Epoxy Unidirectional Laminates. Part I: Experimental Studies, *Materials*, 12, 2019.

[13] Tabrizi I. E., Kefal A., Zanjani J. S. M., Akalin C., Yildiz M., Experimental and Numerical Investigation on Fracture Behavior of Glass/Carbon Fiber Hybrid Composites Using Acoustic Emission Method and Refined Zigzag Theory, *Composite Structures*, 233, 2019.

[14] Gutkin R., Green C.J., Vangrattanachai S., Pinho S.T., Robinson P., Curtis P.T., On Acoustic Emission for Failure Investigation in CFRP: Pattern Recognition and Peak Frequency Analyses, *Mechanical Systems and Signal Processing*, 25(4), 2011, pp. 1393–1407.

[15] Yilmaz C., Akalin C., Gunal I., Celik H., Buyuk M., Suleman A., Yildiz M., A Hybrid Damage Assessment for E-and S-Glass Reinforced Laminated Composite Structures under in-Plane Shear Loading, *Composite Structures*, 186, 2018, pp. 347–354.

[16] Mahato K., The Composition of Fractional Hankel Wavelet Transform on Some Function Spaces, *Applied Mathematics and Computation*, 337, 2018, pp. 76–86.

[17] Burrus C., Gopinath R., Guo H., *Introduction to Wavelets and Wavelet Transform - A Primer*, Prentice Hall, 1998.

[18] Fletcher P., Sangwine S.J., The Development of the Quaternion Wavelet Transform, *Signal Processing*, 136, 2017, pp. 2–15.

[19] Abdulkareem M., Bakhary N., Vafaei M., Noor N.M., Mohamed R.N., Application of Two-Dimensional Wavelet Transform to Detect Damage in Steel Plate Structures, *Measurement*, 146, 2019, pp. 912–923.

[20] Zhu L.-F., Ke L.-L., Zhu X.-Q., Xiang Y., Wang Y.-S., Crack Identification of Functionally Graded Beams Using Continuous Wavelet Transform, *Composite Structures*, 210, 2019, pp. 473–485.

[21] Liu C.-L., *A Tutorial of the Wavelet Transform*, 2010.

[22] Knitter-Piątkowska A., *Wykorzystanie Transformacji Falkowej Do Wykrywania szkodzeń w Konstrukcjach Obciążonych Statycznie i Dynamicznie*, Politechnika Poznańska, 2011.

[23] Berger J., Coifman R., Goldberg M., Removing Noise from Music Using Local Trigonometric Bases and Wavelet Packets, *AES: Journal of the Audio Engineering Society*, 42, 2012.

[24] Rzeczkowski J., Samborski S., de Moura M., Experimental Investigation of Delamination in Composite Continuous Fiber-Reinforced Plastic Laminates with Elastic Couplings, *Materials*, 13(22), 2020.

[25] Samborski S., Numerical Analysis of the DCB Test Configuration Applicability to Mechanically Coupled Fiber Reinforced Laminated Composite Beams, *Composite Structures*, 152, 2016, pp. 477–487.

Addresses:

- MSc Eng. Jakub Skoczylas, Lublin University of Technology, Faculty of Mechanical Engineering, Nadbystrzycka 36, 20-618 Lublin, Poland
  j.skoczylas@pollub.pl
  ([*]*corresponding author*)
- Assoc. Prof. DSc Eng. Sylwester Samborski, Lublin University of Technology, Faculty of Mechanical Engineering, Nadbystrzycka 36, 20-618 Lublin, Poland
  s.samborski@pollub.pl
- PhD Eng. Mariusz Kłonica, Lublin University of Technology, Faculty of Mechanical Engineering, Nadbystrzycka 36, 20-618 Lublin, Poland
  m.klonica@pollub.pl

The design and execution of a laboratory micro hydroelectric power plant

Elisabeta Spunei, Ionel Turcu, Alina Vişan[*]

Abstract. *The paper presents a laboratory micro hydroelectric power plant destined to applicative activities. The hydraulic turbine is a Pelton turbine, rebuilt by fast prototyping in Geomagic Design and printed on a 3 D printer. The turbine casing and the afferent elements are made in-house. The hydrogenator is synchronous being an alternator from a Dacia vehicle. The hydrogenerator load is constituted by 3 groups of light bulbs. We analysed the working of the micro-hydroelectric power plant in idle run and for different loads. As a result of the analysis we found out that it stably works for different loads and by its open construction it is useful for developing students ability to understand the phenomena. The installation designed and executed is useful for the engineering students as the pandemic forbids the thematical visits in hydro-energetic facilities.*

Keywords*: micro hydroelectric power plant, renewable energy, Pelton turbine, 3D printer*

1. The present stage related to the production of the electric power in hydro-energetic installations

The use of renewable sources of energy for the production of electric power contributes to the reduction of gas emissions with greenhouse effect. Thus, the European Union decided that in 2030 at least 32% of the raw final energy consumption should be ensured from renewable sources [1], hence the need to implement solutions for the production of electric energy from unpolluted sources.

An implemented solution is the use of water for the production of electric energy, micro-hydro energy being considered one of the most profitable energetic technologies [2]. Thus, more and more countries have built hydroelectric power plants or micro hydroelectric power plants which should ensure their power supply need.

On the international level, there are solutions which use drinking water, water used in irrigations and water used for the production of electricity [3-5]. For the production of electricity using micro-hydro energy, in Spain they proposed the use of water from all overflows [6], and in Belgium they intend to pump water which is 500 m deep in a deallocated mine [7].

When the turbine is placed directly on the supply pipe with water, the investment costs are very much reduced as compared to the classical variant of placing a turbine and the environment is not negatively influenced by this one [8].

In the case of locations with no national power supply network some solutions are implemented which consist of more than two combined systems of renewable energy (solar, wind, hydro-energetic) and a storage system. In some cases, these systems are completed and with diesel-generator able to supply energy in the situation in which the other systems are not working [9].

Where there is a power supply network for consumers, all the needs of electricity can be satisfied and the excess can be provided in the national network, the supply producers becoming consumers [10].

For an optimal working these systems need to be properly designed, depending on the functional objectively pursued (minimal total cost, maximum performance, minimal loss in the exploitation period, the static and dynamic performances) [11-13] thus it will work safely [14-17].

In the pandemic conditions, when the access to the hydro-power facilities is restricted, in order to provide students with an adequate understanding of a micro hydro power plant functioning, one was built in the laboratory. After the analysis of its operation, we remarked that they are working adequately, being able to ensure the need of energy for the configured consumers.

2. Design and achievement of the laboratory micro hydroelectric power plant

The block diagram of the main components which constitute the laboratory micro hydroelectric power plant are presented in figure 1. The electric generator is of the tree-phased synchronous type being in fact an alternator of a Dacia 1300 vehicle, having the following technical characteristics [18]:
- Working voltage U – 14 V;
- The maximal load current I_{max} – 30 A.

The maximal power P_{max} calculated results:

$$P = U \cdot I = 420 \ [W] \tag{1}$$

The supply of the operating winding of the synchronous generator is achieved by an accumulator of 12V, 10A by means of the K1collector, the power provided being redressed by means of a diode block/circuit. The adjustment of the tension in the energizing circuit is achieved by a make-and-break relay and the electric values provided are monitored by a voltmeter and an ampermeter.
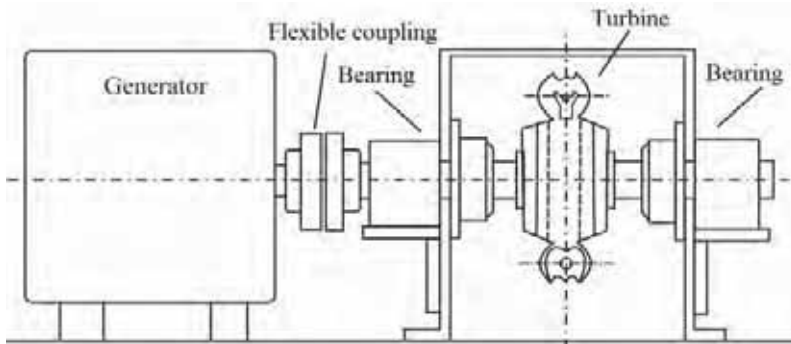
Figure 1. The main components of the laboratory
micro hydroelectric power plant.

The supply of the operating winding of the synchronous generator is achieved by an accumulator of 12V, 10A by means of the K1collector, the power provided being redressed by means of a diode block/circuit. The adjustment of the tension in the energizing circuit is achieved by a make-and-break relay and the electric values provided are monitored by a voltmeter and an amperemeter.

The connection between the electric generator and the hydraulic turbine is achieved by an elastic hitch.

The hydraulic turbine is made of:
- casing made of transparent polycarbonate;
- the rotor of Pelton turbine rebuilt by fast prototyping in Geomagic Design and built with the help of a 3D printer made of PLA (polylactic acide) using the technology FDM (fused deposition modeling) [19, 20];
- the metallic shaft supported on 2 roller bearings (radial-axial bearing) on which the rotor of Pelton turbine is imbedded. At the exit from the casing the shaft has sealing semerings on both sides;
- injector designed in the Autodesk Inventor software and placed on the turbine casing which by means of a screw on the thread end offers the possibility to modify the injector position concerning the water flow control;
- the drainage coupling placed in the turbine casing used for the evacuation of the turbined water.

Figure 2 shows a Pelton turbine bucket, Figure 3 presents a Pelton turbine, both of them rebuilt in Geomagic Design™, and Figure 4 shows an image from the process of 3D printing of the Pelton turbine.
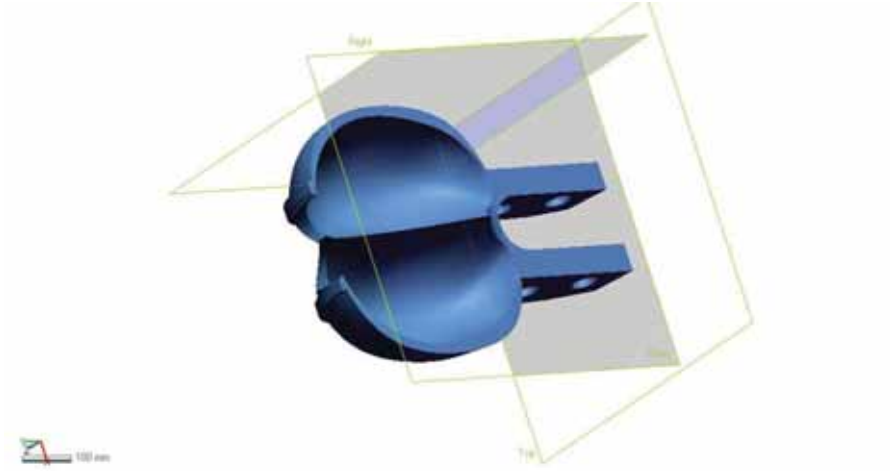
Figure 2. Pelton turbine bucket.
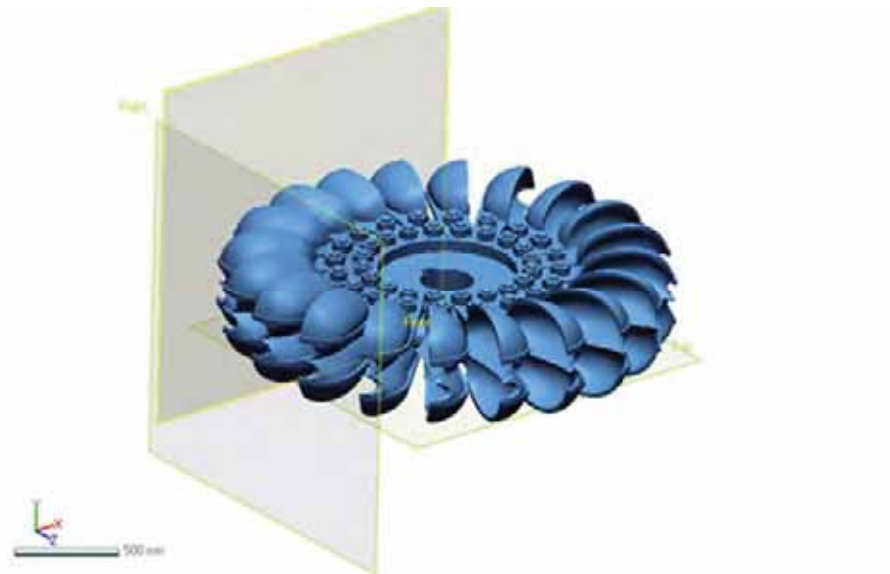
Figure 3. Pelton turbine.
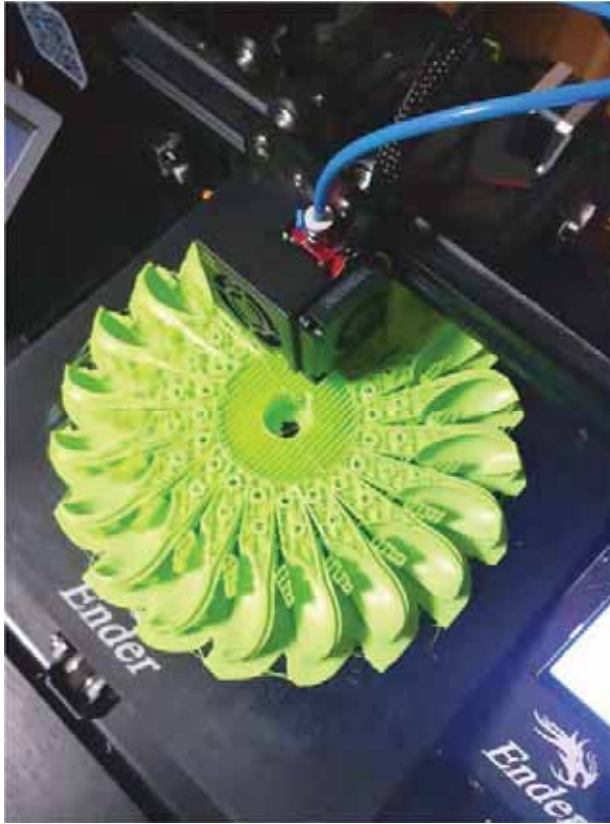
Figure 4. The Pelton turbine during the printing process.

The water supply for the laboratory micro hydroelectric power plant was achieved from the city network which has a pressure of 4 bars and 12 light bulbs, 35W were the consumers. In order to vary the load, these were connected in 3 turns, with 4 bulbs in a turn, the total power being:

$$P_r = P_{bulb} \cdot no_{bulb/row} = 140 \text{ [W]} \tag{2}$$

The supply diagram of the excitation winding of the synchronous generator and the supply of consumers is presented in figure 5 and in figure 6 there is an image with micro hydroelectric power plant achieved and mounted in the laboratory.
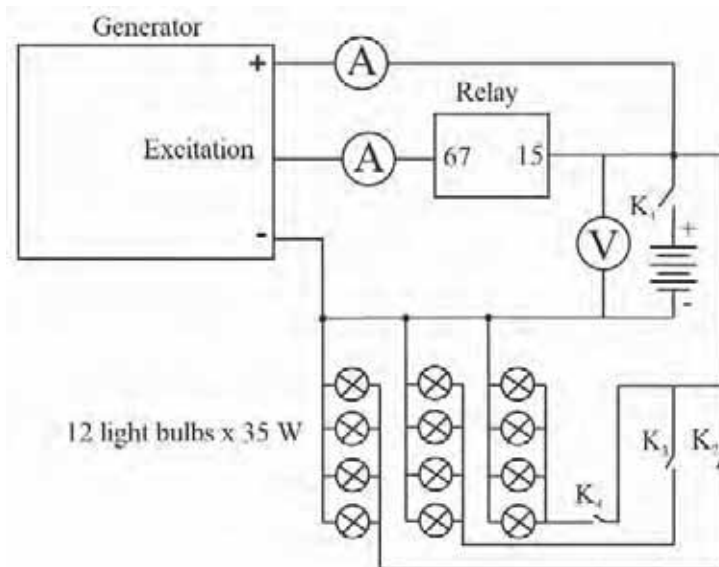
Figure 5. Supply electric diagram for the excitation winding
of the generator and consumers.

Figure 6. The laboratory micro hydroelectric power plant.

3. Analysis of the laboratory micro hydroelectric power plant operation

The analysis of the operation was achieved in 2 stages: at the assembly place where the water supply of the turbine was doing at the pressure of 2 bars and in the laboratory where the pressure of water at the entrance of the turbine was of 3,5 bars.

In the first stage the excitation power was adjusted by the regulating relay around 1,5 A. For the revolution of the generator there were 840 rot/min, the power provided was 14,5 V. At the coupling of the load the power of the load had the values in table 1.

Table 1. The values of the load current

Load power [W]	Load current [A]
140	10
280	13,5
420	17

After mounting the micro hydropower plant in the laboratory the speed was measured in idle operation, the mode of the speed variation being presented in figure 7. The maximum speed for the idle operation of the micro hydropower plant was 1112,2 rot/min, this being reached in 1,3 seconds.

We did some analysis referring to the operation of the micro hydropower plant with 1/3, 2/3 in load and nominal load.

For the analysis of the operation with 1/3 load, we connected a row of bulbs and we observed the fact that the value of the current in the circuit of the consumer is 13,7 A, and the voltage supplied was 11,5 V, the current measured in the excitation circuit being 2,62 A. The mode of the speed variation at operation with 1/3 of load is presented in figure 8 where we observe that the maximal speed is 877 rpm and it is reached in 0,82 seconds.

For the analysis of the operation with 2/3 load two rows of bulbs were connected. In this situation the current in the consumer circuit is 14 A and the voltage supplied is 11,2 V. The variation mode of the speed at operation with 2/3 load is presented in figure 9 where we observe that the maximal speed is 768,6 rpm and it is reached in 0,49 seconds.
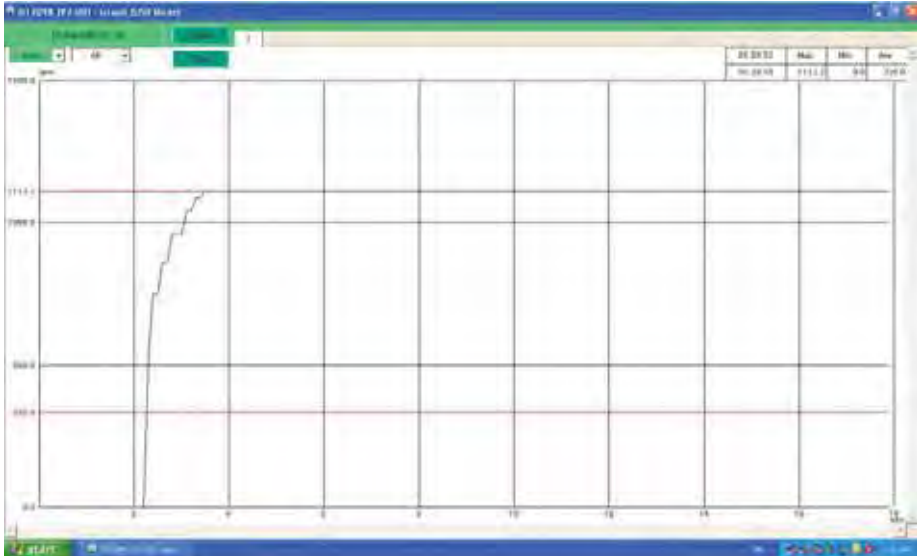
Figure 7. The mode of the speed variation at the start of the micro hydropower plant in idle operation.
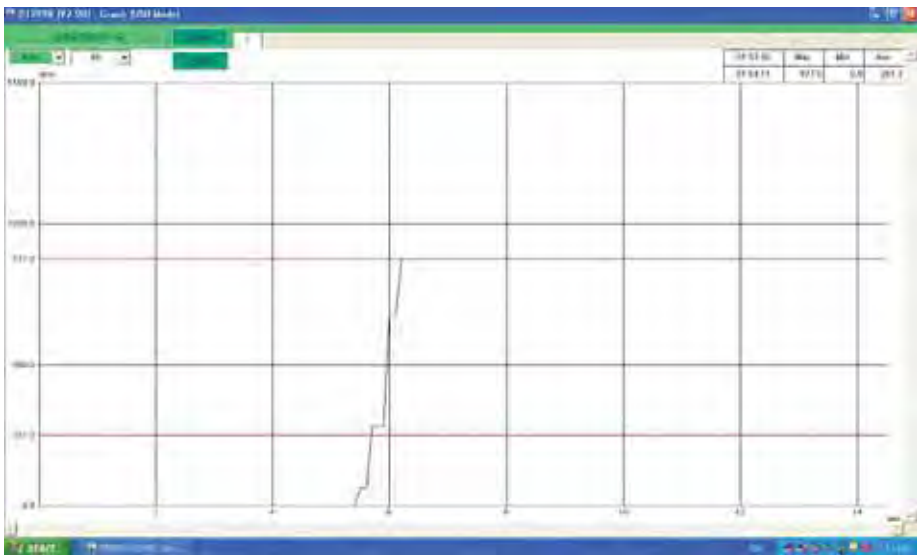
Figure 8. The mode of the speed variation at the start of micro hydroelectric power plant and operation in 1/3 load.
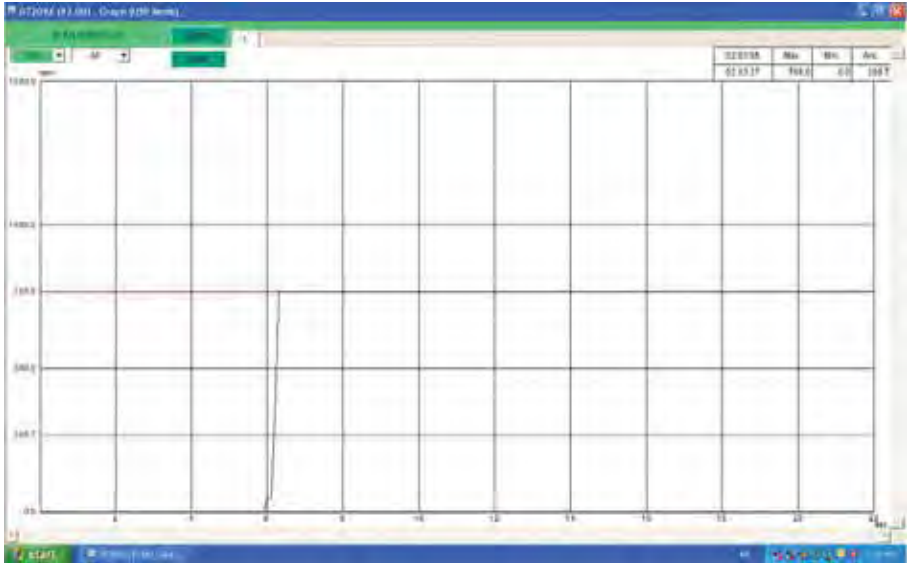
Figure 9. The variation mode of speed at the start of micro hydroelectric power plant and operation with 2/3 load.
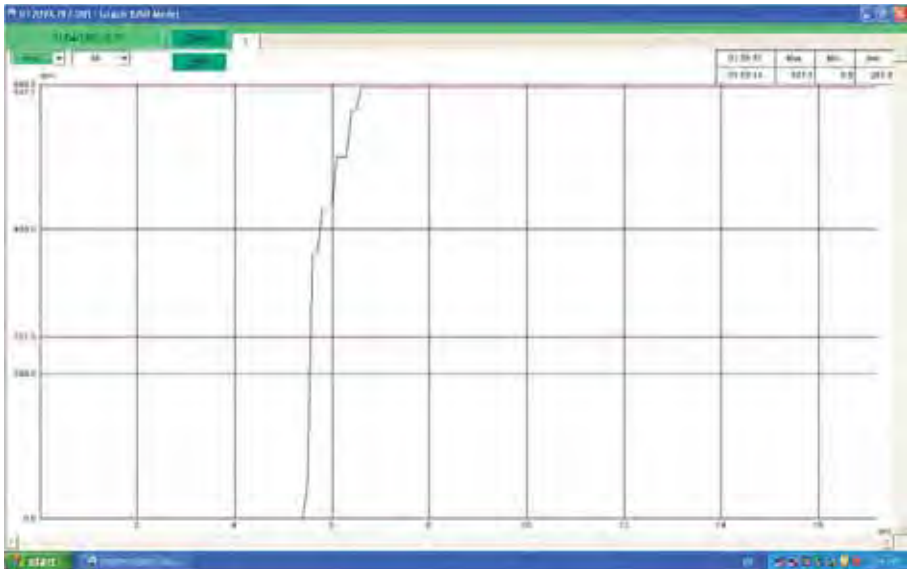
Figure 10. The variation of the number of revolutions at the start of the micro hydroelectric power plant and its operation at nominal load.

For the analysis of operation at nominal load all the bulbs in the circuit were connected in the consumer circuit being 17,9 A and the tension supplied is 10,2 V. The mode of speed variation at start and operation in nominal load is presented in figure 10 where we observe that the maximal speed is 597,1 rpm and this is reached in 1,18 seconds.

4. Conclusion

The providers of turbines or hydraulic micro-turbines have a catalogue with models experimentally tested, which have been initially designed based on the measurements achieved on industrial turbines.

Generating the geometry of the Pelton rotor by fast prototyping in Geomagic Design offers the possibility of reducing the design time as compared to the classical variant and brings the following advantages: fast achievement of components, very high precision, low-cost price.

After analysing the functioning micro hydroelectric power plant designed and executed in the laboratory we found out that it stably functions being able to provide the necessary electricity for consumers.

References

[1] Share of energy consumption from renewable sources in Europe, https://www.eea.europa.eu/data-and-maps/indicators/renewable-gross-final-energy-consumption-5/
(downloaded at September 3rd, 2021).

[2] Manzano-Agugliaro F., Taher M., apata-Sierra A., Juaidi A., Montoya F.G. An overview of research and energy evolution for small hydropower in Europe, *Renewable sustainable energy reviews*, 75, 2017, pp. 476-489.

[3] Mitrovic D., Chacon M.C., Garcia A.M., Morillo J.G., Diaz J.A.R., Ramos H.M., Adeyeye K., Carravetta A., McNabola A., Multi-Country Scale Assessment of Available Energy Recovery Potential Using Micro-Hydropower in Drinking, Pressurised Irrigation and Wastewater Networks, Covering Part of the EU, *Water*, 13, 2021, Article number: 899.

[4] Ali A., Baig F.S., Memon A.H., Designing Hydel Power Generation Capacity using a Mini/Micro Hydro Power Plant at Left Bank Outfall Drain Drainage System, near Goth Ahori, Jhuddo, Sindh, *Mehran university research journal of engineering and technology*, 39, 2020, pp. 554-563.

[5] Kamran M., Asghar R., Mudassar M., Abid M.I., Designing and economic aspects of run-of-canal based micro-hydro system on Balloki-Sulaimanki Link Canal-I for remote villages in Punjab, Pakistan, *Renewable energy*, 141, 2019, pp. 76-87.

[6] Garcia A.M., Diaz J.A.R., Morillo J.G., McNabola A., Energy Recovery Potential in Industrial and Municipal Wastewater Networks Using Micro-Hydropower in Spain, *Water,* 13, 2021, Article number: 691.

[7] Morabito A., Spriet J., Vagnoni E., Hendrick P., Underground Pumped Storage Hydropower Case Studies in Belgium: Perspectives and Challenges, *Energies*, 13, 2020, article number: 4000.

[8] Berrada A., Bouhssine ., Arechkik A., Optimisation and economic modeling of micro hydropower plant integrated in water distribution system, *Journal of cleaner production*, 232, 2019, pp. 877-887.

[9] Muh E., Tabet F., Comparative analysis of hybrid renewable energy systems for off-grid applications in Southern Cameroons, *Renewable energy*, 135, 2019, pp. 41-54.

[10] Syahputra R., Soesanti I., Planning of Hybrid Micro-Hydro and Solar Photovoltaic Systems for Rural Areas of Central Java, Indonesia, *Journal of electrical and computer engineering,* 2020, vol. 2020, article number: 5972342.

[11] Spunei E., Piroi I., Piroi F, Optimizing Structural Dimensions and Costs of a Synchronous Generator Depending on the Current Blanket, *Analele niversităţii Eftimie Murgu, Fascicula de Inginerie,* 19(1), 2012, pp. 303-310.

[12] Spunei E., Piroi I., *The importance of choosing the value of current density in the stator windings on the cost and efficiency of the synchronous generator*, 7th International Conference and Exposition on Electrical and Power Engineering, EPE 2012, IEEE Catalog number CFP1247S-DVD, 25-27 Oct., Iaşi, 2012.

[13] Spunei E., Piroi I., Comparative Analysis Between Stationary and Dynamic Parameters of a Synchronous Generator, with the Main Variable of the Air Gap Magnetic Induction, 11th International Conference on Applied and Theoretical Electricity (ICATE), Oct. 25-27, 2012, Craiova, *Analele niversităţii din Craiova, Seria Inginerie Electrică*, 36(36), Editura Universitaria, 2012, pp. 386-389.

[14] Espinoza O., Tiwary A., Assessment of autonomous renewable energy system operability under extreme events and disasters, *Sustainable energy technologies and assessments*, 44, 2021, article number: 100995.

[15] Delgado J., Ferreira J.P., Covas D.I.C., Avellan F., Variable speed operation of centrifugal pumps running as turbines. Experimental investigation, *Renewable energy*, 142, 2019, pp. 437-450.

[16] Arani H.A., Fathi M., Raisee M., Nourbakhsh S.A., The effect of tongue geometry on pump performance in reverse mode: An experimental study, *Renewable energy*, 141, 2019, pp. 717-727.

[17] Morabito A., Hendrick P., Pump as turbine applied to micro energy storage and smart water grids: A case study, *Applied energy*, 241, 2019, pp. 567-579.

[18] Tocaiuc G., *Echipamentul electric al automobilelor*, Editura Tehnică Bucureşti, 1982.

[19] Nedelcu D., Cojocaru V., Ghican A., Periș-Bendu F., Avasiloaie R., Considerations Regarding the Use of Polymers for the Rapid Prototyping of the Hydraulic Turbine Runners Designed for Experimental Research on the Model, *Materiale Plastice*, 52(4), 2015, pp. 475-479.

[20] Nedelcu D., Pop F., Cojocaru V., Hopota A., Prototiparea rapidă a unui rotor Pelton, *Ştiinţa şi Inginerie*, 2012, pp. 335-342.

Addresses:

- Lect. Dr. Eng. Elisabeta Spunei, Babeș-Bolyai University, Faculty of Engineering, 1-4, Traian Vuia Square, 320085, Reşiţa, Romania
  elisabeta.spunei@ubbcluj.ro
- Eng. Ionel Turcu, Babeș-Bolyai University, Faculty of Engineering, 1-4, Traian Vuia Square, 320085, Reşiţa, Romania
  ionel.turcu@stud.ubbcluj.ro
- Lect. Dr. Alina-Dana Vişan, Babeș-Bolyai University, Faculty of Letters, Horea Street, Cluj-Napoca, Romania
  alina.visan@ubbcluj.ro
  (*corresponding author*)

Effect of amended soil using different fertilizer applications on phenology of Cassava in Edo State South-South Nigeria

Cletus Jude Odighi, Yahaya Olotu[*], Edeki Ahmansi, Bada Olatubosun

Abstract. *Three experimental fertilization treatments of fertigation (FERT), Nitrogen-Phosphorus-Potassium (NPK), and poultry organic fertilizer (ORG) were applied on a cassava (TMS 30573) cultivation at the rate 300 kg/ha for NPK and ORG, while fertigation was injected at 1.5 litres/minutes. The results were compared with the control and unfertilized field using the same cassava cultivar. The results from the four treatments indicated that the cassava phenological development significantly responded to fertilizer applications. At 183-day after planting (DAP), the plant height under FERT was higher than NPK, OGR and CON by 19.0 cm, 60 cm and 80 cm. Conversely, under ORG, the leaf emergency (*le*) steady increased to 42 leaves at 183 DAP, whereas NPK reached peak (*le*) at 161 DAP and dropped to 41 at 183 DAP. Also, under the FERT and CON, le dropped to 38 and 33 leaves at 183 DAP. The rate of leaf death (*ld*) is significant at P<0.001 under fertigation, NPK and ORG, while insignificant under control treatment. Projected cassava yield per hectare estimated from phenological and morphological development indicated that ORG showed high possibility of producing cassava yield increase of 2.5 tons/hectare over FERT, 3.2 tons/hectare, 4.8 tons/hectare under NPK and CON respectively.*

Keywords: Cassava-TMS 30573, Fertilization, Phenological development, Cassava yield, Treatment

1. Introduction

Cassava is one of the most important crops due to its large chain value addition. Several food items as garri, funfun, pupuru are a by-product of cassava. Manihot esculenta Crantz is also an essential calorie for human and animal well-being. [1] indicated that cassava is the third important calories source after rice and rice mostly in tropical countries. Also, the crop is increasingly used in the pharmaceutical and beer industries [9]. The global population explosion and an

emerging increase in cassava usage as direct and indirect consumption, drug and beer manufacturing have greatly increased the demand for the crop. The study of [1] revealed that cassava's demand has tremendously increased due to its wide range of uses. Presently, three is a large gap between the cassava yield and population growth in Nigeria. Conversely, an average cassava yield of 22.0 tons/ha is not sustainable to attain intended cassava yield potential.

Having established an existence between a large cassava yield gap and a growing population, it is important to increase its production to reduce possible deficits, improve food security and economic growth. The finding from the study of Hillock (2014) showed that global cassava's yield represents 46% and 36% over the African continent. Despite that Nigeria is the largest cassava importing, most of the cassava importing regions in Nigeria have been experiencing a reduction in yield per hectare due to nutrient depletion, prevailing weather conditions, and farm management. However, all the factors attributed to cassava yield per hectare could be achieved by choosing and planting a cassava stem variety suitable for a given agro-ecological zone regarding climate (temperature, rainfall e.t.c), nutrients, and pest resistance. Also, agronomic and farm practices are very imperative to achieving improved cassava yield. [3] reported that cassava yield could be increased by planting suitable cassava varieties and application of the required amount of fertilizer

Constant cultivation without fertilizer application will likely lead to nutrient depletion and low cassava yield. Amendment of nutrient-depleted soils is commonly achieved through the use of fertilizers as NPK, Urea, and organic manures both from plants and animals. [8] observed over Sub-Saharan Africa that cassava yield increase with fertilizer application. It is important to determine the rate, amount, and type of fertilizer to use in response to soil type and condition. Also, the information on the soil analysis is significant to fertilizer application. [4] revealed that nitrogen (N) and potassium (K) are the major nutrients required for cassava yield. 4R Nutrient Stewardship principle is recommended to be used in applying fertilizer for cassava cultivation.

Hence, this study aims to evaluate and compare the phenological development of cassava under three fertilizer treatments (URE fertigation, NPK, organic manure) with the control treatment. The results obtained will be useful to select appropriate fertilizer for optimum cassava yield in Edo State, Nigeria.

2. Materials and Methods.

2.1. Site description

Field experiments were carried out at the Teaching and Demonstration of Auchi Polytechnic, Auchi located at latitude 7.0465^0N and longitude 6.2701^oE. The soil has a high percentage of sand with low fertility due to continuous cultivation and erosion. Auchi is located within a tropical savanna climate with

annual average precipitation and air temperature of 1,205 mm and 28^{0}C. The highest and lowest dry period is February and July with a maximum temperature of 38°C and 29°C.

2.2. Land preparation

The vegetation on the area (trees and grasses) was removed using Axe, cutlass, hoe, and motor saw. The area was tilled mechanically using plough and harrow. While the marking out (the division into treatment plots) was done using measuring tape and pegs. A cassava variety of TMS 30573 was planted on the 18th March 2021. The cassava stake of 26 cm long was manually planted on the ridge's crest at a spacing of 2 m.

2.3. Experimental design

The design of the experiment was 4 * 4 randomized complete block design with three replications. The size of each plot is a 4 m * 6 m and contained 6 rows of 6 m length with a planting distance of 2 m. A total of four (4) plots including a control treatment were constructed. The plant was fertilized with NPK at a dose of 15:15: 15 at the rate of 300 kg/ha after two months of a plantation at plot A, while fertigation of NPK (15:15: 15) was done at 1.5 litres per minute on plot B. Organic manure was used to plot C before tillage at the rate of 300 kg/ ha. Hence, plot D is the control treatment where no form of soil amendment was carried out. Each of the plots was subjected to the same supplementary water application of 5 mm for every three (3) days interval for plant germination and establishment. The rate of germination was determined 40 days after planting. The germination rate was 80% in plot A, 100% in plot B, 80% in plot C, and 75% in plot D. The weeding activities were carried out using convection and application of herbicide (Force Up). Cassava phenological development (plant height, plant width, leaf emergency, leaf death) was measured every five days over each of the plots. Statistical metrics of ANOVA and T-test were used to compare different treatments on the cassava growth parameter. Signal 1.0 version was used for the smart plot of the phenological parameter. The least significant difference (LSD) and multiple range test (DUNCAN) were used to compare the mean at a 1% confidence interval. Some of the field activities were shown in plates 1-4.
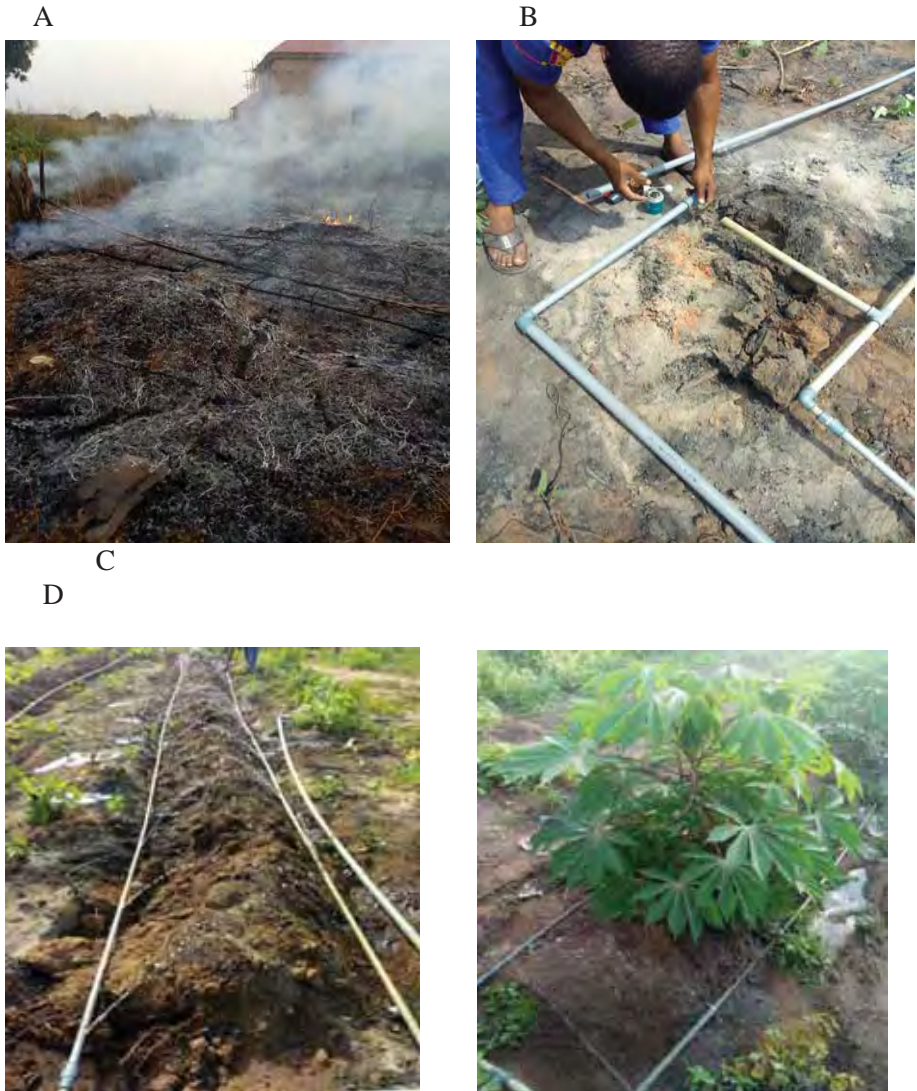
Plate 1: Land clearing (A), Installation of irrigation system (B), Operation of irrigation system (C) and Growing cassava plant (D).

3. Results and Discussion

3.1 Cassava germination

The germination of planted cassava stake was observed at exactly 20 days after the day of planting. The survival and germination showed that plot A recorded a 100% germination rate (GR), while plots B, C, and D indicated GR of

80%, 75%, and 80% respectively. A similar finding was obtained by [3] revealed that MKUC 34-114-106 cassava cultivar had survival and GR of 95.4% and 96.7%.

3.2. Cassava phenology under soil amendment

The growth parameters of cassava were measured at 25 days after planting (DAP) across the plots. The plant height (Ph) increased suddenly with solid NKP, fertigation, and organic manure while under control treatment, the Ph started to increase at 69 DAP. Average plant of 160.0 cm was obtained in plot B (fertigation), 141.0 cm in plot A (Solid NPK fertilizer), 100.0 cm at plot C (organic manure), and 80 cm under control treatment at 183 DAP as shown in Fig 1a. The finding revealed that the plant growth response abruptly to fertigation and NPK soil amendments. The control treatment could be attributed to the depletion in the soil nutrient due to its continuous cultivation. However, the steady development of cassava phenology under organic manure could be best be explained by the long period required for the decomposition processes. The finding is similar to the study of [5] which revealed that under fertigation or any soil amendment to improve soil nutrients may improve the yield of cassava.

Conversely, the developmental pattern took different dimensions for the leaf emergency and death. Le abruptly increased with the NPK treated plot (A) and got to the peak of 48 leaves at 161 DAP and dropped to 41 leaves at 183 DAP. Fertigation treatment also showed a similar pattern with the highest Le of 38 leaves at 183 DAP. A close observation of the organic manure treated plot indicated a steady increase in Le in the number of leaf emergencies from 40 DAP to 42 leaves at 183 DAP whereas the Le recorded showed a low increase compared to organic manure treatment with the highest leaf emergency of 33 leaves at 183 DAP (Fig. a-c). Hence, it is obvious that fertilization has a significant effect on cassava phenological development. [6;7] showed that fertilization has significant effects on phenological and morpho-physiological stages by cassava. Therefore, the absence of fertilization of plot D (Control) could be attributed to low leaf emergency. Fig. 1d shows that the lowest death rate (LDR) occurred at treatment at peak leaf (*ld*) at 25 leaves at 183 DAP, while ld of 40 leaves was estimated at 183 DAP at plot A (Organic manure) and B (fertigation) the ld was at 37 and 35 leaves at 183 DAP respectively.
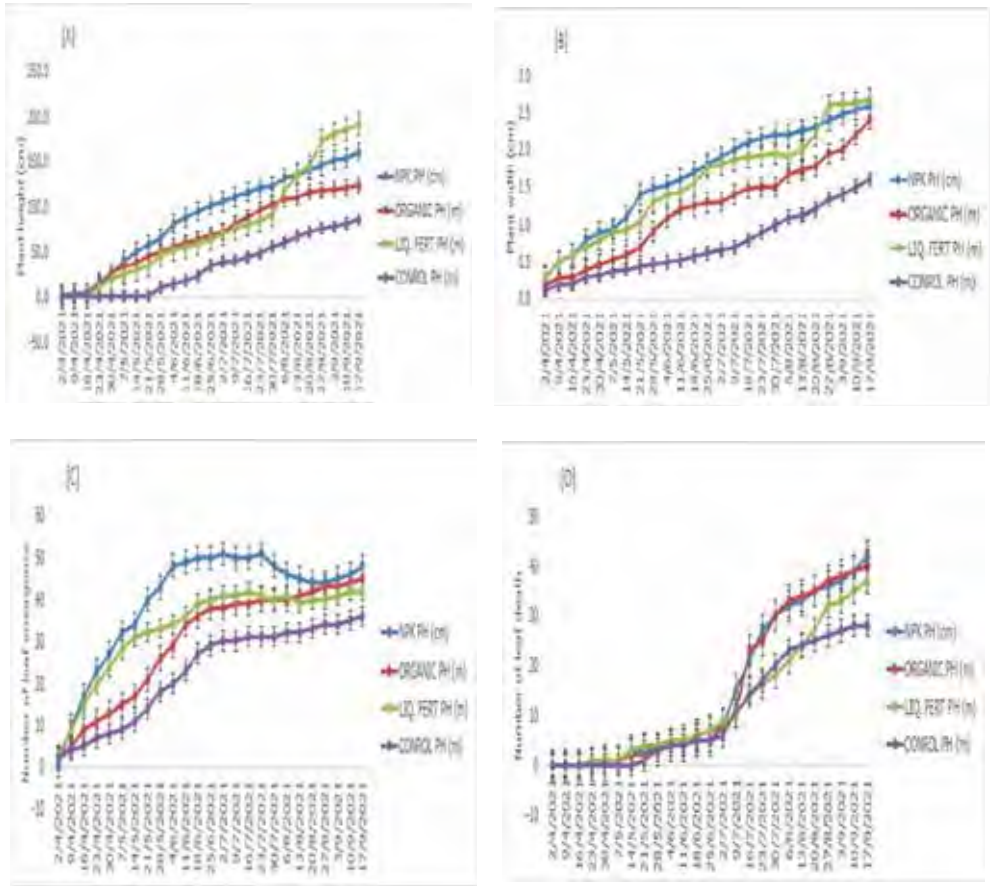
Figure 1. Cassava phenological development-plant height (a), plant width (b), leaf emergency (c), and leaf death (d).

3.3. Cassava growth trend

The result in Table 1 presents statistical metrics of the cassava phenological development (PD) under regime fertilized and unfertilized treatments. PD such as plant height (Ph), plant width (PW), and leaf emergency (Le) are significant with the control treatment at $P > 0.001$. However, under the fertigation treatment, Ph, Le, and Ld are significant at $P < 0.001$, while Ph and Pw are significant at $P < 0.001$ but insignificant with leaf emergency and plant width. All the growth parameters (Ph, Le, Ld) indicated a highly significant level at 1% under organic treatment except plant width (PW) at $P > 0,023$ respectively.

Table 1 Statistical metrics for experimental treatments

Treatments	Phenology	Mean	Median	Variance	Std. Dev.	Std. Error	T-Test	Sign
Control	Plant height (Ph)	40.5	40.0	879.8	29.6	6.47	6.26	*0.001
	Plant width (Pw)	0.7	0.6	0.2	0.4	0.07	9.36	*0.001
	No of leaves (Le)	20.3	25.0	166.7	12.9	2.44	8.31	*0.001
	Leaf death (Ld)	9.6	4.5	117.5	10.8	2.05	4.76	0.001
Fertigation	Plant height (Ph)	91.3	76.0	3178.9	56.4	12.31	7.43	0.001
	Plant width (Pw)	4.1	1.9	57.2	7.5	1.43	2.86	0.001
	No of leaves (Le)	32.4	37.0	117.3	10.8	2.00	15.90	*0.001
	Leaf death (Ld)	13.8	9.5	153.7	12.4	2.30	5.90	*0.001
Fertilizer-NPK	Plant height (Ph)	101.3	111.0	159.0	39.9	8.70	12.10	*0.001
	Plant width (Pw)	5.6	2.0	145.0	12.1	2.28	2.46	0.207
	No of leaves (Le)	39.5	45.0	184.6	13.5	2.60	15.40	0.001
	Leaf death (Ld)	17.9	11.5	277.4	16.6	3.00	5.70	*0.001
Organic Fertilizer	Plant height (Ph)	80.9	81.0	1040.7	32.3	7.03	11.50	*0.001
	Plant width (Pw)	4.6	1.3	102.9	10.1	1.92	2.40	0.023
	No of leaves (Le)	30.3	37.0	175.7	13.2	2.50	12.10	*0.001
	Leaf death (Ld)	17.1	9.5	255.9	15.9	2.02	5.6	*0.001

3.4. Physiological dynamic of cassava under different treatment

Plant width (Pw) and plant height (Ph) under all the treatments indicated a positive and strong relationship. Under plot A (NPK treatment), the coefficient of determination (R2) is 0.8806, while in plots B, C, and D, the R^2 values are 0.9545, 0.9156, and 0.9146. Generally, fertilization improved plant growth and this implies that increases in plant height also led to increases in plant width, leaf area index (LAI), and storage root yield. Hence, it is clear that cassava yield prediction from the phenological relationship indicated that organic manure fertilizer may likely produce the largest cassava yield per hectare based on the analysis in Fig.2. The finding is similar to the study of [10;11] that revealed organic fertilizer has essential nutrients like zinc which is responsible for chlorophyll production, protein synthesis, and enzyme components which simulates plant growth and yield.
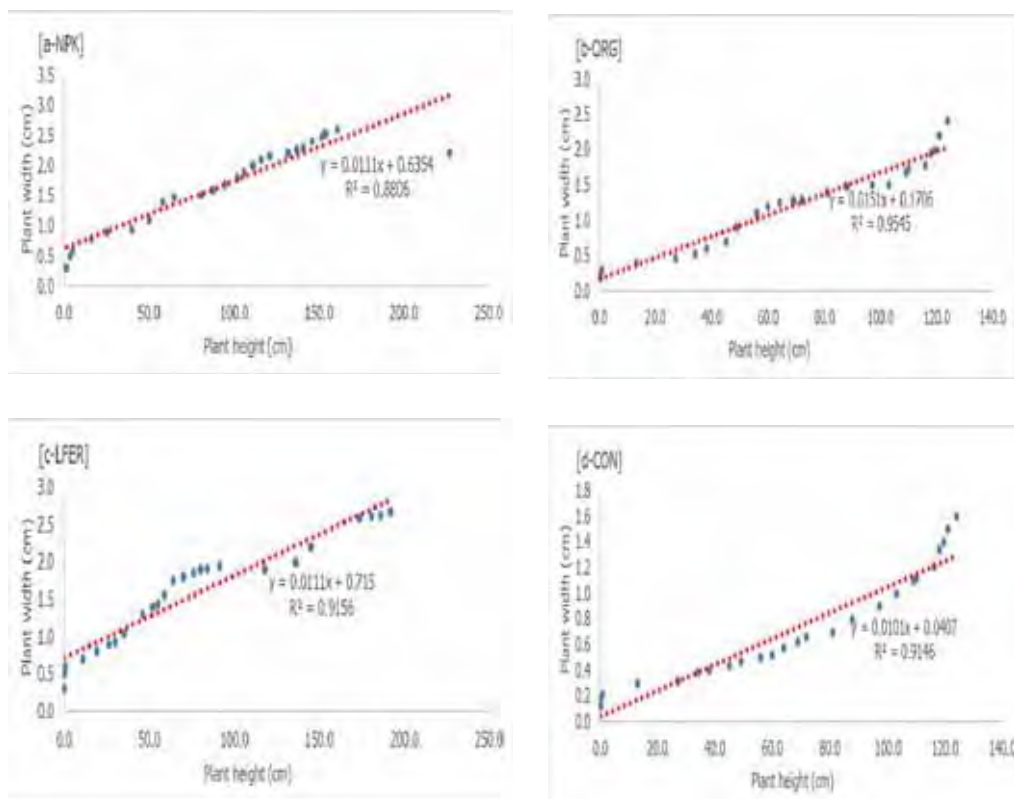
Figure 2. Plant width and plant height under NPK (a-NPK), organic fertilizer (b-org), fertigation (c-lfer), and control (d-CON)
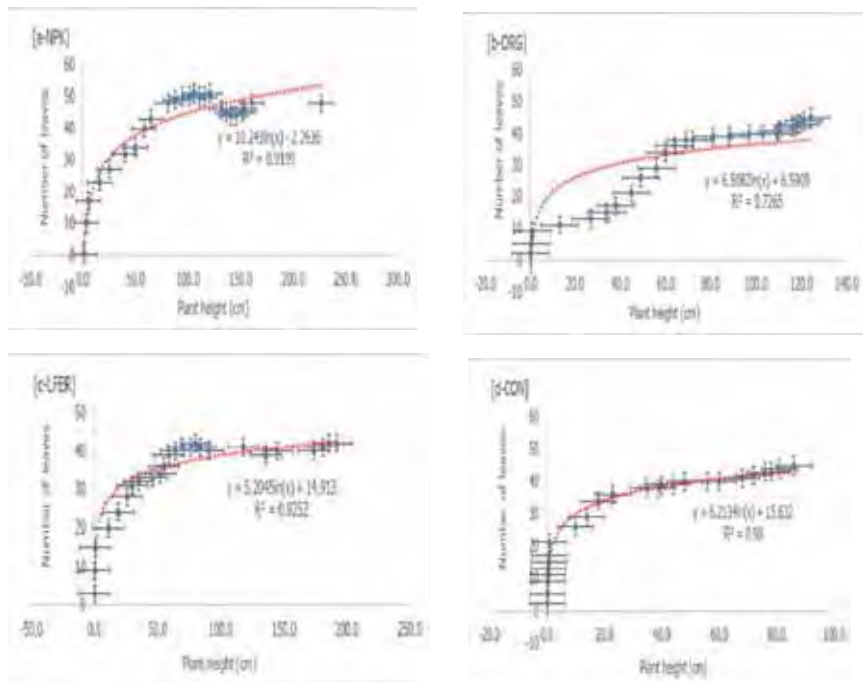
Figure 3. Leave number and plant height under NPK (a-NPK), organic fertilizer (b-org), fertigation (c-lfer), and control (d-CON).

Fig. 3 shows the relationship between the leaf emergency and plant height for each of the fertilized and uncontrolled treatments. The R^2 value under NPK treatment is 0.919, whereas, in fertigation, organic fertilizer, and unfertilized treatment, the R2 is 0.7265, 0.9252, and 0.980. The accumulation of potassium, nitrogen and phosphorous accumulation resulted in the early plant leaf emergency and an increase in cassava stem height and diameter. However, the observation under fertigation with the least R2 (0.7265) could probably be due to pest infection

4. Conclusion

The study investigates the effects of various fertilizer applications on the phenological development of cassava TMS 30573 variety compared to unfertilized treatment in Edo State. The overall results show that fertilization improves cassava growth and development. The investigation revealed that under fertigation and N.P.K fertilizer, plant height, plant width, and the number of

65

leaves suddenly increased from the early stage of cultivation, whereas a steady rise in physiological under organic fertilization was observed. Therefore, cassava growth under organic fertilizer tends to grow better due to its lower leaf death rate and increase in cassava root storage compared to fertigation, NPK, and unfertilized soil. Conversely, the use of NPK fertilizer and fertigation will lead to an early harvest and improved yield per hectare, but organic fertilizer can produce higher under longer periods. Hence the choice of fertilizer application somehow depends on the purpose of cultivation. For instance, if the cassava is to meet early market force, it is recommended to apply either fertigation or NPK fertilizer and for other purposes organic fertilizer is highly recommended.

References

[1] Luar M.P., Apolonio O., Arnold V., Dale F. C., Thomas O., *Cassava Response to Fertilizer Application,* Journal of Agricultural Science, 12(8), 2015, pp. 140-150.
[2] Hillock R.J., *Addressing the Sub-Saharan Africa,* Journal of Agriculture, 43(2), 2014, pp 16-20.
[3] Sungthonguises K., Laoken A., Polthanee A., *Effect of fertilizer application on growth and yield of Manihot esculenta Crantz*, Journal of Agricultural Science, 12(8), 2020, pp. 152-160.
[4] Agbaje G.O., Akinlosotu T.A., *Influence of NPK fertilizer on tuber yield of early and late-planted cassava in a forest alfisol of south-western Nigeria,* African Journal of Biotechnology, 3(10), 2004, pp. 547-551.
[5] Kayode O., *Effects of NPK fertilizer on tuber yield, starch contact and dry matter accumulation of white guinea yam (D. rotundata) in aforest alfisol of South Western Nigeria.* Experimental Agric., 21, 1985, pp. 389-393.
[6] Mwamba S., Kaluba P., Moualeu-Ngangue D., Winter E., Chiona M., Benson H. *Physiological and Morphological Responses of Cassava Genotypes to Fertilization Regimes in Chromi-Haplic Acrisols Soils. Agronomy,* 11, 2021, 1757.
https:// doi.org/10.3390/agronomy11091757
[7] CGIAR, 2015. Research for Results. *From roots to riches: improved cassava reduces poverty, hunger and climate change.*
https://library.cgiar.org/bitstream/han

[8] Biratu G.K., Elias E., Ntawunuhunga P., Sileshi G.W., *Cassava response to the integrated use of manure and NPK fertilizer in Zambia*. Heliyon, 4(8), 2018, pp 16-20.

[9] Okoth O., Yermiyahu U., *Improvement in Cassava Yield per Area by Fertilizer Application, Cassava-Biology, Production, and Use*, Andri Frediansyah, IntechOpen, 2021, DOI: 10.5772/intechopen.97366. Available from: https://www.intechopen.com/chapters/76250

[10] Anusontpornperm S., Nortcliff S., Kheoruenromne I., *Hardpan formation of some coarse-textured upland soils in Thailand. Paper Presented at Management of Tropical Sandy Soils from Sustainable Agriculture*, November 27-December 2005, Khon Kaen, Thailand.

[11] Cock J.H., Franklin D., Sandoval G., Juri P., *Ideal cassava plant for maximum yield. Crop* Sci. 1979, 19, 271–279. [CrossRef]

Addresses:

- **Mr Cletus Jude Odighi, Department of Agricultural & Bio Environ-mental Engineering, Auchi Polytechnic, Auchi,** odighicltus@gmail.com
  (*corresponding author*)

- **Engr (Dr) Yahaya Olotu, Department of Agricultural & Bio Envi-ronmental Engineering, Auchi Polytechnic, Auchi,** realyahaya@yahoo.com
  (*corresponding author*)

- **Edeki Ahmansi, Department of Agricultural & Bio Environmental Engineering, Auchi Polytechnic, Auchi**

- **Bada** Olatubosun, **Department of Statistics, Auchi Polytechnic, Auchi**

ynamic modeling of defecti e gears

Alin-Virgil Bloju, Zoltan-Iosif Korka*

Abstract. *The use of geared transmissions has a long history and a rich experience, which has allowed the development of an intense research activity that has led to modern design methods, mostly standardized and execution technologies that have become traditional. As the fundamental sciences have provided more and more in-depth and refined knowledge, namely performance algorithms of optimal synthesis, the design in the field of gear transmissions has evolved by integrating in the calculation methods a growing number of elements. of influence (materials, geometry, dimensional and shape deviations, heat treatments, kinematic, energetic, dynamic factors, etc.). Automated modeling and simulation currently allow the prediction of behavior - from all points of view of a transmission - during operation.*

Keywords*: transmissions, modeling, simulation, calculation methods*

1. Introduction

Due to high service load, harsh operating conditions or fatigue, there may be a cause for a number of different drive-pattern [1]. Drive failures are responsible for approximately 60% of speed damage [2]. Most of these defects occur in the form of cracks, exfoliations or chipping [2]. According to Syncrude Canada Ltd, fatigue crack and tooth tongs, known as pitting, were the most common defects[3]. Cracks are a non-lubrication fault mode while pinching is a type of lubrication-related fault [2]. Many researchers have shaped the cracks in the gear and their effect on the stiffness of the teeth [4]. However, research on python modeling and its effect on the stiffness of the year-grenadier is limited. This reference focuses on the fault modeling in the form of pinching and investigating its effect on the thimple gear rigidity a pair of gears with external teeth.

According to the American society for metals (ASM) manual [5], pinch occurs when fatigue cracks are established on the surface of the tooth or just below the surface of the tooth. The chipping is usually surface cracks caused by metal-metal contact of sparsness, or occurs due to the low thickness of the lubricant film. On high-speed gears, with smooth surfaces and good oil film thickness, splits can occur due to cracks that start under the surface of the teeth side faces. These cracks may be

induced by the inclusion in the gear material, which acts as tension concentrators and propagates below and parallel to the tooth surface. The pinches form when the cracks cross the tooth surface and cause the material to separate. When several pits join, a larger pit (or an exfoliation) forms. Pinching can also occur due to contamination of the lubricant with foreign particles. These particles create points of tension in the oil film, reducing its load and thus promoting the initiation of the pitting.

Tan et al [6] have experimentally measured the growth of the pectates at different loading levels. In order to ensure the bearing of the lubricating film, SAE 20W-50 type oil has been used within a relatively short time. But it has poor wear properties. The experimental tests were carried out at a rotational speed of 745 rpm at different torque moments: 220Nm, 147Nm and 73Nm.

For the conditions with higher applied torque moments (220Nm and 147Nm), the pitching was manifested over the full width of the teeth and was visible on most of the gear teeth. For the lower torque applied (73 Nm), the pitching spread over the width of the gear teeth at a much slower speed and was located only a few teeth. Prolonged operating time has spread splashes on the gear teeth. Figure 1 shows the time progression of the affected area from 6,3% to 41,7% of the gear tooth surface under the test conditions at 73 N m and 745 rpm.
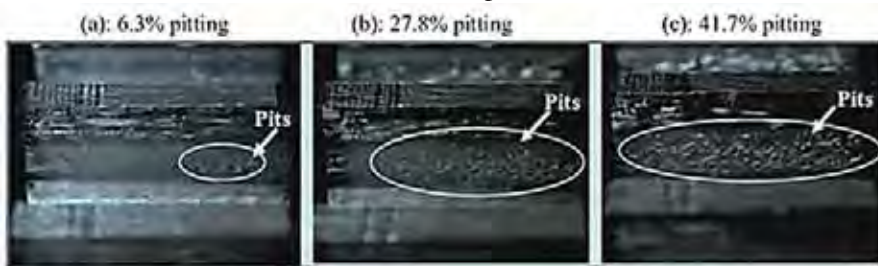
igure 1. Pinch rise under 73 N m and 745 rpm operating conditions [6].

Hand-produced ruffles, to simulate the tetching, were practiced on the teeth of the gear by several researchers to explore experimentally the symptoms corresponding to the defect of a box. Gelman et al [2] made tooth surface depths by artificial etching along the tilt line of a single tooth to imitate the pitching. Lee and colab. [7] created a pinch on the top dusty tooth, removing by processing a small part of the tooth material. Combet et al [5] manually produced pinches on the side of five teeth. The chipped teeth were not successive, but separated by six flawed teeth. Öztürk et al [8] they first created circular pinches on a tooth using an electro-erosion machine. Then they added several such recesses of the same size to the same tooth. Also, they were created on the deep neighboring teeth to materialize the initiation of the

pitting fault. Hoseini et al [3] artificially created circular chipping on a planetary gear, using electrical erosion processing. The number of pinches was varied to mimic slight, moderate and severe damage, as shown in Figure 2. In this study, we have also shaped the drive teeth pinching using circular holes, as was done in [3,8].

a.   b.   c.
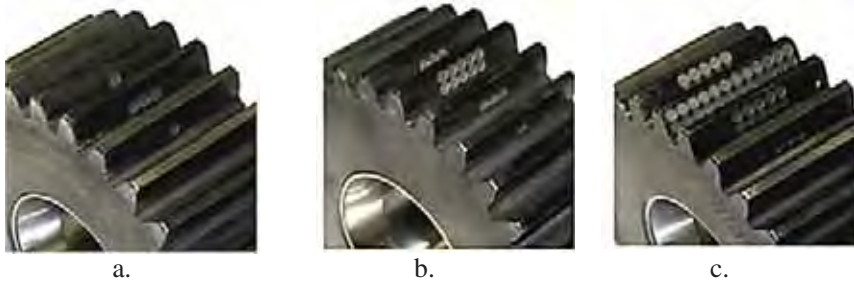
igure 2. Gears with a Pitting gear created by artificial cipas [3]
(a-pitting light, b-moderate; c-severe pitting)

Several researchers have investigated the effect of a single pinch or exfoliation on the limable stiffness of the gear over time. Chaar et al [9] and Choy et al respectively. [10] changed the form of variation of the rigidity of the gear to simulate the assembly defect. They did not provide any principle or equation to determine the rigidity of the gear as the pup-re defect increased. Cheng et al [16], Aboul-Seoud et al [12] respectively Chaar et al [1] analyzed the effect of a single stump on the variable stiffness in time of the gear. The pinypid was shaped as a rectangular shape, as shown in Figure 3. In Cheng's model, the length of the pinch a and the width of the pinch b were fixed, while the severity of the pups was determined by the depth of the pinching c. In the model of Aboul-Seoud, the pinched width b and the size of the pebure were fixed, while the severity of the pinch was determined by its length a.
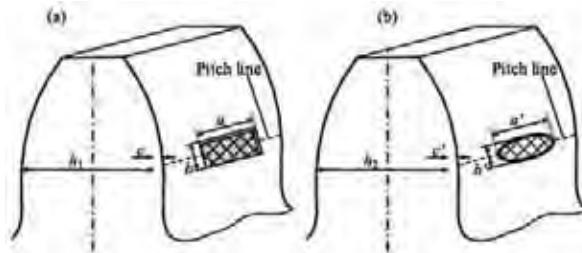
igure 3. Chipping patterns for assessment of rigidity of gear networks.(a);(b)

Chaar et al [1] developed two models in their study. One is the same as Cheng's model [11], while the other is the same as the model of Aboul-Seoud [12]. RAC et al [13] evaluated the effect of cipire/pyttering on the variation in time of the stiffness of a gear using the final element method. Only one pinch was shaped in elliptical form, as shown in Figure 3 (b). The size of the pinch was fixed, but the effect of the defect position on the rigidity of the gear was investigated. Three pinched positions were examined, namely the unipolar gear area (when a pair of teeth engages), the bipolar contact area (when two pair of teeth are in simultaneous mesh) and the transition area from unipolar to bipolar gear. MA and colab [14] have investigated the effect of tooth cidation on the rigidity of the gear. A unique rectangular exfoliation has been modeled and investigated the effects of width, length and exfoliation site on rigidity. All the above studies to assess the rigidity of the gear pair shall focus on the existence of a single pinch. Their methods cannot be used to assess the rigidity of the drive on wheels with several pits on one tooth. Yang and Lin's study [15] addressed this shortcoming. Later, Tian and colab [16] added the shear-care energy to the potential energy method. The potential energy method has been used to assess the rigidity of gears without defects [14,15], on gears with cracks [4,11,16], on single chipped gears on one tooth [12], on gears with a chipped tooth [16], on gears with a change in the tooth profile [14], plastic tooth-deflection gears [14] and alignment-fault gears (mounting) [18]. The energy method was used in this study to assess the stiffness of the anaging of a pair of external gears with several shells on one tooth.

In this research, the tooth-pinch was shaped as circular. The equations to test the rigidity of the drive with several pinches on one tooth have been inferred using the method of potential energy. A case study was then presented to illustrate the effect of pitting on the rigidity of an agrenal. Three levels of pitching severity have been modeled: Light, moderate and severe. Finally, the proposed method was compared to a model using the finished element to verify its accuracy.

2. Calculation of the stiffness of gears with Pitting

For this purpose, the stumps have been shaped in circular form, as in [3,8]. The potential energy method [15,17] was used to write the rigidity equations for the gear pair. In [15, 17] angre-naing is assumed to be free of friction, no manufacturing errors and no transmission error. The gear body is treated as rigid. The rigidity of the drive has been calculated according to the rotation angle of the drive. In the first stage, the rigidity equations of the gear were obtained with a single weird tooth. These equations were then extended to gears with more pinches per tooth.

2.1. Calculation of the stiffness of gears with a single shank on the tooth

For assessment of the rigidity of the drive without fault, in [17] the tooth was modeled as a beam in the bracket as shown in Figure 4(a).
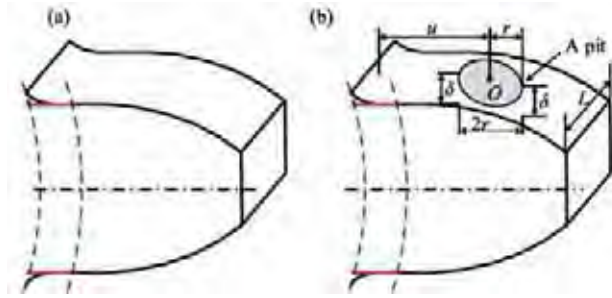
igure 4. Tooth modeling: (a) a tooth model for gears without damage and (b) the proposed single shank tooth model.

In the first stage, only one circular chip was considered as shown in Figure 4. The acre delimits the pinch is located on the side of the tooth. The position and size of a single shank can be fully characterized by three variables: *(u, r, δ)*, where u represents the distance between the tooth leg and the center of the circle of the peeling, r is the radius of the chip and $δ$ is the depth of the chip. The position of the chip in the direction $δ$ of the tooth (the width of the tooth is as shown in Figure 4.b) is not unrred in the proposed method.

2.2 Cur y shear and axial compressi eness

Depending on the properties of the volute curve, the action line of the two networks is tangent to the base circles of the gear and normal to the volute profile of the tooth. The action force F which is along the action line may be broken down into two orogonal forces F_a and F_b, as shown in Figure 5.

$$F_a = F \sin \alpha_1 \tag{1}$$
$$F_b = F \cos \alpha_1 \tag{2}$$

Applying the potential energy method, the bending, shear and axial compression energies stored in a tooth can be expressed as follows [15]:

$$U_b = \frac{F^2}{2k_b} = \int_0^d \frac{[F_b(d-x) - F_a h]^2}{2EI_x} \, dx, \tag{3}$$
$$U_s = \frac{F^2}{2k_s} = \int_0^d \frac{1.2F_b^2}{2GA_x} dx, \tag{4}$$

$$U_a = \frac{F^2}{2k_a} = \int_0^d \frac{F_a^2}{2EA_x} dx, \tag{5}$$
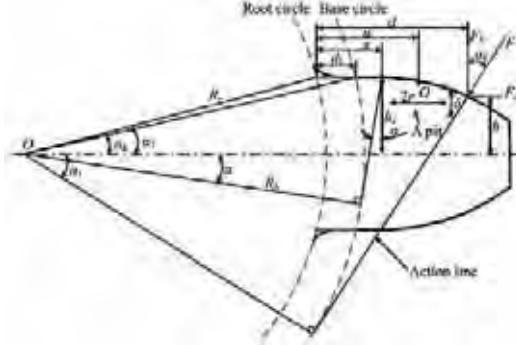
igure 5. Spring force on a single-shank gear tooth.

Where k_b, k_s and k_a represent the stiffness to bend, shear and axial compression respectively, E and G repretighten the young module and the shear module respectively, i.e. the distance between the point of contact of the gear and the center line of the tooth, d is the distance between the point of contact of the gear and the gear train's backside, A and I_x indicate the area and time of the inertia area of the tooth section, i.e. the distance from the root of the tooth x.

Depending on the characteristics of the curve, h, h_x, d, x, A_x and I_x of a perfect gear tooth can be expressed as follows [17]:

$$h = R_b[(\alpha_1 + \alpha_2)\cos\alpha_1 - \sin\alpha_1], \tag{6}$$

$$h_x = \begin{cases} R_b \sin\alpha_2, & \text{if } d_1 < x \leq d_1 \\ R_b[(\alpha + \alpha_2)\cos\alpha - \sin\alpha], & \text{if } d_1 < x \leq d' \end{cases} \tag{7}$$

$$d = R_b[(\alpha_1 + \alpha_2)\sin\alpha_1 + \cos\alpha_1] - R_r\cos\alpha_3, \tag{8}$$

$$x = R_b[(\alpha + \alpha_2)\sin\alpha + \cos\alpha] - R_r\cos a_3, \tag{9}$$

$$A_x = 2h_x L, \tag{10}$$

$$I_x = \frac{1}{12}(2h_x)^3 L = \frac{2}{3}h_x^3 L, \tag{11}$$

Where R_b, R_l and L represent the radius of the base circle, the radius of the root circle and the tooth width of the outer wheel, h, signifies the height of the section whose distance to the tooth root is x, α_2 is the angle of rotation of the teeth on the

73

base circle, α_3 describes the approximate angle of half of the root circle and α is the angle of rotation of the gear (see Fig.5). Angle expressions are given as follows [17].

$$\alpha_2 = \frac{\pi}{2Z} + \tan \alpha_0 - \alpha_0, \tag{12}$$

$$\alpha_3 = arcsin\left(\frac{R_b \sin \alpha_2}{R_r}\right), \tag{13}$$

Where Z is the number of teeth of the outer wheel and α_0 is the pressure angle.

For a hollow tooth gear, the expressions h, h_x, I_x și A_x are different from those given above for a perfect gear tooth. In addition, the contact width of the teeth is not constant L. We use ΔL_x și ΔA_x și ΔI_x to represent the reduction in the width of the teeth contact, the zone and the moment of the inertia zone of the teeth section, i.e. the distance to contact with the gear. For a single pipet model on a tooth, in Figure 4.b, the expression ΔL_x și ΔA_x și ΔI_x is as follows:

$$\Delta L_x = \begin{cases} 2\sqrt{r^2 - (u - x)^2}, & x \in [u - r, \ u + r] \\ 0, & others \end{cases} \tag{14}$$

$$\Delta A_x = \begin{cases} \Delta L_x \delta, & x \in [u - r, \ u + r] \\ 0, & others \end{cases} \tag{15}$$

$$\Delta I_x = \begin{cases} \frac{1}{12}\Delta L_x \delta^3 + \frac{A_x \Delta A_x (h_x - \delta/2)^2}{A_x - \Delta A_x}, & x \in [u - r, \ u + r] \\ 0, \end{cases} \tag{16}$$
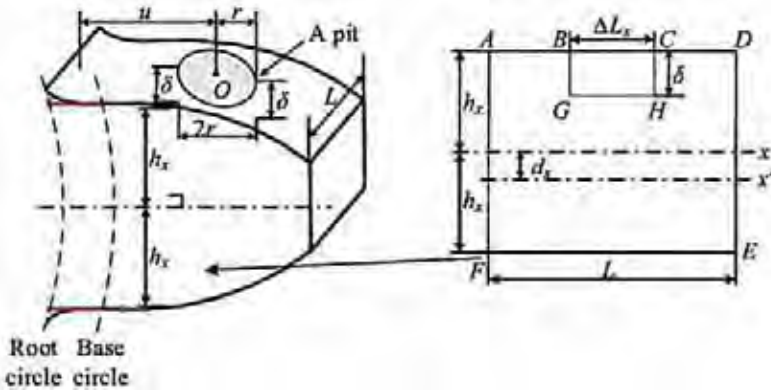
igure . A section of a single shank tooth.

Figure 6 shows a section of the tooth of a gear with a single shank. Let's use I_x și I_{x2} to represent the moments of inertia of the a-B-C-D-E-F and A-B-G-H-C-D-E-F tooth sections in relation to the x-axis respectively. Use I_x to represent the moment of inertia of the area in section A-B-G-H-C-D-E-F about the x' axis, where x' is the

center-center axis of the a-B-G-H-C-D-E-F. Folo-sind the theory of the parallel axis [15, 19], we can achieve:

$$I_x = I_{x2} + \frac{1}{12} \Delta L_x \delta^3 + \Delta L_x \delta \left(h_x - \frac{\delta}{2} \right)^2, \qquad (17)$$

$$I_{x2} = I_{x'} + (2h_x L - \Delta L_x \delta)(d_x)^2, \qquad (18)$$

By combining equations (17) and (18) we can obtain:

$$I_{x'} = I_x - \frac{1}{12} \Delta L_x \delta^3 - \frac{A_x \Delta A_x (h_x - \delta/2)^2}{A_x - \Delta A_x}, \qquad (19)$$

Use $\Delta I_x = I_x - I_{x'}$ to represent the reduction in the zones of inertia in the section of the tooth. We can obtain the equation (16).

Given a gear tooth with a circular hollow, we can calculate ΔL_x și ΔA_x and ΔI_x for any section of the teeth whose distance to the point of contact with the gear is x. In addition, pu-TEM notes from EC. (5) ca x is a function of the angle of rotation of speed (noted with the ά). Therefore, for any given angle of rotation, we can calculate the values ΔL_x and ΔA_x and ΔI_x using EC. (14), (15) and (16) respectively. In addition, ΔL_x and ΔA_x and ΔI_x are all independant of the position of the chip in the direction of the width of the tooth. Therefore, the position of the chip along the width of the tooth is not required in these equations.

Replacement of equation (1), (2), (6) to (9), (14) to (16) in (3), the bending rigidity of an external gear tooth with a circular toothpick can be obtained:

$$\frac{1}{k_b} = \frac{\left[1 - \frac{(Z - 2,5)\cos \alpha_1 \cos \alpha_3}{N \cos \alpha_0} \right]^3 - (1 - \cos \alpha_1 \cos \alpha_2)^3}{2EL \cos \alpha_1 \sin^3 \alpha_2}$$

$$+ \int_{-\alpha_1}^{\alpha_2} \frac{3\{1 + \cos \alpha_1 [(\alpha_2 - \alpha)\sin \alpha - \cos \alpha]\}^2 \ (\alpha_2 - \alpha)\cos \alpha}{E\left(2L[\sin \alpha + (\alpha_2 - \alpha)\cos \alpha]^3 - 3\frac{\Delta Ix}{R_b^3} \right)} d\alpha. \qquad (20)$$

Replacing equations (1), (7) to (10), (14) to (15) in equation (5), the axial compressive stiffness of an external gear tooth can be obtained with a circular toothpick:

$$\frac{1}{k_s} = \frac{1.2(1 + v)\cos^2 \alpha_1 \left(\cos \alpha_2 - \frac{Z - 2.5}{Z \cos \alpha_0} \cos \alpha_3 \right)}{EL \sin \alpha_2} +$$

$$\int_{-\alpha_1}^{\alpha_2} \frac{1.2(1 + v)(\alpha_2 - \alpha)\cos \alpha \cos^2 \alpha_1}{E\left(L[\sin \alpha + (\alpha_2 - \alpha)\cos \alpha] - \frac{\Delta A_x}{2R_b} \right)} d\alpha. \qquad (21)$$

Replacing equations (1), (7) to (10), (14) to (15) in equation (5), the axial compressive stiffness of an external gear tooth can be obtained with a circular toothpick:

75

$$\frac{1}{k_a} = \frac{sin^2\,\alpha_1\left(\cos\alpha_2 - \frac{Z-2.5}{Z\cos\alpha_0}\cos\alpha_3\right)}{2EL\sin\alpha_2} + \int_{-\alpha_1}^{\alpha_2} \frac{(\alpha_2 - \alpha)\cos\alpha\,sin^2\,\alpha_1}{E\left(2L[\sin\alpha + (\alpha_2\,\alpha)\cos\alpha] - \frac{\Delta A_x}{R_b}\right)}\,d\alpha. \quad (22)$$

Expression ά1, is given [18]:

$$\alpha_1 = \theta - \frac{\pi}{2Z_1} - \tan\alpha_0 + \alpha_0 +$$

$$\tan\left[arccos\frac{Z_1\cos\alpha_0}{\sqrt{(Z_2+2)^2 + (Z_2+Z_1)^2 - 2(Z_2+2)(Z_2+Z_1)cos\left(arccos\frac{Z_2\cos\alpha_0}{Z_2+2} - \alpha_0\right)}}\right] \quad (23)$$

Where Z_1 și Z_2 represent the number of teeth in the box, and respect θ is the gearbox's SI rotation angle and we can define $\theta = 0$ when the pinched tooth starts to mesh.

With regard to the pair tooth of the rib tooth, equations (20) to (22) can still be used to calculate the rigidity of its network as long as it is an external gear tooth. However, the expression of α_1 is expressed as [16]:

$$\alpha_1 = \tan\left(arccos\frac{Z_2 - \cos\alpha_0}{Z_2+2}\right) - \frac{\pi}{2Z_2} - \tan\alpha_0 + \alpha_0 - \frac{Z_1}{Z_2}\theta. \quad (24)$$

2.3. ertzian contact stiffness

From the results obtained by Yang and Sun [11], the radio contact stiffness, for a pair of perfect external wheels, is linearized to a constant throughout the whole line of action, irrespective of both the contact position and the depth of the interpenetration.

$$k_h = \frac{\pi EL}{4(1-v^2)'} \quad (25)$$

Where E, L, v, the boardweight denotes the mode of Young, and the width of the tooth and the Poisson report respectively.

For a pair of toothed wheels, the contact width of the tooth is L-ΔL_x and not L. If the torque meter is used for the measurement of the torque meter, the torque meter shall be set to a minimum of 5 % of the input torque.

$$k_h = \frac{\pi E(L - \Delta L_x)}{4(1-v^2)}, \quad (26)$$

Where Ddlx, is the reduction in the width of contact between the teeth (see equation (14).

2.4. ifference in stiffness of the gear train with se eral tooth pitting

In section 1, we derived the rigidity equations of the drive network with a single stump. These equations can be easily extended to gears with several circular splashes on one tooth. As long as the circular splits do not overlap with each other

76

and all the circles are within the area of the tooth surface, the hertzian contact strength, bending rigidity, shear stiffness and axa-to-a compressive stiffness can be obtained by equations (27), (28), (29) and (30) respectively:

$$k_h = \frac{\pi E\left(L - \sum_1^N \Delta L_{xj}\right)}{4(1 - v^2)}, \tag{27}$$

$$\frac{1}{k_b} = \frac{\left[1 - \frac{(Z - 2.5)\cos \alpha_1 \cos \alpha_3}{Z \cos \alpha_0}\right]^3 - (1 - \cos \alpha_1 \cos \alpha_2)^3}{2EL \cos \alpha_1 \sin^3 \alpha_2}$$
$$+ \int_{-\alpha_1}^{\alpha_2} \frac{3\{1 + \cos \alpha_1[(\alpha_2 - \alpha)\sin \alpha - \cos \alpha]\}^3 (\alpha_2 - \alpha)\cos \alpha}{E(2L [\sin \alpha + (\alpha_2 - \alpha)\cos \alpha]^3) - 3\sum_1^N \frac{\Delta I_{xj}}{R_b^3}} d\alpha, \tag{28}$$

$$\frac{1}{k_s} = \frac{1.2(1 + v)\cos^2 \alpha_1\left(\cos \alpha_2 - \frac{Z - 2.5}{Z \cos \alpha_0}\cos \alpha_3\right)}{EL \sin \alpha_2}$$
$$+ \int_{-\alpha_1}^{\alpha_2} \frac{1.2(1 + v)(\alpha_2 - \alpha)\cos \alpha \cos^2 \alpha_1}{E\left(L[\sin \alpha + (\alpha_2 - \alpha)\cos \alpha] - 0.5\sum_1^N \frac{\Delta A_{xj}}{R_b}\right)} d\alpha, \tag{29}$$

$$\frac{1}{k_a} = \frac{\sin^2 \alpha_1\left(\cos \alpha_2 - \frac{Z - 2.5}{Z \cos \alpha_0}\cos \alpha_3\right)}{2EL \sin \alpha_2} + \int_{-\alpha_1}^{\alpha_2} \frac{\left(\alpha_2 - \frac{Z - 2.5}{Z \cos \alpha_0}\cos \alpha_3\right)}{E\left(2L[\sin \alpha + (\alpha_2 - \alpha)\cos \alpha] - \sum_1^N \frac{\Delta A_{xj}}{R_b}\right)} d\alpha, \tag{30}$$

Where N is the number of circular toothcuts on a tooth surface; ΔL_{xj}, ΔA_{xj} and ΔI_{xj} is the reduction of the tooth contact width, area and moment zone of inertia caused by the circular sheet, ΔL_{xj}, ΔA_{xj} and ΔI_{xj} can be obtained using equations (14), (15) and (16) respectively.

Users may apply these equations to assess the rigidity of the gear train at any given ro-speed angle, even if they are not familiar with the theory of these networks.

3. Conclusions

Fault feature analysis of gear tooth spall plays a vital role in gear fault diagnosis. Knowing the characteristic of fault features and their evolution as a gear tooth fault progresses is key to fault severity assessment. This thesis provides a comprehensive (both theoretical and experimental) analysis of the fault vibration features of a gear transmission with progressive localized gear tooth pitting and spalling. A dynamic model of a one-stage spur gear transmission is proposed to analyze the vibration behavior of a gear transmission with tooth fault. The proposed dynamic model considers the effects of Time Varying Mesh Stiffness (TVMS), tooth surface roughness changes and geometric deviations due to pitting and spalling, and also incorporates a time-varying load sharing ratio, as well as dynamic tooth contact friction forces, friction moments and dynamic mesh damping ratios. The gear dynamical model is validated by comparison with responses obtained from an

experimental test rig under different load and fault conditions. In addition, several methods are proposed for the evaluation of the TVMS of a gear pair with tooth spall(s) with curved bottom and irregular shapes, which fills the current research gap on modelling tooth spalls with irregular shapes and randomly distribution conditions. Experiments are conducted and the fault vibration features and their evolution as the tooth fault progresses are analyzed. Based on feature analysis, a new health indicator is proposed to detect progressive localized tooth spall.

References

[1] Chaari F., Baccar W., Ab bes M.S., Haddar M., Effect of spalling or tooth breakage on gearmesh stiffness and dynamic response of a one-stage spur gear transmission, *Eur.J. Mech. A Solids,* 27(4), 2008, pp. 691-705.

[2] Gelman L., Zimroz R., Birkel J., Leigh-Firbank H., Simms D., Waterland B., Whitehurst G., Adaptive vibration condition monitoring technology for local tooth damage in gearboxes, *Insight Non-Destr. Test. Cond. Monit.* 47(8), 2005, pp. 461-464.

[3] Hoseini M.R., Zuo M.J., *iterature review for creating and uantifying faults in planetary gearboxes*, Technical Report, Reliability Research Lab, Mechanical Department, University of Alberta, 2009.

[4] Ma H., Zeng J., Feng R., Pang X., Wang Q., Wen B., Review on dynamics of cracked gear systems, *Eng. Fail. Anal.* 55, 2015, pp. 224-245.

[5] Blau P.J., *ASM andbook, Vol. 18 - Friction, lubrication, and wear technology*, ASM International, 1992.

[6] Tan C.K., Irving P., Mba D., A comparative experimental study on the diagnostic and prognostic capabilities of acoustics emission, vibration and spectrometric oil analysis for spur gears, *Mech. Syst Signal Process*. 21(1), 2007, pp. 208-233.

[7] Ozti.irk H., Sabuncu M., Yesilyurt I., Early detection of pitting damage in gears using mean frequency of scalogram, *J. Vib. Control* 14(4), 2008, pp. 469-484.

[8] Choy F.K., Polyshchuk V., Zakrajsek J.J., Handschuh R.F., Townsend D.P., Analysis of the effects of surface pitting and wear on the vibration of a gear transmission system, *Tribol. Int.* 29(1), Feb. 1996, pp. 77-83.

[9] Abouel-seoud S.A., Dyab E.S., Elmorsy M.S., Influence of tooth pitting and cracking on gear meshing stiffness and dynamic response of wind turbine gearbox, *Int. J. Sci. Adv. Technol*. 2(3), 2012, pp. 151-165.

[10] del Rincon A.F., Viadero F., Iglesias M., de-Juan A., Garcia P., Sancibrian R., *Effect of cracks and pitting defects on gear meshing*, Proc. Inst. Mech. Eng. Part CJ. Mech. Eng. Sci. 226(11), 2012, pp. 2805-2815.

[11] Ma H., Li Z., Feng M., Feng R., Wen B., Time-varying mesh stiffness calculation of spur gears with spalling defect, *Eng. Fail. Anal*. 66, 2016, pp. 166-176.

[12] Yang D.C.H., Lin J.Y., Hertzian damping, tooth friction and bending elasticity in gear impact dynamics, *J. Mech. Des*. 109(2), 1987, pp. 189-196.

[13] Tian X., Zuo M.J., Fyfe K.R., *Analysis of the vibration response of a gearbox with gear tooth faults*, In: Proceedings of the Presented at the 2004 ASME International Mechanical Engineering Congress and Exposition, Anaheim, California USA, 2004, pp. 785-793.

[14] Liang X., Zuo M.J., Patel T.H., *Evaluating the time-varying mesh stiffness of a planetary gear set using the potential energy method*, Proc. Inst. Mech. Eng. Part CJ. Mech. Eng. Sci. 228(3), 2014, pp. 535-547.

[15] Chen Z., Shao Y., Dynamic simulation of spur gear with tooth root crack propagating along tooth width and crack depth, *Eng. Fail. Anal*., 18(8), 2011, pp. 2149-2164.

[16] Pandya Y., Parey A., Failure path based modified gear mesh stiffness for spur gear pair with tooth root crack, *Eng. Fail. Anal*. 27, 2013, pp. 286-296.

[17] Chen Z., Shao Y., Mesh stiffness calculation of a spur gear pair with tooth profile modification and tooth root crack, *Mech. Mach. Theory*, 62, 2013, pp. 63-74.

[18] Cao Z., Shao Y., Zuo M.J., Liang X., *Dynamic and uasi-static modeling of planetary gear set considering carrier misalignment error and varying line of action along tooth width*, Proc. Inst. Mech. Eng. Part CJ. Mech. Eng. Sci. 229(8), 2015, pp. 1348-1360.

[19] Sainsot P., Velex P., Duverger O., Contribution of gear body to tooth deflections - a new bidimensional analytical formula, *J. Mech. Des.* 126(4), 2004, 748.

Addresses:

- Drd.Eng. Alin-Virgil Bloju, Babeș-Bolyai University, Faculty of Engineering, Piața Traian Vuia, nr. 1-4, 320085, Reşiţa, alin.bloju@ubbcluj.ro
- Assoc. Prof. dr. eng. habil. Zoltan-Iosif Korka, Babeș-Bolyai University, Faculty of Engineering, Piața Traian Vuia, nr. 1-4, 320085, Reşiţa, zoltan.korka@ubbcluj.ro
(* corresponding author)

An o er iew about the feasibility
of the hydrogen power plants

Marius Savu Lolea, Andrea Amalia Minda*
Emeric Remus Szabo, Daniela Tabita Negrea

Abstract. *In order to make the decision to implement a project from any domain, several aspects must be analyzed in the preliminary stage, leading to the justification of the practical realization of the project. Feasibility is based on technical-economic criteria but also involves other impact factors, such as social and ecological. In the case of hydrogen, there are not many countries with experience in the field, but in the future it is expected that hydrogen technologies will expand, from production, transport, storage, distribution and use. There are more and more factors that encourage the development of hydrogen projects and the funding proposed through European environmental agreements is a real challenge for specialists. Therefore, the authors of the paper aimed to analyze several aspects of the feasibility of hydrogen production and storage projects with the identification of implementation conditions: benefits, efficiency, costs, sources of funding, entities involved, constraints or legislative framework.*

Keywords*: hydrogen projects, feasibility, economic criteria, funding*

1. Introduction

As it follows from the strategy and documents of the European Union (EU) administration and legislature, on the road to a climate-neutral Europe and a cleaner planet in general, it is important to rethink energy supply and create a fully integrated energy system under the European Green Pact [12]. The green transition of the EU economy should provide access to clean, safe and affordable energy for companies and final consumers. But it is not an easy task because as energy production and consumption generated 75% of EU greenhouse gas emissions in 2018, and it still depends on imports for 58% of total energy, especially oil and gas [17]. Beyond supporting the implementation of renewable energy sources at European level, a new challenge has appeared, due to several advantages: the hydrogen.

Hydrogen can contribute to the storage of electricity and can be used as fuel in transportation or building heating as it is non-polluting. However, for the most part,

obtaining it today is generally done through polluting processes.These processes must be eliminated by gradually moving to comprehensive ecological processes for the production of "green" hydrogen. Green hydrogen, produced from renewable energy resources, is considered one of the solutions for countries around the world to achieve climate neutrality by 2050, the main challenges for its production being high costs and resource availability. In Romania, the hydrogen is currently used mainly in the chemical industry, in refineries and for ammonia production. It is also used in welding processes. Given the need to reduce the harmful environmental impact, it is important that countries around the world start developing projects quickly to implement the necessary hydrogen infrastructure. Future projects require high material, human or financial investment and public-private partnerships and non-reimbursable financing must be used, which are available to EU countries, and a significant number of legislation acts are being developed to support hydrogen production and storage facilities. As in other economic sectors, before obtaining funding, the technical-economic possibilities for practical implementation of projects must be identified, through a preliminary feasibility study by applying specific analysis criteria and impact factors on human society and the natural environment.

2. ydrogen properties.   ydrogen storage problems

Hydrogen is the lightest of all gases. It is very often found in nature in compounds with other elements and is the most abundant element in the universe. Hydrogen is a component of water, minerals and acids, as well as an essential part of all hydrocarbons and essentially all other organic substances being the third element of compounds to spread in the earth's crust. In fact, 98% of the known universe - especially the sun and stars - are made of hydrogen. Hydrogen cannot be found in nature in its pure state, so it cannot be mined in the same way as oil or coal. Hydrogen must be extracted from chemical compounds [18].

Hydrogen is a substance that comes in gaseous form at normal atmospheric temperature and pressure. In fact, hydrogen is found in solid form up to about 14 K (- 259 $^\circ$C) when it passes into the liquid phase and at about 20 K (- 253 $^\circ$C) it vaporizes and passes into the gas phase. Under normal conditions of pressure and temperature, hydrogen has a very low density of about 0.08988 kg / Nm^3 [18].

At present, hydrogen is produced in large quantities from fossil fuels by steam reforming of natural gas and partial oxidation of coal or heavy hydrocarbons. These methods can take advantage of economies of scale and are currently the cheapest and most established techniques for the large-scale production of hydrogen [3]. They can be used in the short to middle term to meet hydrogen fuel demand and enable the proving and testing of technologies related to hydrogen production, storage, distribution, safety and use. However, in the long term, it is clearly unsustainable that the hydrogen economy is driven by hydrogen derived from hydrocarbons. The

manufacture of hydrogen from fossil fuels using reformation and gasification processes always yields carbon dioxide as a by-product [3]. A more promising route of hydrogen production without carbon dioxide release is the high-temperature pyrolysis (decomposition in the absence of oxygen) of ydrocarbons, biomass and municipal solid waste into hydrogen and (solid) carbon black accompanied by its industrial use and/or easy sequestration. At present, the cost of this process is significantly higher than that of steam reforming of natural gas [3].

Nuclear hydrogen production can be made by lowtemperature electrolysis, high-temperature electrolysis, thermochemical, and hybrid processes. Low temperature electrolysis is simply splitting water into hydrogen and oxygen using electrical power which possesses a high amount of electricity consumption (~1,23 V/mol H_2O)[4]. High-temperature electrolysis, which can also be called steam electrolysis, is a method to split steam into hydrogen and oxygen. Electrical energy requirement for splitting steam is lower than that of liquid water, and higher efficiencies can be obtained by using heat as a part of energy source [4].

Regardless of the source from which hydrogen is extracted, a production process is needed and it involves energy consumption. The great advantage, however, is that for the generation of hydrogen it is not strictly necessary to use energy from fossil fuels, but you can use electricity from renewable sources (RES): hydraulic, solar, wind, geothermal, biomass [1]. The scheme of a production system based on electrolysis and storage of hydrogen energy from RES, through fuel cells, is shown in Figure 1[5].
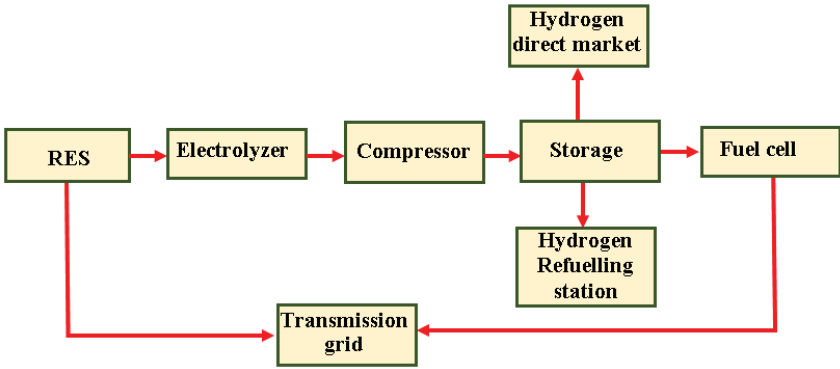
igure 1. Scheme of a renewable hydrogen storage system

Hydrogen can be stored in all forms of aggregation but problems can occur when an explosive mixture occurs in the presence of air, because hydrogen, mixed with oxygen in a proportion of 5–85%, is flammable and therefore dangerous [1]. When stored under pressure in metal containers, special care must be taken to remove leaks.

A means of storing hydrogen is ammonia (NH_3), from which it can be released by a catalytic reforming process.

In recent years, other storage techniques have been developed, using graphite nanotubes. Hydrogen is stored between layers of nanotubes with diameters of 5–10 nm. Thus, about 30 liters of hydrogen are stored for every gram of graphite. The disadvantage is that the charging time of a 25 liter tank is 4÷24 hours and can only be done 4-5 times [1]. Hydrogen can be stored in metal-organic networks using a series of synthetic porous materials, polymers with attached titanium atoms, glass microspheres of 10–300 m [1]. The storage capacity of hydrogen by different methods is shown in Table 1.

Table 1. Hydrogen storage capacity by different methods

Storage type	Moles of hydrogen/cm^3
H_2 gas at 100 bar	0,81
Liquid H_2	7,0
Hidride MgH_2	11,1

Table 2 shows some of the solid storage properties of hydrogen in magnesium compounds called hydrides. Mg. Other hydrides are sodium, lithium or calcium and aluminum or boron.

Table2. Hydrogen storage properties in Mg-based alloys

Material type	Minimum mass storage capacity H_2[%]	Bearing pressure at 300ºC [atm]	Temperature [ºC]	Reaction kinetiks [min]	Reaction Enthalpy [kJ/mol H_2]
$Mg_{75}Ti_{12}Fe_4Ni_8$	4,75	Abs 1,5 desorb.1,5	300÷360	1,36,6	73,67
$Mg_{75}Ti_{12}Fe_8Ni_4$	5,33	Abs 1,4 desorb.1,2	300÷360	1,14,5	71,79

One form of intense hydrogen storage discussed by specialists in the last period is that in gaseous form in underground caverns and especially in disused salt mines. A research project in this sense is being developed in partnership and in Europe, in which Romania also participates and which is called HyUnder [10]. The project will be briefly presented in Chapter 4 of this paper.

3. Cost of hydrogen. Technical and economic criteria of analysis

The feasibility analysis of hydrogen projects aims to identify potential constraints and appropriate solutions in terms of technical, economic, regulatory and managerial aspects. Typical feasibility reports for major infrastructure should include information on: demand analysis, available technology, production plan, staffing

requirements, project size, location, physical inputs, timing and implementation, deployment and financial planning phases etc [13].

There are many decision-support instruments in the scientific literature that can perform an impact assessment of an hydrogen energy system. The most widely financial applied decision support methods are life-cycle assessment (LCA), cost-benefit analysis (CBA) and multi-criteria decision analysis (MCDA)[2].

From a technical point of view, for the first time in electrolysis processes, the specific energy consumption on component terms must be analyzed in order to determine the yield of the transformation of the detected substance into hydrogen. Thus, the financial criterion will be linked by evaluating the costs of incoming electricity with the amount of hydrogen at the exit from the electrolysis plant. This will establish the profitability of this process. In most electrochemical reactions, the amount of electricity consumed in electrolysis is higher than the theoretical one (corresponding to Faraday's law, which defines them) because the losses in the process must be covered [9].

The specific energy consumptions are obtained by reporting the amount of energy actually used in the mass, respectively the volume of product obtained in electrolysis and can be expressed with the formulas [9]:

$$CSE_{mass} = \frac{U_{pr} \cdot I \cdot t}{m} \tag{1}$$

and

$$CSE_{volume} = \frac{U_{pr} \cdot I \cdot t}{V} \tag{2}$$

where: m – practical mass of product obtained; V – the volume of hydrogen released.

In order to be able to appreciate the degree of discrepancy between the theoretical and practical values (there are losses and secondary reaction substances), the notion of transformation yield was introduced, with several components one being the electrical current yield η_c, which is calculated with the relationship [9]:

$$\eta_c = \frac{Q_t}{Q_p} \cdot 100, \ \% \tag{3}$$

In which: Q_t – theoretical Quantity of electricity; Q_p – the Quantity of electricity practically consumed.

The electricity yield can also be calculated depending on the amount of transformed substance:

$$\eta_c = \frac{m_p}{m_p} \cdot 100, \ \% \tag{4}$$

where: m_p – the mass of product practically obtained; m_t – theoretical mass of product.

It is still possible to calculate the energy, noted with simbo η_W, which expresses the ratio between the quantity of theoretically required electricity, W_t and of electric energy practically consumed, W_p, in an electrochemical reaction:

$$\eta_W = \frac{W_t}{W_p} \cdot 100, \ \% \tag{5}$$

Replacind with $W = V \cdot I \cdot t = W \cdot Q$, results:

$$\eta_W = \frac{V_t \cdot Q_t}{V_p \cdot Q_p} \cdot 100 = \frac{Q_t}{Q_p} \cdot 100, \ \% \tag{6}$$

In which: V_t – theoretical electrolysis voltage (decomposition voltage); V_p – work voltage (terminal voltage).

The third type of yield is the voltage yield, which can be calculated with the formula:

$$\eta_W = \frac{U_{min}}{U_{pr}} \cdot 100 = \frac{E}{U_{pr}} \cdot 100, \ \% \tag{7}$$

where: U_{min} – minimum electrolysis voltage; U_{pr} – practical working voltage;
E – the electromotive voltage of the considered system.

The main financial indicators specific to investments in hydrogen project achievement, are [7]:

a). Total costs of investments. As a first step in financial evaluation of project, the total costs of investments(I) included direct(I_d) and indirect costs(I_i):

$$I \quad I_d \quad I_i \tag{8}$$

Where, I_d reprezented the cost of materials and equipments and I_i is related to design, authorization, project's check, unforeseable expenses etc;

b).Yearly total cost: Can be calculated using the following relationship:

$$C_{tot} = \frac{I}{D_a} + C_p \tag{9}$$

In which D_a is analysis period, in years and C_p – the cost of production;
In the energy domain, the yearly costs of production can be assessed using the next formula:

$$C_p \quad C_{comb,t} \quad C_{EE} \quad C_{OM \ R} \tag{10}$$

Where, $C_{comb,t}$ represents the early expenses with fuel; CEE- are the yearly expenses with electric energy; $C_{OM\&R}$ – The costs of operating, maintnance and repairs whitout fuel involvment;

c). Total costs C, are expressed with the following formula:

$$C \quad I \quad C_p \, D_a \tag{11}$$

85

d). Costs of hydrogen, is calculated as a ratio between the yearly total costs and the production capacity in physical measuring units, namely[7]:

$$C_H = \frac{c_{tot}}{Q_f} \tag{12}$$

Where, C_H reperesents the yearly costs of Hydrogen and Qf – the production capacity in physical measuring units;

e). Specific investment. Is calculated as a ratio between total investment and the production capacity in prhisical measuring units, namely[7]:

$$i_s = \frac{I}{Q_f} \tag{13}$$

in which, i_s represent the specific investment .

To assess the cash flow resulting from hydrogen production, the Hydrogen Levelized Cost indicator is used - $PC_{Leverized}$ - which is a measure of the current average net cost of hydrogen production for a plant. It is used to plan investments and to compare different methods of hydrogen production. It is calculated as the ratio of all costs updated over the analysis period of a plant divided by a weighted amount of hydrogen delivered.

For the calculation of the levelized production costs of hydrogen, can use the next standard formula, given in [6]:

$$PC_{Leverized} = \frac{\sum_{t=1}^{n} \frac{C_{CapEx,t} + C_{OpEx,t} + C_{Elec,t}}{(1+d)^t}}{\sum_{t=1}^{n} \frac{m_t}{(1+d)^t}} \tag{14}$$

The terms from Equation (1) have the following meanings:

n- analysis period(years), t – year index, $C_{CapEx,t}$ – Costs of capital expeditures in year t; $C_{OpEx,t}$ – Costs of operation expeditures in year t; $C_{Elec,t}$ – Costs of electricity in year t; m_t – Mass of produced hydrogen in year t; d – Asumed discounting factor(5%).

Once the investment costs, revenues and operating costs and sources of funding have been determined, it is possible and useful to determine the financial sustainabi-lity of the project [13]. A hydrogen project is financially sustainable when it does not involve the risk of running out of money in the future. Project beneficiaries must closely monitor how, over the time horizon of the project, the sources of funding (including income and any cash transfers) will consistently correspond to the required periodic payments. Sustainability occurs if the cumulative net flow of cash receipts and payments generated is positive for all considered years.

The indicators needed to test the financial performance of the hydrogen project are:

- The Financial Net Present Value of project (FNPV),
- Financial Internal Rate of Return (FIRR).

FNPV is defined as the amount that results when the planned investment and operating costs of the project (updated as appropriate) are deducted from the present value of the expected revenue. [13]:

$$FNPV \quad \sum_{t=0}^{n} a_t \cdot S_t = \frac{S_0}{(1+i)^0} + \frac{S_1}{(1+i)^1} + \cdots + \frac{S_n}{(1+i)^n} \qquad (15)$$

Where S_t is the cash flow balance at time t, a_t - the financial factor chosen for the update at time moment t and i -the reference discount rate.

4.   ydrogen pro ects at national le el.   unding sources

If they meet the conditions for eligibility and financial score, hydrogen-based projects can be funded from several non-reimbursable sources. Hydrogen plants can be included in the infrastructure, environmental protection, energy efficient and renewable energy program. At the same time, the financing of the project on hydrogen can be done through guaranteed bank funds or through public-private partnerships.

The European Commission (EC) launched on 8 July 2020 the strategy for integrating hydrogen production, storage and use into the energy system, as part of Green Deal [11]. Through "Hydrogen strategy for a climate-neutral Europe", EC targets 38 actions on an integrated energy system, in which hydrogen contributes to the decarbonisation of industry, transport, electricity production and buildings across countries of EU.

Also, through the European Hydrogen Strategy, the European Commission has set certain targets for the use of hydrogen, funded and achieved in stages, as follows [11]:

• From 2020 to 2024, support the installation of at least 6 gigawatts of renewable electricity electrolysis plants in the EU and the production of up to one million tonnes of renewable hydrogen;

• From 2025 to 2030, hydrogen must become an intrinsic part of the integrated European energy system, with at least 40 gigawatts of electrolysis plants generated by RES in hydrogen and the production of up to ten million tonnes of renewable hydrogen in the EU;

• In the period 2030-2050, renewable hydrogen technologies are encouraged to reach maturity and to be widely implemented in all sectors difficult to decarbonise.Through the project called „HyUnder", worth 2 million euros, carried out over a period of 2 years and in which Romania participated along with France, Germany, Romania, Spain, Netherlands and England, it was aimed to identify the possibilities of underground storage of hydrogen. In our country, four points with old salt mines were identified located in Ocnele Mari, Ocna Mureş, Târgu Ocna and Cacica. In Spain also, four good locations have been found as mentioned in [8]. All locations are old brown coal mines and since the beginning all sites were defined as interesting

options for hydrogen storage due to its good location near wind resources and also vicinity to the electric and natural gas grids.

In line with the hydrogen strategy [11], the JTM (Just Transition Mechanism) was created, which is the transition mechanism to green energy provided in the European Green Deal for the period $2020 \div 2030$, with allocated funds. on three distinctive pillar.

A synthesis of future funding for projects, studies and research in the field of green hydrogen, for 10 EU countries, with the largest budget allocations in the period $2021 \div 2027$, is presented in Table 3.

Table 3. Just Transition Machanism allocation(EUR million)

Country	Proposed JTF allocation	Total estimated funding under pillar 1	Estimated expected investments to be mobilized under pillars 1,2,3
Poland	2000	7692	27344
Germany	877	4614	13387
Romania	**757**	**2704**	**1011**
Czech Rep.	581	2074	7761
Bulgaria	458	1710	6205
France	402	1825	5807
Italy	364	1301	4868
Spain	307	1397	4445
Estonia	294	1049	3923
Nederlands	220	1045	3174
Finland	165	749	2383
Slovakia	162	580	2170
Ireland	125	569	1.811

With a number of 1350 pages, the new proposal document prepared by the Romanian government for PNRR (National Recovery and Resilience Plan) which supports the recovery from the economic crisis caused by the COVID 19 pandemic, provides for the allocation of 29.2 billion eruo funds by the European Commission for interval $2021 \div 2026$. Approved on September 27 , 2021, PNRR has a lot of green hydrogen-based projects in addition to other renewable energy projects. Among the hydrogen projects we mention: hydrogen networks combined with natural gas, 420 hybrid buses with electricity(together with fast and slow charging stations) / hydrogen in the county residences, 240 electric/hydrogen buses in other types of localities, 1000 minibuses electric/ hydrogen minibuses purchased for Community purposes, two railways with hydrogen trains (12 trains), RES hydrogen generation and capture facilities, etc.

The "HyLaw" project - "Hydrogen Law and removal of legal barriers to the deployment of fuel cells and hydrogen applications", is a report that brings together a package of laws and regulations on hydrogen and the removal of legal barriers to the use of fuel cells and applications hydrogen-based [14]. This is a pilot project that aims to stimulate the market uptake of hydrogen and fuel cell technologies, giving market developers a clear view of the applicable regulations, while drawing the attention of decision makers to the legal barriers that need to be removed. . The project is the result of the cooperation of 23 partners from: Austria, Belgium, Bulgaria, Denmark, Finland, France, Germany, Hungary, Italy, Latvia, Norway, Poland, Romania, Spain, Sweden, Portugal, Netherlands and the UK, being coordinated by Hydrogen Europe.

5. Electricity RES based Market impact on ydrogen production

One of the most important factors which has influence about the technical and economic feasibility of hydrogen projects is the cost of energy. It should be noted that the electricity in the RES is attractive for powering the electrolyzers only if the installations are owned by the hydrogen producer. In this situation, after the amortization of the investment in renewable energy power plants, the cost of electricity generated can be considered close to zero, if operating and maintenance costs are excluded. Instead, the purchase of electric energy(EE) from certified RES producers that sell on the energy exchange, electricity is no longer attractive even if it is cheaper than electricity from fossil fuel power plants.

In the context of the economic crisis triggered by the COVID 19 pandemic, the EE prices from the RES have risen sharply and the energy market is fluctuating. This is also due to the fact that, on the one hand, there is demand and on the other hand, the purchasing power of consumers decreases or there are increased precautions and interest in financial savings, with a more careful analysis of the Energy Market.

Table 4. Transactions results

Day number	Mean price of transaction for EE[RON/MWh]		
	Month1	Month 2	Month 3
	July	August	September
Day1	257,70	402,00	441,25
Day 2	300,05	288,00	363,75
Day 3	289,30	212,50	365,03
Day 4	365,25	400,75	365,04
Day 5	402,39	411,05	548,10
Total period	322,94	342,86	416,63

In order to observe the fluctuations of the electricity prices on the market, it is sufficient to follow the evolution of the transactions with EE coming from RES on the energy exchange managed by the Commercial Operator from Romania [19].

The results of the RES market investigation of electricity for trading periods consisting of five days in three consecutive months, July August and September, 2021, are presented in the the Table 4.

The graphics evolution of EE transactions results from RES analyzed market is shown in Figure 2.
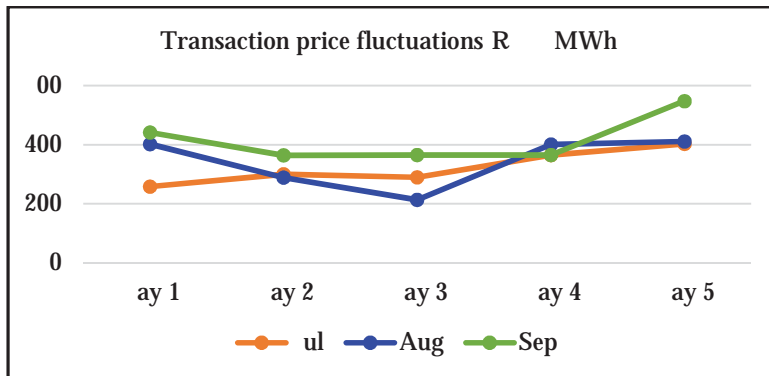
igure 2. Results of EE transactions from the RES dedicated market

The chart shows significant fluctuations in trading prices, with average percentage increases for the periods analyzed as follows: August compared to July recorded an average price increase of 5.81% and September compared to August of recorded an average increase in the trading price of 17.71%. Thus, between September and July there was an increase of 23.52% in the average trading price of EE in RES, which is a significant value. But, the most spectacular jump of the EE price in RES occurred on the stock exchange on 11.10.2021, the first trading day of the month when it was traded with the price of 820,01 RON / MWh with an increase of 96, 82% compared to the mean price in September [19].

The research carried out by the authors is important especially in view of the fact that large energy companies in Romania, which operate in the field of renewable energy sources, such as Enel Green Power [15] or Hidroelectrica [16], have shown interest in entering the market for hydrogen from renewable energies. In partnership with the Austrian company Verbund AH, the Romanian company Hidroelectrca S.A., wants to produce ecological hydrogen through the "Green Hydrogen & Blue Danube" project and to transport it by river to the riparian countries in Europe.

Beyond the ecological aspect and the continuous restoration, RES are also important because they are rewarded by the state with green certificates that are traded separately and increase the profitability of EE production.

. iscussion

RES as well as the cheap electricity produced from them allow the creation of electrical networks interconnected with hydrogen networks obtained by electrolysis and fuel cells. This creates facilities that allow the storage and use of energy at flashes or peak loads. The conversion efficiency of several RES categories has continuously improved.

About the photovoltaic panels it can be said that they have evolved a lot lately with an increasing efficiency due to new technologies and high-performance materials used in the manufacture of solar cells, which leads to an increase in electricity generated on a smaller area. However, electrolysis processes are high consumers of electricity, which makes the large-scale production of hydrogen in this way still quite expensive. Then, in the absence of hydrogen transmission infrastructure, it is necessary that the electrolysis stations be located near the RES or the electric discharge stations from the RES plants in order to keep the costs low. Last but not least, the problem of efficient storage of large quantities of hydrogen and easy to evacuate must be solved for easy integration into the transmission and distribution.

7. Conclusions

Romania is a country that has been producing hydrogen for a long time for various industrial uses. An energy industry or an entire hydrogen-based economy is a solution to a number of problems, but especially to those related to energy supply and security. Hydrogen must be seen as an alternative energy vector that relaxes the problem of critical infrastructure and helps reduce risks and improve the resilience of the energy sector. It offers long-term potential for a sustainable energy system that can operate without emissions of greenhouse gases and gases, based on commonly available sources. A future hydrogen infrastructure will be developed in years to come, but scientific, technical and commercial studies conducted so far have already highlighted the role of hydrogen in the future energy system based on renewable energy in Romania. The energy and raw materials used to produce hydrogen are preferably local.

Although hydrogen is already an increasingly used fuel on the transport side and its future as a fuel is certified by many specialists, the problem of switching to an extended energy system with storage and conversion to hydrogen is a highly technical problem. whose solution appeals to multiple disciplines covering several fields, from engineering research to social and economic sciences.

Planning the development of hydrogen networks throughout the chain from production to consumption is an essential part of the decision-making process of integration into national energy systems with which they must be associated with the sustainable development of energy. However, it is often difficult to compare different feasibility criteria that may be contradictory, uncertain and heterogeneous and therefore their careful evaluation and analysis is required to make objective recommendations.

References

[1] Badea G, Feiseghi R.A, *ydrogen role in the background of technical-econo-mic current directions*, Conference Paper, May 2012,
DOI: 10.13140/RG.2.1.1397.8720

[2] Bandaru S.A., Beccera V., et.al, A General Framework for Multi-Criteria Based Feasibility Studies for Solar Energy Projects: Application to a Real-World Solar Farm, *Energies Journal*, 14(2204) 2021, pp.1-34
https://doi.org/10.3390/en14082204

[3] Edwards P.P., Kuznetsov V.L., David W.I.F., *ydrogen energy*, Phil. Trans. Of Royal Soc. A), 365, 2007, pp. 1043–1056, DOI:10.1098/rsta.2006.1965

[4] El-Eman S.R, Ozcan H., Dincer I., Comparative cost evaluation of nuclear hy-drogen production methods with the Hydrogen Economy Evaluation Program, *International Journal of ydrogen Energy* (40), 2015, pp.11168-11177,
DOI: 10.1016/j.ijhydene.2014.12.098

[5] Garcia D.A., Barbanera F., et al, Expert Opinion Analysis on Renewable Hy-drogen Storage Systems Potential in Europe, *Energies Journal of Science and Technology*, 9(963), 2016, pp. 1-22., DOI:10.3390/en9110963

[6] Jovan D.J., Dolanc G., Can Green Hydrogen Production Be Economically Via-ble under Current Market Conditions, *Energies Journal of Science and Technology*, 13(6599), 2020, pp. 1-16., DOI: 10.3390/en13246599

[7] Naghiu G.S., Giurca I. et. al, *Comparative Analysis on the Solutions of ydro-gen Production sing Solar Energy with and without Connection to the Power Network*, The 9th International Conference Interdisciplinarity in Engineering, INTER-ENG 2015, 8-9 October 2015, Târgu Mureș, Romania, Procedia Technology, 22, 2016, pp. 781 – 788

[8] Simon J., Ferriz A.M., Correas L.C., *y nder ydrogen nderground Sto-rage at arge Scale: Case Study Spain*, The 9th International Renewable Energy Storage Conference, IRES 2015, Energy Procedia No.73, 2015, pp. 136–144, doi: 10.1016/j.egypro.2015.07.661

[9] Randamente electrochimice/Chimie fizică și electrochimie,
https://alili2001.files.wordpress.com/2014/12/m08_chimfiz.pdf/
(downloaded at September 10rd, 2021)

[10] Proiectul international HyUnder/Scurtă prezentare, https://mfe.gov.ro/wp-content/uploads/2021/01/31e1b03347c949e0e023e510346507ea.pdf (downloaded at September 8rd, 2021)

[11] European Commission, A Hydrogen strategy for a climate neutral Europe , adopted on 8 july, 2020, https://www.hydrogeneurope.eu/

[12] European Commission, The European Green Deal, 13 December 2019 https://ec.europa.eu/clima/policies/eu-climate-action_ro

[13] European Commission, *Guide to Cost-Benefit Analysis of investment projects,* http://ec.europa.eu/regional_policy/sources/docgener/guides/cost/guide2008_en.pdf;

[14] Proiectul HyLaw, Topic: FCH-04-2-2016, Identification of legal-administrative barriers for the installation and operation of key FCH technologies Tip de proiect: "Supporting action", Grant nr. 735977 , Data de început: 1 ianuarie 2017, www.hylaw, www.hydrogeneurope.eu

[15] https://www.enelgreenpower.com/learning-hub/renewable-energies/hydro-gen

[16] https://cdn.hidroelectrica.ro/cdn/aga/2021/2903/nota_aprobare_memorandum_verbund.pdf

[17] https://www.europarl.europa.eu/news/ro/headlines/society/20210512STO04004/energie-din-hidrogen-care-sunt-beneficiile-pentru-ue

[18] http://dezvoltaredurabila.gov.ro/web/wp-content/uploads/2020/06/RAPORT-Prof.-Tudor-Prisecaru.pdf

[19] www.opcom.ro

Addresses:

- Dr. Eng. Marius Savu Lolea, Postdoctoral scientific researcher, University of Oradea, Universității str, no.1,410087, Oradea, Romania mlolea@yahoo.com

- Lect. Dr. Andrea Amalia Minda, Babeș-Bolyai University, Faculty of Engineering, Piața Traian Vuia, nr. 1-4, 320085, Reșița, Romania andrea.minda@ubbcluj.ro (*corresponding author*)

- Ph.D.stud., Eng. Emeric Szabo, University of Oradea, Universității str, no.1, 410087, Oradea, Romania emericremus@gmail.com

- Ph.D. stud., Eng. Daniela Negrea, University of Oradea, Universității str, no.1, 410087, Oradea, Romania dana_negrea1@yahoo.com

atural fre uencies and mode shapes in zero force members of a truss

Dan Pîrșan, Zeno-Iosif Praisach

Abstract. *Trusses are everywhere; they are used in bridges, antenna towers, cranes, even in parts of the International Space Station. And for good reason, they allow us to create strong structures while using materials in very efficient and cost-effective way. Trusses it is essentially a rigid structure made up of a collection of straight members. The type of truss depends on how the horizontal and diagonal beams are arranged.*

Keywords*: trusses, zero-force member, natural fre uency, mode shape*

1. Introduction

Trusses are very popular construction by using a relatively small amount of material for the weight they can support [1]. A single-span truss is like a simply supported beam because it carries vertical loads by bending [3]. A truss is a simple structure whose members are subject to axial compression and tension only and but not bending moment [5]. Early trusses were built without precise knowledge of how the loads are carried by each part of the truss. These trusses were patented as from 1840, at a time when new bridge designs we're being developed to accommodate the expansion of the railroad industry and were patented by Howe (fig. 1, a), Pratt (fig. 1, b) and Warren [8].

Warren truss contains a series of isosceles triangles, or equilateral triangles (fig. 2, a). To increase the span length of the truss bridge, verticals are added for Warren Truss (fig. 2, b). Pratt truss is characterized [9] by having its diagonal members (except the end diagonals) slanted down towards the middle of the bridge span.
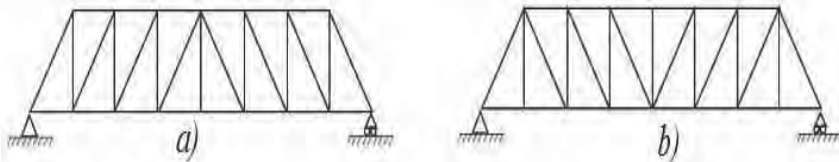
igure 1. Howe and Pratt truss.
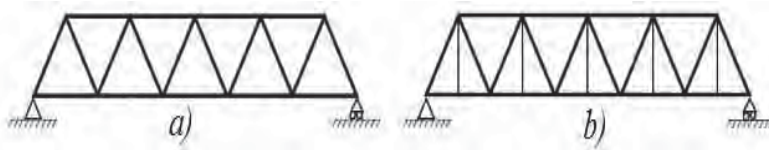
igure 2. Warren truss.

The members of a truss can be subjected at tension, compression or only participate in increasing the rigidity and stability of the truss without being stressed and the latter are called zero force members. In a truss, the zero force elements are hinged beams at both ends, and their dynamic behavior is analyzed in this paper.

2. orces in Trusses

To determine the reactions [4] in the points of support the equilibrium equations from the strength of materials are used: the sum of the forces and reactions on the horizontal is equal to zero; the sum of the forces and reactions on the vertical is equal to zero; the sum of the moments of the external forces and of the reactions in relation to a support is zero.

Below is an explanation of what happens if a force is applied to a triangular element
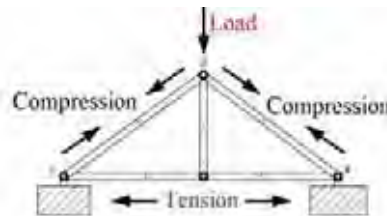
ig 3 Triangle transfers a force.

When a force (the load) is applied to one of the corners of a triangle, it is distributed down each side. The two sides of the triangle are squeezed. Another word for this squeezing is compression. The third side of the triangle is pulled, or stretched sideways. Another word for this stretching is tension [7].

A simple truss is composed of triangles, which will retain their shape even when removed from supports [6]. A truss is considered statically determinate when the static equilibrium equations can be used to find the reactions on that structure. The method of joints analyzes the force in each member of a truss by breaking the truss down and calculating the forces at each individual joint. When using the

95

method of joints to solve for the forces in truss members, the equilibrium of a joint (pin) is considered.

And by solving the reactions in fig. 4 results which are compressive efforts (negative) and which stretching (positive).

There are rules to identify the beam of a triangle not subject to stresses (compression or stretching), respectively zero-force members:

1. If a joint has only two non-collinear members and there is no external load or support reaction at that joint, then those two members are zero force members;

2. If three members form a truss joint for which two of the members are collinear and there is no external load or reaction at that joint, then the third non-collinear member is a zero force member;

3. Zero-force members can be removed (as shown in the figure 4) when analyzing the truss. The zero-force members are used to increase stability and rigidity of the truss, and to provide support for various different loading conditions.
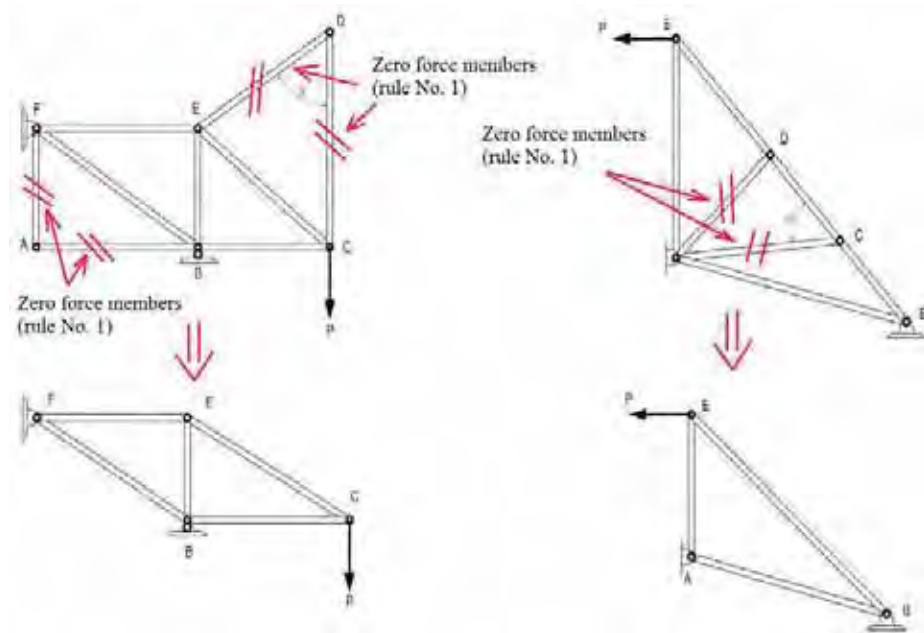
igure 4. Trusses with zero force members (upper side) and without zero force members (lower side).

3. atural fre uencies and modal shape for a hinged hinged beam

As shown above, there can be elements with zero forces in a truss. For this element, the natural frequencies and vibration modes can be calculated as a simply supported beam.

For a continuous structure (beam) the frequencies (f_n) are determined by means of the relation (1) [10]:

$$f_n = \frac{a_n^2}{2\pi}\sqrt{\frac{E \cdot I}{m \cdot \ell^4}} \quad [\text{Hz}] \tag{1}$$

where, $a_n = \sqrt[4]{\omega^2 \dfrac{\rho \cdot A}{E \cdot I}}$ (2) is the dimensionless wave number;

ω [rad/s] – is its own pulsation;
ρ [kg/m^3] – the density of the material;
A [m^2] – cross-sectional area;
E [N/m^2] – is the longitudinal modulus of elasticity;
I [m^4] – moment of inertia of the cross section of the beam;
m [kg] - represents the mass of the beam;
 ℓ [m] - represents the length of the beam;
$n = 1\ldots\infty$ - vibration mode number.

Knowing the geometry of the structure and the material from which the structure is made, in order to determine the natural frequencies with the relation (1) we must know the values of the dimensionless wave number. In the case of free vibrations, the differential equation of the displacement for transverse vibrations of the beam is:

$$\frac{\partial^4 w}{\partial x^4} - \omega^2 \frac{\rho \cdot A}{E \cdot I_z} w = 0 \tag{3}$$

where, w [m] - vertical movement of the neutral axis. The general solution is:

$$W_n(x) = A_n \sin(a_n x) + B_n \cos(a_n x) + C_n \sinh(a_n x) + D_n \cosh(a_n x) \tag{4}$$

The integration constants A_n, B_n, C_n and D_n are determined from the initial boundary conditions: the deflection and the bending moment at the hinged points are zero, respectively (ℓ is the length of the element):

$$\begin{cases} W(0) = 0 \\ \dfrac{\partial^2 W(0)}{\partial x^2} = 0 \end{cases} \tag{5} \qquad\qquad \begin{cases} W(\ell) = 0 \\ \dfrac{\partial^2 W(\ell)}{\partial x^2} = 0 \end{cases} \tag{6}$$

It is obtained such a system of 4 equations with 5 unknowns, which results in the frequency equation:

$$\sin(a_n \ell) = 0 \tag{7}$$

with solutions: $a_n = \pi, 2\pi, \ldots n\pi$, respectively the modal function:

$$W_n(x) = \pm \sin(a_n x)$$

(8)

The first 6 vibration modes for a simply supported beam of length L = 1 with the normalized function (+ 1) are illustrated in figure 5:
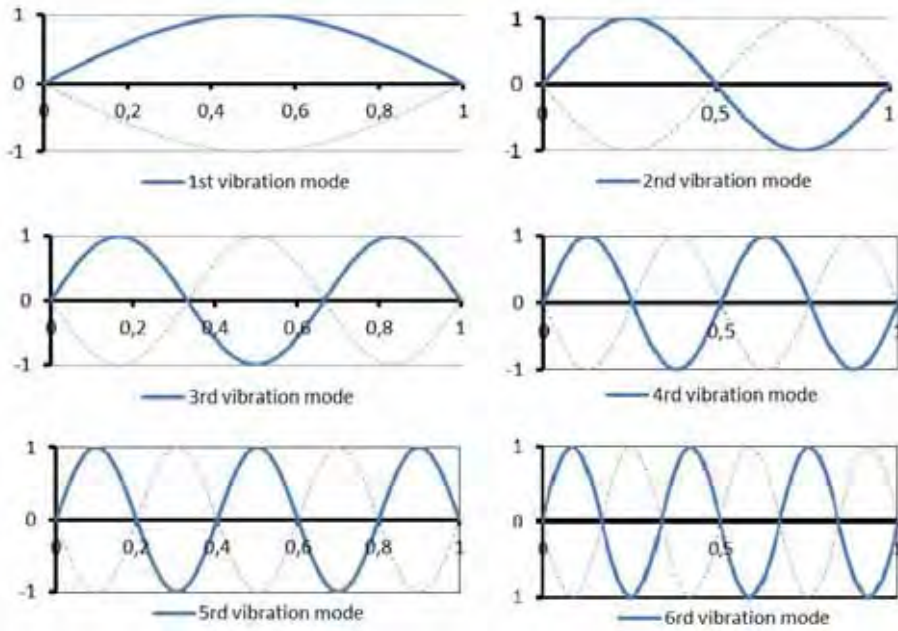
igure 5. The first 6 vibration modes for simply supported beam.

4. Conclusion

The main conclusions, which highlight the essential elements of the research are:

- if a joint has 3 membres and no external load, or if 2 of the membres are co-liniar, the third non-coliniar member is a zero-force member;
- were put evidence the internal tensions which appears in a triangular element with lattice beams when an external force is applied;
- the rules for zero force in elements of trusses were highlighted;
- for these elements, which are considered as a simply supported beam, the first 6 modes of vibration were drawn.

Knowing the modal function that describes the vibrational movement of the element, we can determine the energy function that allows us to locate the damage for the monitored structure [2].

References

[1] Collins M.D., Michael P., *Diagonal Compression Field Theory-A Rational Model for Structural Concrete in Pure Torsion*, ACI Journal, Proceedings 71(8), Aug. 1974, pp. 396-408.

[2] Praisach Z.I., Gillich G.R., Protocsil C., Muntean F., *Evaluation of Crack Depth in Beams for Known Damage ocation Based on Vibration Modes Analysis*, Conference: Acoustics & Vibration of Mechanical Structures, Timisoara, Applied Mechanics and Materials, 430, 2013, pp. 90-94,.

[3] Al-Nahlawi K.A., Wight J.K., *Experimental and Analytical Study in Shear for ightly Reinforced Concrete Beams*, Department of Civil Engineering, Report UMCE No. 89-7, University of Michigan, June 1989.

[4] Gillich G.R, Praisach Z.I., Detection and Quantitative Assessment of Damages in Beam Structures Using Frequency and Stiffness Changes, *Key Engineering Materials*, 569, pp. 1013-1020, 2013.

[5] Bratu P., *Analiza Structurilor Elastice-Comportarea la acțiuni statice și dinamice*, Editura Impuls, 2011.

[6] Bratu P., *Vibrațiile sistemelor elastice*, Editura Tehnică, 2000.

[7] Faraji M., Dardel M., Pashaei M.H., Natural Frequency, Mode Shape, Bukling and Post-Bukling Analysis of MEMS with Various Clamped Position, *Journal of Science and Engineering*, 1(2), 2013, pp. 103-120.

[8] Marti P., *se Of Truss Models in Detailing,* Annual Convention of the American Concrete Institute, Phoenix, Mar. 8, 1984, 24 p.

[9] Irvine T., *Natural Fre uencies of Beams Subjected to a niform Axial oad, Revision C*, vibrationdata.com, 2011.

[10] Gillich G.R., Negru I., Protocsil C., Stanciu E., Minda P.F., *Evaluarea integrității structurilor mecanice,* Editura Eftimie Murgu, Reșița, 2018.

Addresses:

- PhD. Pirsan Dan, Babeș-Bolyai University, Faculty of Engineering, Piaţa Traian Vuia, nr. 1-4, 320085, Reşiţa, Romania
  dan.parsan@ubbcluj.ro
- Lect. Dr. Eng. Habil. Zeno-Iosif Praisach, Babeș-Bolyai University, Faculty of Engineering, Piaţa Traian Vuia, nr. 1-4, 320085, Reşiţa, Romania
  zeno.praisach@ubbcluj.ro

Statistical analysis of measured wind speed data s appealing spreadsheet applications

Cristian Paul Chioncel, Nicoleta Gillich*, Gelu-Ovidiu Tirian

Abstract. **Once the wind data is measured, the values are processed, based on statistic approach, as accurately as possible, to provide a clear over-view of the locations wind potential, being the basis of any wind farm project, representing the go or no-go in further subsequent design steps. The probability density distributions are derived from time-series data, identifying the associated distributional parameters. The wind energy potential of the locations is studied based on the Rayleigh and Weibull models, implemented with the help of Excel computations, and representing tools, to understand the wind characteristics. Based on the statistical analysis of wind conditions presented here, the results of current study can be used to make a sustainable energy yield for any location.**

Keywords: **wind energy, statistical analysis, Excel, wind data**

1. Introduction

The Intergovernmental Panel on Climate Change (IPCC) report published in august 2021, highlights ‚code red’ for global heating, driven by human. [1] Measures to counteract, not just trends, but in the meantime a recognized scientific reality, the global heating, are defined at the European Union level in the Green Deal, identifying and fixing targets on different levels focused on no net emissions of greenhouse gases by 2050 and economic growth decoupled from resource use [2]. In increasing the share of renewable energies as well as energy sustainability, the wind energy, will have a significant role. [3]

Once the technologies enable to build bigger wind turbines (higher pills, larger rotor diameter and consequently more installed power per wind turbine), locations that until now were not suitable for exploiting the wind potential, even under certain subsidy conditions, can become now interesting.

The character of this energy source is a stochastic one, the most important parameter, the wind speed, and his direction, are, for a given location, mostly randomly in time. Wind data analysis and accurate wind energy potential assessment are critical factors for suitable development of wind power application at a given location.

[4] Knowing the statistical properties of the wind speed is essential for computing parameters which describe the potential of a location, independent of the wind turbine characteristic. One such parameter is Wind Power Density (WPD), predicting the energy output of a wind energy conversion system, related to the power characteristic of the turbine. Thus, a proper analysis and understanding of statistical wind speed data are crucial, as well as for the structural and environmental analysis [5] as for the performance of wind energy conversion system [6] and the assessment of the wind energy potential. The probability distribution of wind speeds over a certain time interval correlated with the wind rose, form together the main information needed to estimate, for a given site, the wind energy output.

The main decision of exploiting the wind potential of a certain locations is based on the analysis of measured wind speed data. [7] Mainly, various mathematical tools, focuses on obtaining and subsequent interpretation of the wind speed characteristics, as the **Weibull** or **Rayleigh** functions, simplify the presentation as well the interpretation, of a wide range of wind speed data [4]. Therefore, a lot of software tools have been developed, integrating different features. The presents paper wants to emphasis how applications focused on a spreadsheet, as Excel, can provide a very powerful tool in wind data processing. [8]

2. Wind data   statistical representation and a ailable power

Calculations of energy, and later power, available in the wind is based on physics and geometry knowledge, figure 1. [9]

Starting from the basic definition of the kinetic energy (KE) of an object with mass **M** and velocity **V** is given by:

$$KE = \frac{1}{2}Mv^2. \tag{1}$$

To find the kinetic energy of the wind, we make the analogy of the air parcel that cross the rotor surface of the wind turbine over a given time with a puck, described through a cross-sectional area (**A**) and a thickness (**D**), with a certain volume (**Vol**). Considering that the density of air volume is given by the report mass per volume, as well as the velocity (**v**) of the air parcel that can be expressed as the time (**T**) needed for the air parcel to cross the wind turbine blades, the expression of the kinetic energy gets:

$$KE = \frac{1}{2}(\rho \cdot Vol)v^2 = \frac{1}{2}(\rho \cdot A \cdot D)v^2 = \frac{1}{2}(\rho \cdot A \cdot v \cdot T)v^2 =$$

$$KE = \frac{1}{2}\rho \cdot A \cdot T \cdot v^3 \tag{2}$$

The available power (P) in the air parcel can be expressed dividing energy by time, relation (3), [10] and if afterwards the power expression will be divided with

the air parcels cross-sectional area (A), we get the so-called wind power density (WPD), relation (4), a parameter that has no dependence on the wind turbine characteristics:
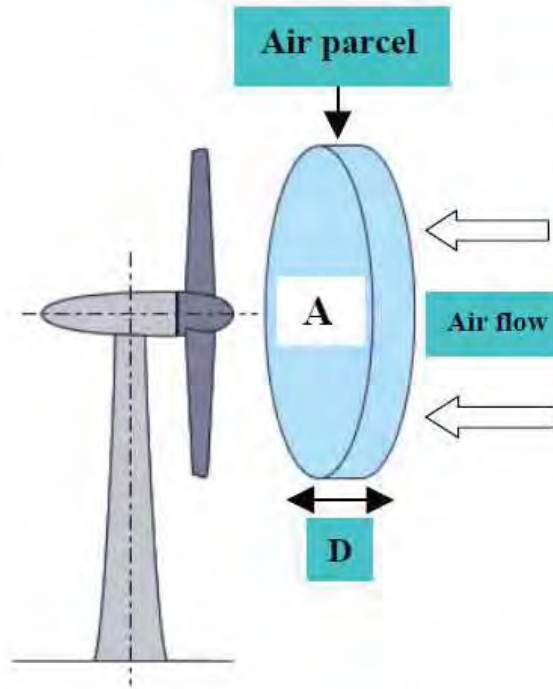
igure 1. Illustrative for the physics of wind power

$$P = \frac{1}{2}\rho \cdot A \cdot v^3 \tag{3}$$

$$WPD = \frac{1}{2}\rho \cdot v^3 \tag{4}$$

Generally, the locations that fits for exploitation of the wind potential, are priority described based on the **wind class** ranking rather mean wind speed or wind power density (WPD), the wind power classes, seven in number, being associated with a variation range of the WPD.

The usual method of obtaining the frequencies of different speeds is classification. The measured speed values (i.e. the values averaged over a period of 1 or 10 minutes) are divided into classes of 1 m/s and displayed as a frequency distribution. These metrologically recorded relative frequency distributions can be described analytically by the two-parametric Weibull distribution with the shape parameter **k** and the scaling factor **A**, figure 2. [10] The shape of the Weibull curve is described by

the shape parameter **k** taking usually values between 1 and 3. Figure 3 shows curves of the Weibull function for different shape parameters at an average wind speed of 4 m / s. [4]
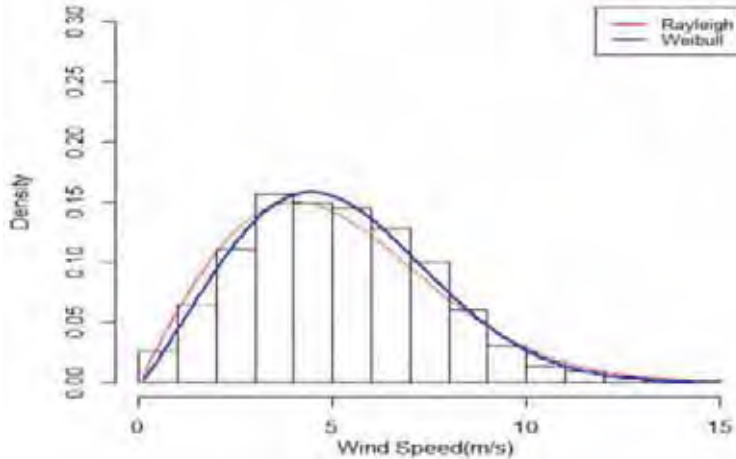
igure 2. Example of a frequency distribution fitted with Weibull and Rayleigh curves [10]
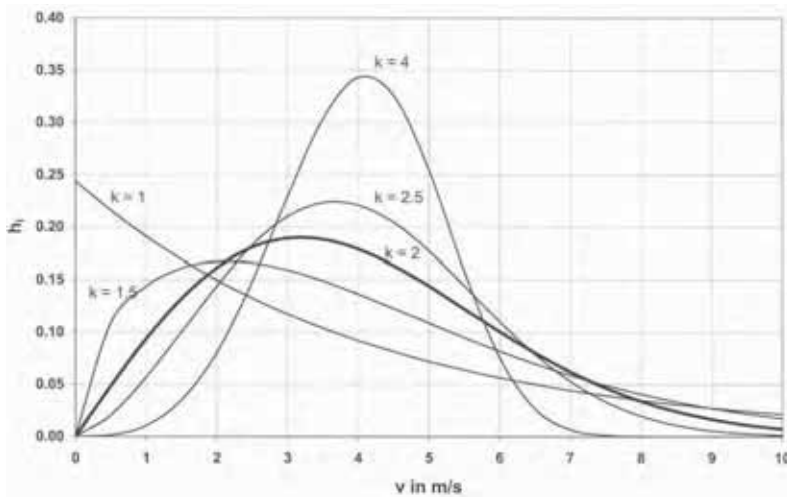
igure 3. Wind speed distribution based on the Weibull function for a mean wind speed **v**=4 m/s; **k**=2 Rayleigh distribution

As an important parameter in computing more exactly the wind potential for each location intervenes the air density, ρ, that depends on a series of factors, as:

103

elevation above sea level, atmospheric pressure, air temperature. To obtain a first overview of the location's possibility of wind exploitation, the use of $\rho = 1.225$ kg/m^3 is widespread, which does not lead to huge error in the WPD estimation process. [10]

The WPD expression (4) contains the assumption of computing it considering the mean wind speed, but to obtain a more accurate estimation of WPD, must be done a summation over time, as follows

$$WPD = 0.5 \cdot \frac{1}{n} \sum_{i=1}^{n} (\rho_i \cdot v_i^3), \tag{5}$$

were **n** representing the wind speed readings, v_i and ρ_i are the **j**th (1st, 2nd, 3rd, etc.) readings of wind speed and air density. [11] The most accurate result, since wind speed **v** and air density ρ will change with every new measurement, would entail a calculation for every data interval. The WPD can be interpreted as if an energy source with this determined average power would be constantly available at the considered location and in the considered period. [10]

3. Statistical analysis on gi en wind data set using Microsoft Excel spreadsheet applications

The provided analysis we will use wind date measured for a year [12], consisting of wind speed related to hours per year. Based on that information, **Excel** gives us the opportunity to create a histogram from the wind data. [13] For this we will compute the percentage of the time/hours the wind blows with a certain wind class related to the analyzed time (one year) by dividing each position in the **Hours per year** column to the total sum (8760 hours = 1 year), obtaining the frequency of occurrence. To represent the histogram, we select and represent the first, **A**, and third, **C**, column (figure 4) in a graph, for which the bar chart fits best, figure 5.

If we want to compute the **Weibull Density Function**, Excel has for this the WEIBULL.DIST(x, alpha, beta,cumulative) [14] function, were, in our case, x represents the wind speed, alpha – the shape factor, usually know as **k** for which we will use the value two, beta what we know as lambda, for what we will use 7, and then we are asked rather we want to keep a cumulative distribution function, TRUE, or a probability density function, FALSE, that we will use: WEIBULL.DIST(A3, 2, 7, FALSE). Summing all the computed range of values, we obtain a value close to one (≈ 1.01). Plotting the two columns, **A** and **D**, figure 4, we obtain what is expected to be a Weibull curve, figure 6.

Next, we will look at the power in the wind, comparing it using the annual average speed (4) versus using the wind distribution (5). If we compute and use the medium wind speed for the given wind data, figure 4 Column F, the resulted WPD is 226.28 W/m^2, figure 4 Column E. If we multiply this value with the number of hours per year, 8.760 **h**, we obtain 1982204.53 Wh/m^2, representing the total power per unit area, as an average, that will go through at that given site for the average

wind speed of the location. If we do now the same but for each of our bins, and sum the column H, figure 4, we obtain 383.56 W/m², which multiplied by the total number of hours per year, will lead us to 3359999.33 Wh/m². The proportion between W/m² and Wh/m² are similar, 383.56 W/m² / 226.28 W/m² ≈ 1.7, that means we obtain almost twice as much power out per unit area using the Weibull distribution! This reflects what really happens with the evolution of the wind, rather than the situation with a constant speed value (average wind speed).

	A	B	C	D	E	F	G	H
2	Bin / wind speed (m/s)	Hours per year	Frequency of occurrence	Weibull Probability Density Function	Product (A x B)	Medium wind speed	WPD with medium wind speed	Power in the Wind
3	0.5	47	0.0053653	0.020304305	23.5	7.1753995	226.2791	0.0004
4	1	181	0.0206621	0.039991783	181			0.0124
5	2	434	0.0495434	0.075233506	868			0.23781
6	3	582	0.0664384	0.101902959	1746			1.0763
7	4	753	0.0859589	0.117783231	3012			3.30082
8	5	903	0.1030822	0.12252511	4515			7.73116
9	6	1037	0.118379	0.117465862	6222			15.3419
10	7	1058	0.1207763	0.105108412	7406			24.8558
11	8	954	0.1089041	0.088446801	7632			33.4553
12	9	781	0.0891553	0.07033331	7029			38.9965
13	10	613	0.0699772	0.053029636	6130			41.9863
14	11	460	0.0525114	0.038000134	5060			41.9356
15	12	330	0.0376712	0.025925144	3960			39.0575
16	13	235	0.0268265	0.016861821	3055			35.3627
17	14	153	0.0174658	0.010466079	2142			28.7556
18	15	101	0.0115297	0.006204629	1515			23.3476
19	16	61	0.0069635	0.003515498	976			17.1134
20	17	35	0.0039954	0.001904722	595			11.7777
21	18	21	0.0023973	0.00098729	378			8.38849
22	19	12	0.0013699	0.000489767	228			5.63753
23	20	6	0.0006849	0.000232596	120			3.28767
24	21	3	0.0003425	0.00010578	63			1.90295
25	22	0	0	4.60777E-05	0			0
26	23	0	0	1.92289E-05	0			0
27	24	0	0	7.68899E-06	0			0
28	25	0	0	2.94648E-06	0			0
29								
30	Total	8760	1	1.016894317				383.562

Sheet1 ⊕

igure 4. Analyzed wind data in Excel
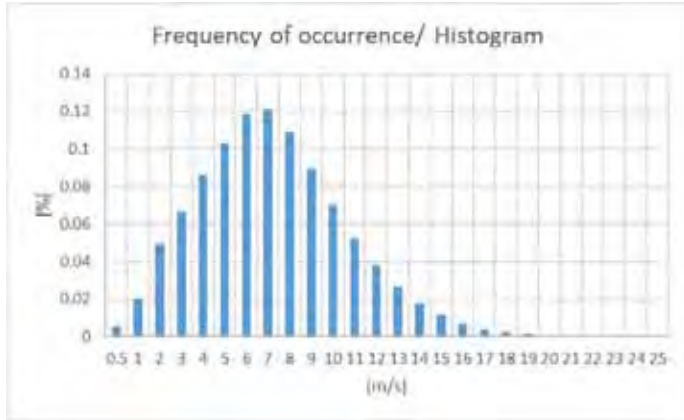
igure 5. Histogram of wind data in Excel
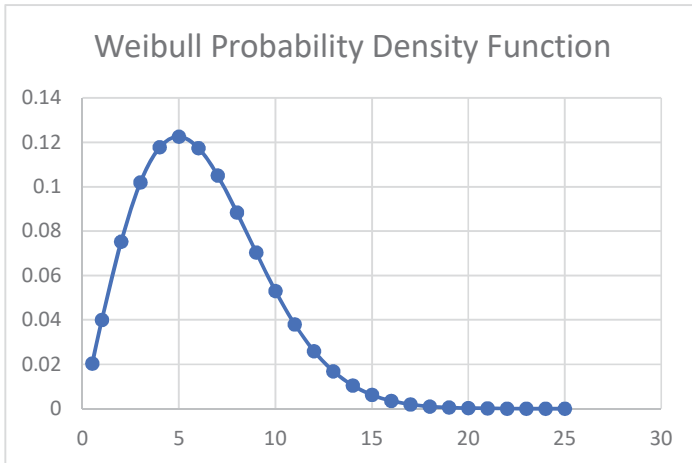
igure . Weibull distribution

4. Conclusion

The paper reflects a part of the main statistical analysis that can be applied on measured wind data appealing spreadsheet applications, in this case **Microsoft Excel**. The statistical computation on the wind speed datas have showed a high level of transparency for the user, being able to follow and understand much better the entire computational steps, the existing connections and interaction between certain parameters, and, as well, the big advantage of not having to resort on specialized developed programs, which requires acquisition fee, and, usually, additional maintenance costs.

References

[1] Intergovernmental Panel on Climate Change – Climate Change 2021 Report, https://www.ipcc.ch/report/ar6/wg1/ (downloaded at September, 2021).

[2] A European Green Deal, https://ec.europa.eu/info/strategy/priorities-2019-2024/european-green-deal_en (access August, 2021)

[3] The significant role of wind energy, https://climatechange-theneweconomy.com/cop23-series-wind-turbines/, July, 2018.

[4] Chioncel C.P., Chioncel P., Gillich N., Overview of Classic and Modern Wind Measurement Techniques, Basis of Wind Project Development, **Analele Universitatii "Eftimie Murgu" Resita**, **Fascicula de Inginerie**, 18(3), 2011, pp. 73-80.

[5] Kidmo D.K., Danwe R., Doka S.Y., Djongyang N., Statistical analysis of wind speed distribution based on six Weibull Methods for wind power evaluation in Garoua, Cameroon, **Revue des Energies Renouvelables**,18, N°1 (2015), pp. 105–125.

[6] Chioncel C.P., Dordescu M., Lazar M.A., Tirian G.-O., **Wind turbine power and optimum energy, at variable wind speeds**, IEEE 24th International Conference on Intelligent Engineering Systems, July 8-10, 2020, Reykjavík, Iceland.

[7] Ayodele T.R., Jimoh A.A., Munda J.L, Agee j.T., Statistical analysis of wind speed and wind power potential of Port Elizabeth using Weibull parameters, **Journal of Energy in Southern Africa**, 23(2), May 2012, pp. 30-38.

[8] Extreme Wind Speeds Software: Excel, https://www.itl.nist.gov/div898/winds/excel.htm

[9] Chioncel C.P., Gillich N., Spunei E., Tirian G.-O., **Overview of the main topics in wind energy systems planning**, IOP Conf. Series: Materials Science and Engineering 477, 2019, 012059.

[10] Kwamboka J.O., Kamau J.N., Saoke C.O., Analysis of the Wind Energy Characteristics and Potential on the Hilly Terrain of Manga, Nyamira County, Kenya, **International Journal of Innovative Science and Research Technology**, 3(3), 2018, pp. 672-677.

[11] Jung C., Schindler D., The role of air density in wind energy assessment – A case study from Germany, **Energy**, Volume 171(C), 2019, pp. 385-392.

[12] Susan Stewart, **Wind Turbine Systems**, Department of Aerospace Engineering http://www.aero.psu.edu

[13] Zaheer U., Muhammad A., D.A. Khan, **Teaching physics using Microsoft Excel**, IOP Conf. Series: Physics Education, 52(5), 2017.

[14] https://support.microsoft.com/en-us/office/weibull-dist-function

Addresses:

- Assoc. Prof. Dr. Eng. Cristian Paul Chioncel, Babeş-Bolyai University, Faculty of Engineering, Piaţa Traian Vuia, nr. 1-4, 320085, Reşiţa, Romania, cristian.chioncel@ubbcluj.ro
- Prof. Dr. Eng. Nicoleta Gillich, Babeş-Bolyai University, Faculty of Engineering, Piaţa Traian Vuia, nr. 1-4, 320085, Reşiţa, Romania nicoleta.gillich@ubbcluj.ro
  (*corresponding author*)
- Assoc. Prof. Dr. Eng. Gelu-Ovidiu Tirian, Politehnica University Timisoara, Faculty of Engineering, Str. Revoluţiei nr. 5, 331128, Hunedoara, Romania, ovidiu.tirian@fih.upt.ro

Aspects about bouncing of plough caused by random excitations of the land

Carmen Nicoleta Debeleac

Abstract. *In this paper the author deals aspects about the vertical motion (named bouncing) of a tractor with plough mounted on the rear frame, during displacement over the random excitation surface of the agricultural land. Final results of the simulation process, performed on the model of tractor-plough with 3 degree of freedoms, show the difference between digging depth function as velocity motion and longitudinal profile of the terrain. Thus, the deviation of the plough depth from the reference depth is evaluated.*

Keywords*: tractor, plough, bouncing, random excitation, digging depth*

1. Introduction

This paper deals with dynamic vertical behavior of a plough tractor during the working process when moving on agricultural land. Sometimes, uncontrolled vibrations can occur in the tractor and the wheels sometimes depart from the land. This phenomenon is called bouncing" and creates to impact dynamics which causes excessive vibration, along with sideslip and poor steering performance which can lead to overturning [1]. Bouncing becomes particularly serious when tractors run on slopes or a field with irregular surface. Due to the motion upon the road irregularities, the structural elements of the tractor are subjected to vertical oscillations, which affect the operation of front and rear suspensions differently [2]. In the same mode, the working accessories that are mounted at the front or rear of the tractor body are affecting [3,4]. The objective of the present study was to analyze the impact dynamics model of the bouncing tractor on an uneven profile of agricultural land using numerical simulation.

2. Mathematical Model

It is considered the movement of the aggregate (tractor with working accessory) as a whole in the vertical plane, when moving over irregularities encountered on agricultural land. Based on equivalent model of a tractor plowing with gauge wheel (fig. 1), its behavior under action of external forces in the vertical longitudi-

nal plane that are appearing to accelerated motion when moving on slope surface should be studied.

Available working accessories are mounted on the base machine (tractor) by suspension linkages using specific mechanisms at the tractor frame. During the technological process, the positions of these mechanisms change insignificantly sometimes, but there may also be situations in which it negatively influences the dynamics of the plowing unit as a whole. For this reason, the following simplifying hypotheses are introduced:

a) during operation the tractor wheels maintain permanent contact (punctual) with the surface of the agricultural land;

b) variation over time of the irregularities of the agricultural land surface is described as a random function;

c) wheels are modeled as identical viscous-elastic elements with linear characteristics (K_{tT}, C_{tT});

d) each wheel of the tractor moves over irregularities with speed v. The amplitudes of the unevenness were noted as follows: with h_1 that corresponding to the front wheels, h_2 to the rear wheels of the tractor and h_4 to the plough wheel.

The study of the vertical oscillations of the tractor will be performed on the equivalent dynamic model and schematic view of this approach is depicted in Figure 2.
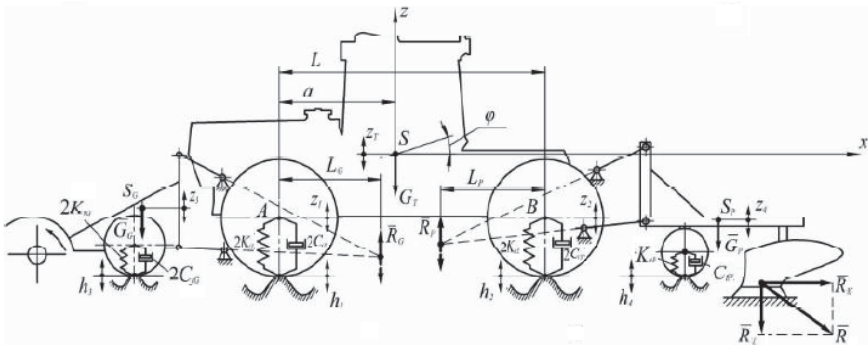
igure 1. Model for dynamic behavior investigation of the tractor in longitudinal-vertical plane [5].

For only tractor base, the model has two degrees of freedom, with oscillation in the vertical direction (z_T) of the center of mass (S) of the tractor and, respectively, with angular oscillations (φ) of the frame around the same point S. In addition, the plow has a gauge wheel for continuously monitors the contact with the profile of the agricultural land (denoted with h_4), and their dynamic behavior is characterized by stiffness K_{tP} and damping coefficient C_{tP}. The dynamic plough model has a degree of freedom described by moving the center of gravity (S_P) of the equipment

in the vertical direction (z_4). The forces acting on the plough are: the weight G_P; the reaction force R_P as a result of the attachment of this equipment to the tractor frame; the component in the vertical direction R of the resistance R at the working tool of the plough. The use of Lagrange equations of the second kind are suitable to describe the motion of the tractor body and, respectively, for the plough mounted on the rear of the tractor [6].

$$
\begin{cases}
\dfrac{\left[m_T(L-a)^2+J_T\right]}{L^2}\ddot{z}_1+2C_{tT}\dot{z}_1+2K_{tT}z_1+\dfrac{\left[m_Ta(L-a)-J_T\right]}{L^2}\ddot{z}_2=2C_{tT}\dot{h}_1+2K_{tT}h_1+\\
\qquad\qquad +\dfrac{1}{L}\left[R_G(L-L_G)+R_PL_P-G_T(L-a)\right]\\
\dfrac{1}{L^2}\left(m_Ta^2+J_T\right)\ddot{z}_2+2C_{tT}\dot{z}_2+2K_{tT}z_2+\dfrac{\left[m_Ta(L-a)-J_T\right]}{L^2}\ddot{z}_1=2C_{tT}\dot{h}_2+2K_{tT}h_2+\\
\qquad\qquad +\dfrac{1}{L}\left[R_GL_G+R_P(L-L_P)-G_Ta\right]\\
m_P\ddot{z}_4+2C_{tP}\dot{z}_4+2K_{tP}z_4=2C_{tP}\dot{h}_4+2K_{tP}h_4-R_P-G_P-R_z
\end{cases}
\tag{1}
$$

Taking into account all the equations of motion of each subsystem (tractor and plough) a system with three equations is obtained which will be the basis for the numerical simulation of the dynamic behavior of the tractor with plough in vertical plane when moving on an agricultural field with irregular profile.

3. Material and method

In this paper, the Case IH Magnum 340 tractor model was chosen to developing proposed approach. Main parameters of this unit are centralized in the Table 1.

Table 1. Identification model of tractor

Parameter	Value
mass tractor	15 t
mass plough	5 t
distance between tractor axles	6 m
distance between the front axle and the center of gravity	2,2 m
L_P distance for the analyzed case	3 m
R_P reaction force for the analyzed case	6 kN
moment of inertia	10^4 kgm^2
tractor wheel stiffness	10^5 N/m
tractor wheel damping	10^3 Ns/m
plough wheel stiffness	10^6 N/m
plough wheel damping	$1,8 \times 10^3$ Ns/m

111

The resistance force of a ploughing plough is [7]:

$$R_z = k_0 ab, \tag{2}$$

where k_0 - specific soil resistance to ploughing on medium soil [daN/cm^2]; a - ploughing depth [cm]; b - working width [cm].

For $k_0 = 5000$ daN/cm^2, a = 0,2 cm and b = 0,2 cm we obtain digging resistance on vertical direction R = 200 daN. About working velocity, we choose the 2nd gear speed to motion aggregate with plough [2,8]. In this case, the plough resistance to ploughing $R_z = (0,2 ... 0,3)F_t$, taking into account by the thrust F_t developed of the tractor unit [9]. If we considered, in addition, the sliding of the running gears δ having several values ($\delta = 10$-17 %), then the working speed v_W becomes $v_t(1-\delta)$, where v_t represents translation velocity of tractor. Nevertheless, in the considered velocity range, that is within 1,38 and 2,77 m/s (or 5 km/h – 10 km/h), the wheel's rolling resistances can be considered almost constant.

In order to simulate the movement of the tractor under the imposed conditions, the following analytical expression was adopted for the spectral composition of the longitudinal profile of the terrain as a function of the excitation pulsation, namely

$$H(s) = \frac{0,88}{10^{-4} s^4 + 3\,10^{-4} s^3 + 12\,10^{-3} s^2 + 0,11\,s^1 + 5}, \tag{3}$$

whose graphical representation for the pulsation domain 10^{-1} ... 10^2 rad/s is given in the figure 2.
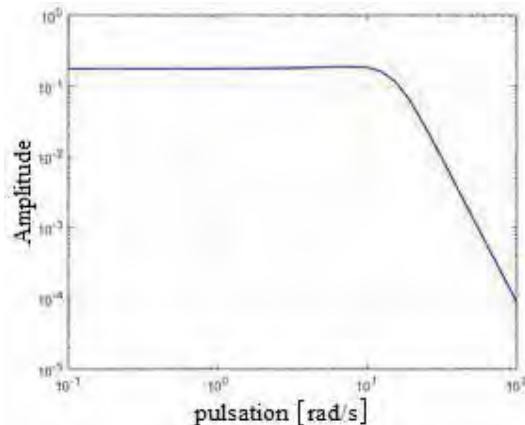
igure 2. Spectral composition of the longitudinal terrain profile.

Applying the Laplace transform to the differential equations that describe the motion of the tractor-plough system we obtain the following system of algebraic equations

$$
\begin{cases}
\left(A_{11}s^2 + A_{12}s + A_{13}\right)Z_1 + A_{14}s^2 Z_2 = \left(f_{11}s + f_{12}\right)H_1 + L\left(f_{13}\right) \\
\left(A_{21}s^2 + A_{22}s + A_{23}\right)Z_2 + A_{24}s^2 Z_1 = \left(f_{21}s + f_{22}\right)H_2 + L\left(f_{23}\right), \\
\left(A_{41}s^2 + A_{42}s + A_{43}\right)Z_4 = \left(f_{41}s + f_{42}\right)H_4 + L\left(f_{43}\right)
\end{cases}
\tag{4}
$$

where L( ) represents the Laplace transformation of the dynamic connection functions f_{13}, f_{23}, f_{43}. The evaluation of the transfer functions G_1, G_2, G_4 it was performed through overlapping effects of the two components of the dynamic equation excitations (those generated by the H land profile and those generated by the dynamic connection functions, respectively). The justification of this approach is given by the linearity of the considered model.

The final expressions of the transfer functions for Case IH Magnum 340 tractor model are as follows

$$
G_1(s) = \frac{-3280s^4 - 320800s^3 + 1{,}362\ 10^6\ s^2 + 7{,}168\ 10^7\ s^1 - 3{,}247\ 10^7}{7500s^5 + 30920s^4 + 3{,}099\ 10^6\ s^3 + 1{,}44\ 10^6\ s^2 + 7{,}2\ 10^7\ s^1},
$$

$$
G_2(s) = \frac{11120s^4 - 1{,}119\ 10^6\ s^3 + 1{,}383\ 10^6\ s^2 + 7{,}182\ 10^7\ s^1 - 1{,}834\ 10^7}{7500s^5 + 30920s^4 + 3{,}099\ 10^6\ s^3 + 1{,}44\ 10^6\ s^2 + 7{,}2\ 10^7\ s^1},
\tag{5}
$$

$$
G_4(s) = \frac{36s^2 + 2\ 10^4\ s^1 - 1141}{100s^3 + 36s^2 + 2\ 10^4\ s^1}.
$$

4. E aluation of the response of the tractor with plough on tra el on agricultural field

The evaluation of the response functions in the time domain of the plough tractor assembly, when moving on lands with irregular profile, was performed considering the respective system under the action of pseudo-random excitations. The regular longitudinal profile was simulated using a harmonic function, with the period $T_m = 2$ m and the amplitude h = 0,050 m, this being the deterministic component of the excitation signal. The random component of the signal was obtained by adding a random signal (white noise type) with the signal / noise ratio (denoted S/N) variable in the range 0,1...10. The first value in the considered range means an approximately smooth longitudinal profile, while the second value indicates a profile strongly affected by random components. The numerical analysis of the dynamic behavior of the tractor-plough assembly under the action of the mentioned excitation, was actually performed for two values of the travel speed from the ad-

missible range: 5 km/h and 10 km/h. The results obtained are presented in figures 3 and 4.

a)

b)
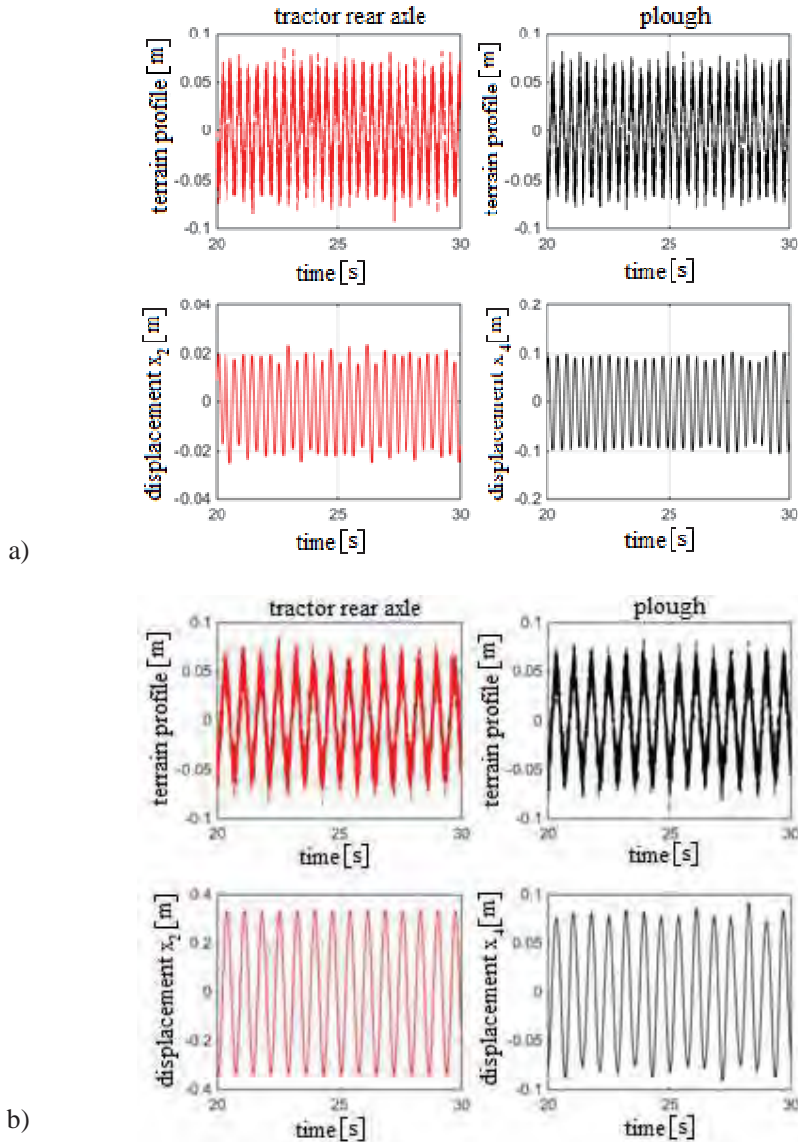
igure 3. The response of the unit tractor - plow for S/N = 10 in the case of:
a) v = 10 km/h; b) v = 5 km/h.
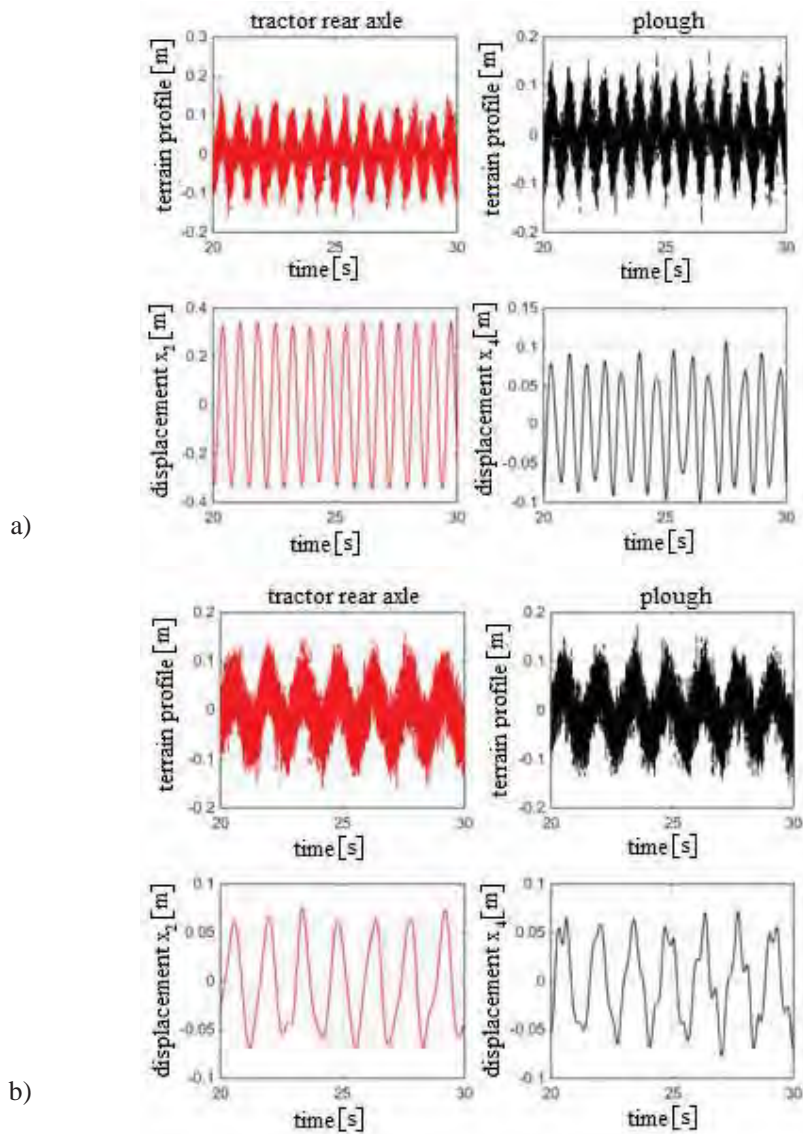
igure 4. The response of the unit tractor - plow for S/N = 0,1 in the case of:
a) v = 10 km/h; b) v = 5 km/h.

Each set of diagrams in these figures contains the excitation signal for each in-
teraction point of the tractor-plough assembly with the terrain profile (out of phase

with the speed of movement), as well as the time response for each degree of freedom considered (the vertical direction of the rear axle and plough axle, respectively). The evaluation of the response of the tractor-plough system allows a comparative analysis of the digging depth of the plow according to the speed of movement and, respectively, the longitudinal profile of the terrain on which the machine moves. The deviation of the digging depth of the plough from the reference depth was evaluated for each case by the difference between the instantaneous value of the excitation at the ground-plow interaction point and the instantaneous value of the vertical displacement of the plow under the dynamic action of the field.

If the reference value is considered h = 0,050 m for maximum amplitude of the land uneven, the maximum percentage values of the deviation from the reference digging depth performed with the tractor (only for rear axle of the tractor and, respectively, for gauge wheel of the plough), in the table 2 are presented.

Table 2. Maximum percentage deviation from the reference digging depth [in %]

ratio S/N	Velocity [km/h]	
	5	10
0,1	296,8	343
10	106,6	147

5. Conclusion

The numerical simulation shows that the developed mathematical model can be further used to study the influence of different constructive and kinematic parameters of the rear-mounted ploughing equipment in order be optimized with the final aim to assess and reduce the oscillations arising during its operation.

The comparative analysis of the results obtained in this study highlights a series of disturbing dynamic evolutions, which manifest themselves on the tractor-plough assembly during the technological work process, with a negative influence on the technological performance in terms of continuous and random variation of the instantaneous digging depth. The results presented in the previous paragraphs lead to the conclusion that in order to obtain the required technological performances, a correlation is necessary between the values of the functional parameters and the effective profile of the land on which the respective activity is carried out. Thus, a speed of movement close to the upper limit of the permissible range can produce, in the conditions of a strongly irregular profile, inadequate deviations from the optimal digging depth, while values of the speed towards the lower limit lead implicitly to a decrease in productivity. Under these conditions, the initial assessment of the state of the running surface of the tractor together with the attached equipment is necessary in order to establish a speed of movement of the machine to ensure an optimum between the deviation from the digging depth and productivity.

References

[1] Watanabe M., Sakai K., Impact dynamics model for a nonlinear bouncing tractor during inclined passage, *Biosystems Engineering*, 182, 2019, pp. 84-94.

[2] Macmillan R.H., *The Mechanics of Tractor Implement Performance. Theory and Worked Examples*. University of Melbourne Publishing House, 2002.

[3] Paraschiv G., Maican E., Paraschiv I., Bucur D., Study on stability at work for tillage aggregates, *Cercetări Agronomice în Moldova*, 2(130), 2007, pp. 5-13.

[4] Stojic B., Poznanovic N., Poznic A., Research and modeling of the tractor tire enveloping behavior, *Journal of Vibration and Control*, 23(2), 2017, pp. 290–304.

[5] Bulgakov V., Adamchuk V., Arak M., Nadykto V., Kyurchev V., Olt J., Theory of vertical oscillations and dynamic stability of combined tractor-implement unit, *Agronomy Research*, 14(3), 2016, pp. 689-710.

[6] Debeleac C., Axinti, G., *Synthesis of Newtonian mechanics with applications. Vol. III. Dynamics*, Galati University Press, 2015.

[7] Bulgakov V., Ivanovs S., Arak M., Kuvachov V., Shymko L., Bandura V., Experimental investigation of the work of a ploughing aggregate, operating according to the system push-pull', *Agronomy Research*, 16(5), 2018, pp. 1950–1959.

[8] Duma Copcea A., Ilea R., Mihuț C., Mechanisation of medium soil ploughing on flat terrain 30 cm deep in the soil, *Scientific Papers Series Management, Economic Engineering in Agriculture and Rural Development*, 17(1), 2017, pp.147-150.

[9] Ormenișan A.N., *Theoretical and experimental research on the influence of automatic adjustment systems of tractor suspension mechanisms on the dynamics and energy of plowing units*, Doctoral Thesis, Transilvania University of Brașov, 2014.

Address:

- Prof. Dr. Eng. Carmen Nicoleta Debeleac, Universitatea Dunărea de Jos" din Galați, Facultatea de Inginerie și Agronomie din Brăila, Călărașilor no 29, Brăila
  carmen.debeleac@ugal.ro